UNIVERSITY OF
KWAZULU-NATAL

INYUVESI
YAKWAZULU-NATALI

A novel *in vitro* anticancer drug delivery strategy using platinum encapsulated gold nanoparticles

Vareessh Maney

Thesis presented in fulfilment of the requirements for the degree of

Master of Science: Biochemistry

In the School of Life Sciences

University of KwaZulu-Natal, Westville

Supervisor

Professor Moganavelli Singh

Durban 2017

SUPERVISOR'S DECLARATION

The research contained in this dissertation was completed by the candidate while based in the Discipline of Biochemistry, School of Life Sciences, of the College of Agriculture, Engineering and Science, University of KwaZulu-Natal, Westville Campus, South Africa. The research was financially supported by National Research Foundation (NRF).

The contents of this work have not been submitted in any form to another university and, except where the work of others is acknowledged in the text, the results reported are due to investigations by the candidate.

As the candidate's supervisor I approve this thesis for submission.

Signed: Professor Moganavelli Singh

Date: November 2017

DECLARATION: PLAGIARISM

I, Vareessh Maney, declare that:

(i) the research reported in this dissertation, except where otherwise indicated or acknowledged, is my original work;

(ii) this dissertation has not been submitted in full or in part for any degree or examination to any other university;

(iii) this dissertation does not contain other persons' data, pictures, graphs or other information, unless specifically acknowledged as being sourced from other persons;

(iv) this dissertation does not contain other persons' writing, unless specifically acknowledged as being sourced from other researchers. Where other written sources have been quoted, then:

a) their words have been re-written but the general information attributed to them has been referenced;

b) where their exact words have been used, their writing has been placed inside quotation marks, and referenced;

(v) where I have used material for which publications followed, I have indicated in detail my role in the work;

(vi) this dissertation is primarily a collection of material, prepared by myself, published as journal articles or presented as a poster and oral presentations at conferences. In some cases, additional material has been included;

(vii) this dissertation does not contain text, graphics or tables copied and pasted from the Internet, unless specifically acknowledged, and the source being detailed in the dissertation and in the References sections.

Signed: Vareessh Maney

Date: November 2017

DECLARATION 2: PUBLICATIONS

My role in each paper and presentation is indicated. The * indicates corresponding author.

Chapter Three

1. Maney,V. and Singh,M*. (2017). An *in vitro* assessment of novel chitosan/ bimetallic PtAu nanocomposites as delivery vehicles for doxorubicin". **Nanomedicine** 12(22): 2625-2640. DOI: 10.2217/nnm-2017-0024.

Signed: Vareessh Maney

Signed: Professor Moganavelli Singh

Date: November 2017

RESEARCH OUTPUT FROM THE DISSERTATION

My role in each paper and presentation is indicated. The * indicates corresponding author.

Publications:

1. Maney,V. and Singh,M*. (2017). An *in vitro* assessment of novel chitosan/ bimetallic PtAu nanocomposites as delivery vehicles for doxorubicin". Nanomedicine 12(22): 2625-2640. DOI: 10.2217/nnm-2017-0024. ***Impact factor = 4.727.*** (Appendix A)

Manuscripts in preparation:

1. Maney, V and Singh, M*. *In vitro* target activated delivery of 5-fluorouracil using chitosan polymerised PtAu bimetallic nanocomposites.

Conference Presentations:

1. Oral Presentation- Maney,V and Singh,M. (2017) "An *in vitro* assessment of chitosan/bimetallic PtAu Nanocomposites as delivery vehicles for doxorubicin" . BIT's 7th Annual World Congress of Nano Science & Technology-2017 (Nano S&T-2017), 24-26 October, Fukuoka, Japan.
2. Poster Presentation- An *in vitro* assessment of novel chitosan/ bimetallic PtAu nanocomposites as delivery vehicles for doxorubicin. University of KwaZulu-Natal, postgraduate research day, 23 May 2017. ***Awarded 1st prize***.
3. Poster Presentation- An *in vitro* assessment of novel chitosan/ bimetallic PtAu nanocomposites as delivery vehicles for doxorubicin. University of KwaZulu-Natal, college research day, 26 October 2017.

ABSTRACT

Nanomedicine, the amalgamation of nanotechnology and medicine is poised to revolutionise clinical oncology through advancements in diagnostics, therapy and monitoring. In the endless battle against cancer, classic chemotherapeutic drugs have proven effective in the short term. However, they lack targeting specificity, are rapidly extruded by drug efflux pumps, are metabolised *in vivo* and can cause deleterious effects to healthy organs. To mitigate these underlying bottlenecks and harness the full therapeutic potential of the array of anticancer drugs available, innovative strategies are needed to temporarily regulate the drug release at the desired anatomic site, improve their tumour penetration and subcellular distribution, thus preventing unwanted toxicity to healthy tissues and organs. Research into the design of hybrid bimetallic nanoparticles has sparked increased attention, owing to their enhanced chemical, optical, surface and mechanical properties compared to their monometallic parent nanoparticle. Of these modern nanoconstructs, platinum (core)-gold (shell) bimetallic nanoparticles (PtAuBNps) have emerged as promising drug delivery vehicles, imbued with properties of both individual elements through synergism. With the boom in nanomedicine, these desirable features hold an indubitable promise in cancer therapy. However, these systems are at a nascent stage of development, requiring full screening of their therapeutic potential and carrier capabilities *in vitro*.

In this investigation, PtAuBNps were chemically synthesised, functionalised with chitosan and encapsulated with doxorubicin (DOX) and 5-fluorouracil (5-FU) respectively. All PtAuBNps and their nanocomposites were physicochemically characterised using attenuated total reflection Fourier transform infrared spectroscopy (ATR-FTIR), UV-Vis spectroscopy, transmission electron microscopy (TEM) and nanoparticle tracking analysis (NTA). The BNps presented as small (<150 nm), circular and homogeneous particles, with the drug laden nanocomposites showing good colloidal stability (< 24.0 mV). Drug binding efficiencies and loading capacity studies confirmed higher drug encapsulation of 5-FU (90.17%) compared to DOX (69.82%). *In vitro* cytotoxicity profiles were determined using the 3-[(4,5-dimethylthiazol-2-yl)-2,5-diphenyl tetrazolium bromide] (MTT) and Sulforodhamine B (SRB) assays, with all drug laden BNps inducing dose dependent, cell specific toxicities, with up to 48% cell death recorded in the cancerous cell lines MCF-7, HepG2 and Caco-2. The PtAuBNps released their chemotherapeutic payloads under pH-triggered disintegration, under simulated

acidic tumour microenvironment conditions through zero-order release kinetics. In addition, the nanocomposites showed good bioadhesive propensity, and the potential to pass through the mucous lining to facilitate oral administration of these drug nanocomposites. Overall, these positive attributes highlight the immense potential of the PtAuBNps as drug carriers for *in vitro* biological applications, and augurs well for optimisations and future research into their theranostic capabilities and clinical application.

Key Words: Nanomedicine; bimetallic nanoparticles; drug delivery; doxorubicin; 5-fluorouracil; chitosan; cytotoxicity; drug release.

DEDICATIONS

This thesis is dedicated to my driving force and perpetual inspiration, my adored parents, Anusha and Kamal Prem Maney. Thank you for every silent sacrifice made towards my upbringing and professional development.

ACKNOWLEDGMENTS

First and foremost, I am thankful to Lord Krishna for bestowing onto me the courage, protection, strength and wisdom to attain my goals thus far.

I would like to express my deep and sincere gratitude to my supervisor, Prof. M. Singh for all her assistance, guidance and support provided during the course of this investigation.

I convey acknowledgements to all my colleagues at the Non-viral Gene Therapy Lab for your help and for creating a competitive and stimulating work environment.

I owe profound gratitude to my family, Kamal-Prem, Anusha, Ashmika and Avishkar Maney. I am forever grateful for your unwavering support, love and encouragement you have all shown me.

Finally, I give my sincere thanks and appreciation to the National Research Foundation (NRF) for the financial assistance, and to the University of KwaZulu-Natal for providing the necessary facilities to make this study possible.

TABLE OF CONTENTS

Page

LIST OF TABLES

LIST OF FIGURES

Chapter Two **Page**

Chapter Three **Page**

Chapter Four **Page**

Appendices Figures **Page**

LIST OF ABBREVIATIONS

5-FU	5-Fluorouracil
Abs	Absorbance
ADC	Actual drug content
ANOVA	One-way analysis of variance
AO/EB	Acridine orange/Ethidium bromide
ATCC	American tissue culture collection
ATR	Attenuated total reflection
Au	Gold
AuNps	Gold nanoparticles
BNps	Bimetallic nanoparticles
Caco-2	Colorectal adenocarcinoma cell line
CS	Chitosan
CSNps	Chitosan nanoparticles
DDS	Drug delivery systems
DMSO	Dimethyl sulfoxide
DNA	Deoxyribonucleic acid
DOPE	Dioleoylphosphatidylethanolamine
DOX	Doxorubicin
ECM	Extracellular matrix
EDTA	N,N,N',N'-ethylenediaminetetraacetic acid
EE	Encapsulation efficiency
EMEM	Eagle's Minimum essential medium
EPR effect	Enhanced permeability and retention effect
EtBR	Ethidium bromide
FBS	Foetal bovine serum
FTIR	Fourier transformed infrared radiation spectroscopy
HEK293	Human embryonic kidney cells
HepG2	Hepatocellular carcinoma
LC	Loading content
MCF-7	Breast adenocarcinoma

MTT	3-(4,5-dimethylthiazol-2-yl)-2,5-diphenyl-2H-tetrazolium bromide
Mw	Molecular weight
MWCO	Molecular weight cut-off
NaBH4	Sodium borohydride
Np	Nanoparticle
NTA	Nano tracking analysis
PBS	Phosphate buffered saline
PEG	Polyethylene glycol
PM	Porcine mucin
Pt	Platinum
PtAuBNps	Platinum (shell)-Gold (core) bimetallic nanoparticles
PtAuCSBNps	Chitosan functionalised platinum-gold bimetallic nanoparticles
PtNps	Platinum nanoparticles
PVP	Polyvinylpyrrolidone
SDS	Sodium dodecyl sulphate
SPR	Surface plasmon resonance
SRB	Sulforhodamine B
TDC	Theoretical drug content
TEM	Transmission electron microscopy
TOPII	Topoisomerase II
TPP	Sodium tripolyphosphate
UV-Vis	Ultraviolet-Visible spectroscopy

LIST OF MATHEMATICAL SYMBOLS

µg	Micrograms
µL	Microliters
µM	Micromole
ºC	Degrees Celsius
α	Alpha
ζ	Zeta
G	Grams
h	Hours
Ic_{50}	The estimated half maximal inhibitory concentration
K_0	Zero-order release constant
K_1	First-order release constant
K_H	Higuchi release constant
K_k	Korsmeyer-Peppas release constant
kV	Kilovolt
M	Molar
Min	Minutes
mL	Millilitre
mM	Millimolar
mV	Millivolt
n	Korsmeyer-Peppas release exponent
Nm	Nanometer
R_0	Initial amount of drug in the nanocomposite
R_∞	Total amount of drug dissolved when the dosage form is exhausted
R_t	Amount of drug released at time t.
Rpm	Revolutions per minute
r^2	Correlation coefficient
SD	Standard deviation
V	Volts
$^v/_v$	Volume to volume ratio
$^w/_v$	Weight to volume ratio

CHAPTER ONE
INTRODUCTION

1.1. Background to the study

Cancer is a multifactorial disease caused by a multistage carcinogenesis process involving a series of cellular, genetic and epigenetic aberrations leading to the progressive transformation of normal cells into cancerous cells (Liu *et al.*, 2014). Cancerous cells acquire several specific phenotypic features including an infinite replicative capacity, autonomous growth signalling, insensitivity to antiproliferative signals, inhibition of apoptosis, sustained angiogenesis, invasion to neighbouring tissue and distant organs (metastasis) and inflammation (Hanahan and Weinberg, 2011, Ross *et al.*, 2012). Cancer therapy that can antagonise any or multiple of these malignant characteristics will prove beneficial towards preventing the development and spread of cancer.

Cancer treatment options are limited to surgery, radiation therapy and chemotherapy. Surgery and radiation therapy are the most effective treatment option for localised types of cancer but are ineffective for metastatic cancers. Chemotherapy makes use of potent cytotoxic drugs to impede cellular proliferation, however without any specificity. Intravenous administration of anticancer drugs are distributed throughout the body via the bloodstream and affect rapidly dividing healthy cells of the bone marrow, gut, lymphoid nodes, spleen, thymus as well as hair follicles (Kakde *et al.*, 2011). In addition, poor accumulation at the target site, intolerable cytotoxicity, rapid degradation, drug metabolism, short circulation half-lives and the development of drug resistance have hampered their therapeutic potential (Hu *et al.*, 2010, Sakhrani and Padh, 2013). During the course of chemotherapy, diminishing effects of the anticancer drug occur due to the overexpression of drug efflux pumps and plasma membrane P-glycoprotein (P-gp) result in the devolvement of drug resistance (Guertin *et al.*, 2016, Janicka and Gubernator, 2016). Thus, major challenges persist in utilising chemotherapy for cancer treatment.

The persistence and complexity of cancer have stimulated a coherent multidisciplinary approach towards understanding cancer biology, genetics, epidemiology, histopathology and chemo-preventive strategies (Danhier *et al.*, 2010, Kawasaki and Player, 2005). The fight against cancer has seen billions of dollars splurged towards the discovery and design of novel therapeutic agents, a strategy fraught with high risk and reward (Prasad *et al.*, 2016). With the

increasing need to develop new drugs with higher therapeutic potential, comes the necessity to augment the current drug repertoire with drug delivery strategies pioneered to improve specificity and efficiency. This would ultimately improve the quality and longevity of cancer patients' lives, especially those who are too weak to endure harsh chemotherapy. For this reason, nanotechnology is touted as possessing the potential and capability to spawn new effective drug delivery systems and transform ineffective drugs into powerful nanomedicines (Bamrungsap *et al.*, 2012).

Nanomedicine is an empowering and expansive discipline of science, having emerged strongly over the past decade. It involves the use of nanoparticulate materials (1-150 nm) for prophylactic, diagnostic, and therapeutic applications, in a bid to improve human health (Misra *et al.*, 2010). Research in this field has shown tremendous progress regarding the design, synthesis and evaluation of nanocarriers which resulted in several marketed nanomedicines (Bregoli *et al.*, 2016). These nano-systems are making significant strides in bridging the gap between indispensable drugs and their associated toxic effects. However, the challenge remains to develop a carrier system that is cost-effective, offers multimodal targeting, has the flexibility to load several chemotherapeutics efficiently and induce site-specific toxicity under controlled release (Kemp *et al.*, 2016). Such a carrier system is yet to come to fruition.

Currently, the only available nanomedicines in clinical use are organic based carriers, with several inorganic nanoparticles recently under clinical trials showing immense potential. Noble metal nanoparticles such as gold (Au), silver (Ag) and platinum (Pt), have an interesting perspective in drug delivery, owing to their remarkable physical, chemical and photonic properties (Dreaden *et al.*, 2012). While gold nanoparticles (AuNps) are inert and non-toxic, platinum nanoparticles (PtNps) possess anticancer properties. It is anticipated that platinum-gold bimetallic nanoparticles (PtAuBNps) will exhibit both individual metal properties as well as novel ones due to their synergistic effects.

There is a paucity of literature regarding noble metal BNps in therapeutics. To the best of our knowledge, there are no studies on the drug delivery performance of PtAuBNps. This study covers the synthesis of PtAuBNps through $NaBH_4$ rapid injection, using PVP as a protecting agent, and functionalising PtAuBNps with chitosan through ionic gelation between TPP with entrapment of two cytotoxic drugs, doxorubicin (DOX) and 5-fluorouracil (5-FU). It was anticipated that the entrapment of cytotoxic agents within the nanocomposites, will lead to better *in vitro* toxicity induction in cancerous cells, site-specific targeting, temporal control

over the drug release pharmacokinetics and the ability to bind to the mucosal layer of the gastrointestinal system.

1.2. Aim and objectives

The aim of the study was to synthesise, functionalise and characterise PtAu bimetallic nanoparticles/nanocomposites and evaluate their ability to deliver model anticancer drugs, DOX and 5-FU to several cancer cell lines *in vitro*.

In order to achieve these aims, the objectives were to:

- Chemically synthesise PtAuBNps.
- Functionalise the PtAuBNps with chitosan.
- Encapsulate DOX and 5-FU within PtAu/Chitosan nanocomposites and assess their encapsulation efficiency, loading capacity and drug release kinetics under *in vitro* simulated conditions.
- Characterise PtAuBNps and their nanocomposites using ATR-FTIR, UV spectroscopy, electron microscopy (EM) and nanoparticle tracking analysis (NTA).
- Evaluate the degree of cytotoxicity induced in selected cancer cell lines *in vitro* using the MTT and SRB assays.
- To examine the role of these nanocomposites in the induction of apoptosis.

1.3. Novelty of the study

The PtAuBNps synthesised previously as reported in literature was used mainly as catalysts for chemical reactions, with limited research conducted into their *in vitro* cytotoxicity as well as their drug delivery capabilities. In literature, PtAuBNps have been reported to be capable of inducing dose dependent cytotoxicity toward cervical cancer cells (SiHa cell line) through apoptosis (Alshatwi *et al.*, 2015). This current study is novel in many aspects, which includes:

- Toxicity profiles of PtAuBNps in different cell lines have not been reported. Assessment of morphological features have only been performed using TEM and SEM. Here we report a more robust and dynamic way of sizing and determining the colloidal stability using NTA.

- PtAu/Chitosan nanocomposites have not been previously reported. Therefore, synthesis and assessments of morphological features, stability, ability to encapsulate DOX and 5-FU, ability to release the active drug under simulated conditions, ability to induce site-specific toxicity, ability to be administered orally and ability to induce apoptosis have not been reported.

Hence this system offers a novel strategy for the delivery of DOX and 5-FU for future *in vivo* applications.

1.4. Outline of dissertation

This thesis is written up as two papers and includes a literature survey chapter and a final overall conclusion.

Chapter 1

This chapter provides an introduction and summarises the background to the study. It serves as a foundation for understanding the rationale, novelty, aim and objectives of the study. It outlines the challenges encountered with current cancer treatment options and explores the possibility of developing efficient chitosan/PtAu bimetallic nanocomposites to attain higher therapeutic efficacy.

Chapter 2

This chapter provides an up to date review of the relevant literature focusing on the complexity of cancer, drug delivery, nanotechnology, PtAuBNps, cellular uptake and intracellular trafficking.

Chapter 3

This chapter is written up as a paper entitled "An *in vitro* assessment of chitosan/ bimetallic PtAu nanocomposites as delivery vehicles for doxorubicin". This paper has been published in Nanomedicine (Appendix A).

Chapter 4

This chapter is written up as a manuscript entitled "*In vitro* target activated delivery of 5-fluorouracil using chitosan polymerised PtAu bimetallic nanocomposites". The chapter

explores the use of chitosan/PtAu bimetallic nanocomposites in facilitating a pH-responsive release of encapsulated 5-FU for cell specific targeting.

Chapter 5

This section rounds off the study and provides an overall conclusion and recommendations for future studies.

References

Alshatwi, A. A., Athinarayanan, J., and Periasamy, V. S. 2015. Green synthesis of bimetallic Au@ Pt nanostructures and their application for proliferation inhibition and apoptosis induction in human cervical cancer cell. *Journal of Materials Science: Materials in Medicine,* 26, 1-9.

Bamrungsap, S., Zhao, Z., Chen, T., Wang, L., Li, C., Fu, T., and Tan, W. 2012. Nanotechnology in therapeutics: a focus on nanoparticles as a drug delivery system. *Nanomedicine,* 7, 1253-1271.

Bregoli, L., Movia, D., Gavigan-Imedio, J. D., Lysaght, J., Reynolds, J., and Prina-Mello, A. 2016. Nanomedicine applied to translational oncology: a future perspective on cancer treatment. *Nanomedicine: Nanotechnology, Biology and Medicine,* 12, 81-103.

Danhier, F., Feron, O., and Préat, V. 2010. To exploit the tumor microenvironment: passive and active tumor targeting of nanocarriers for anti-cancer drug delivery. *Journal of Controlled Release,* 148, 135-146.

Dreaden, E. C., Austin, L. A., Mackey, M. A., and El-Sayed, M. A. 2012. Size matters: gold nanoparticles in targeted cancer drug delivery. *Therapeutic Delivery,* 3, 457-478.

Guertin, A. D., O'neil, J., Stoeck, A., Reddy, J. A., Cristescu, R., Haines, B. B., Hinton, M. C., Dorton, R., Bloomfield, A., and Nelson, M. 2016. High Levels of Expression of P-glycoprotein/Multidrug Resistance Protein Result in Resistance to Vintafolide. *Molecular Cancer Therapeutics,* 15, 1998-2008.

Hanahan, D., and Weinberg, R. A. 2011. Hallmarks of cancer: the next generation. *Cell,* 144, 646-674.

Hu, C. M. J., Aryal, S., and Zhang, L. 2010. Nanoparticle-assisted combination therapies for effective cancer treatment. *Therapeutic Delivery,* 1, 323-334.

Janicka, M., and Gubernator, J. 2016. Use of nanotechnology for improved pharmacokinetics and activity of immunogenic cell death inducers used in cancer chemotherapy. *Expert Opinion on Drug Delivery,* 14, 1-17.

Kakde, D., Jain, D., Shrivastava, V., Kakde, R., and Patil, A. 2011. Cancer therapeutics-opportunities, challenges and advances in drug delivery. *Journal of Applied Pharmaceutical Science,* 1, 1-10.

Kawasaki, E. S., and Player, A. 2005. Nanotechnology, nanomedicine, and the development of new, effective therapies for cancer. *Nanomedicine: Nanotechnology, Biology and Medicine,* 1, 101-109.

Kemp, J. A., Shim, M. S., Heo, C. Y., and Kwon, Y. J. 2016. "Combo" nanomedicine: Co-delivery of multi-modal therapeutics for efficient, targeted, and safe cancer therapy. *Advanced Drug Delivery Reviews,* 98, 3-18.

Liu, M., Jiang, L., and Guan, X. Y. 2014. The genetic and epigenetic alterations in human hepatocellular carcinoma: a recent update. *Protein & Cell,* 5, 673-691.

Misra, R., Acharya, S., and Sahoo, S. K. 2010. Cancer nanotechnology: application of nanotechnology in cancer therapy. *Drug Discovery Today,* 15, 842-850.

Prasad, S., Gupta, S. C., and Aggarwal, B. B. 2016. Serendipity in cancer drug discovery: rational or coincidence? *Trends in Pharmacological Sciences,* 37, 435-450.

Ross, C. R., Brennan-Laun, S. E., and Wilson, G. M. 2012. Tristetraprolin: Roles in Cancer and Senescence. *Ageing Research Reviews,* 11, 473-484.

Sakhrani, N. M., and Padh, H. 2013. Organelle targeting: third level of drug targeting. *Drug Design, Development and Therapy,* 7, 585-599.

CHAPTER TWO
LITERATURE REVIEW

2.1. Introduction

This chapter provides an in-depth review of the relevant literature focusing on the complexity of cancer, drug delivery and the integration of nanotechnology in biological systems for therapeutic purposes. Currently, there is a dearth of scientific knowledge regarding the delivery capabilities and cytotoxicity of these PtAuBNps. With this in mind, the review focuses on the attractive attributes of Au and Pt that has inspired the design of novel chitosan functionalised PtAuBNps as carrier systems for DOX and 5-FU. The various synthesis procedures are elucidated, before highlighting the biomedical potential of chitosan nanocomposites formed by ionic gelation. Finally, the mechanisms of cellular uptake, intracellular trafficking and the biological challenges that drug delivery systems have to overcome are elaborated upon.

2.2. Cancer

Cancer has been a silent killer throughout human existence, with the earliest evidence of malignancy predating to 1.7 million years ago, in fossilised hominin's records (Odes *et al.*, 2016). The oldest textual reference to the disease hails from Egyptian medical papyri written around 3000 BC. A case of breast cancer was vividly described within as a "grave and untreatable bulging mass in the breast" (Lukong, 2017). This medical description remains true till today, as an effective cure remains a daunting objective. However, since then tremendous progress has been made in unravelling the subtleties on how cancer is induced, spreads and resists treatments.

Cancer is an extraordinarily complex and multifaceted disease, deeply rooted in DNA. This devastating disease is believed to be caused by the accumulation of genetic and epigenetic aberrations leading to the overexpression of proto-oncogenes and the loss of function of tumour suppressor genes (Liu *et al.*, 2014). The transition of healthy cells to malignant ones occurs through the acquisition of various phenotypic and functional changes, as seen in Figure 2.1, that promote aggressive growth behaviour and metastatic dissemination. These phenotypic hallmark changes include an infinite replicative capacity, genome alteration, autonomous

growth signalling, insensitivity to antiproliferative signals, inhibition of apoptosis, sustained angiogenesis, altered cellular energetics, metastasis and inflammation (Hanahan and Weinberg, 2011, Ross *et al.*, 2012). The cascade of events set in motion by altered oncogenes, fuel the cancer's survival, malignancy, invasiveness, and drug resistance (Boroughs and DeBerardinis, 2015, Osborne *et al.*, 2004). Only a deeper understanding of the mechanistic and signalling pathways involved during cancer initiation and progression, can pave the way for new therapeutic strategies.

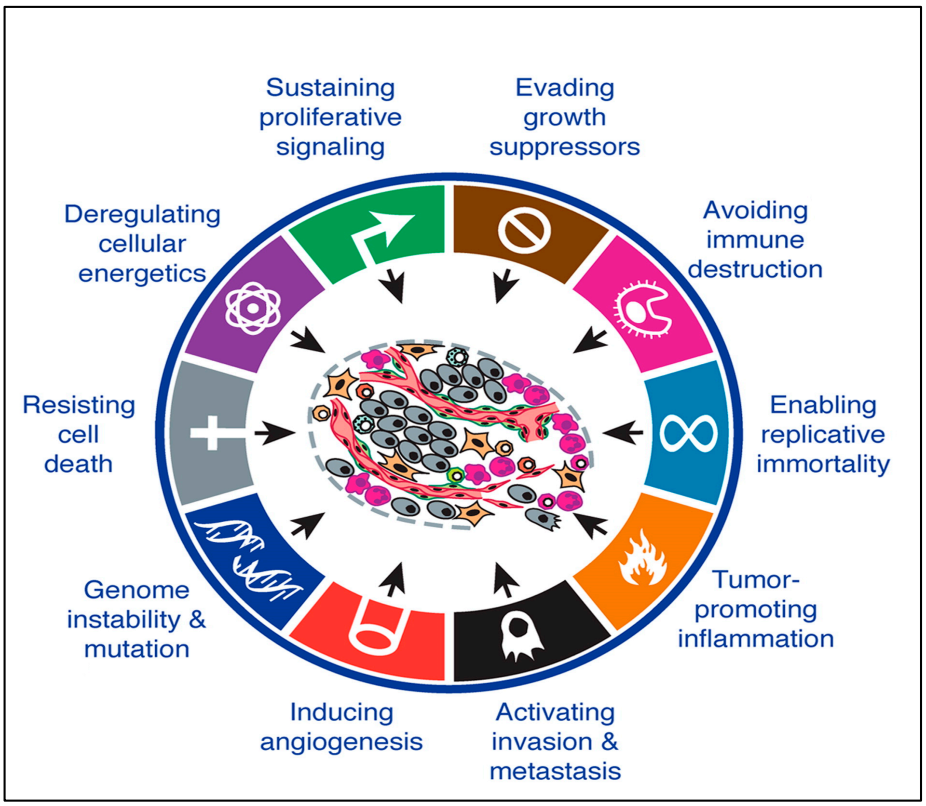

Figure 2.1: Acquired phenotypic characteristics of cancer cells (Hanahan and Weinberg, 2011)**.**

Epidemiological statistics predict an ominous yearly rise in the incidence and prevalence of cancer cases. A sum of 1,688,780 new cancer cases and 600,920 cancer deaths have been projected to occur in the United States by 2017 (Siegel *et al.*, 2017). The conventional cancer treatment modalities consisting of a combination of surgery, radiation therapy and standard chemotherapy, are effective if diagnosed early, but are either too expensive or cause severe side effects in patients (Albain *et al.*, 2009, Rosenblum and Peer, 2014). Surgical excisions may accelerate metastasis, while radiation therapy can result in complications such as osteoradionecrosis, soft tissue necrosis and myelopathy (Coffey *et al.*, 2003, Gomez *et al.*,

2011). Furthermore, both surgery and radiation therapy are local treatment options and do not cure cancer that has metastasised. The intricacy of metastasis makes cancer highly incomprehensible and accounts for more than 90% of all cancer-related deaths (Spano *et al.*, 2012), highlighting the need for systemic non-invasive strategies that in principle can seek out tumours at any anatomical location in the body.

2.3. Anticancer drugs

Chemotherapy is the use of drugs to eradicate neoplastic cells, restrain cellular proliferation and control aggressive tumour growth. Broadly, these chemotherapeutic drugs are classed according to their composite structure and mode of action either as alkylating agents, antimetabolites, natural products and hormones (Eckhardt, 2002). Anticancer drugs are distributed systemically, acting as intracellular poisons, causing cell death by either inducing lesions in genomic DNA or blocking essential metabolic pathways (Savage *et al.*, 2009).

The clinical dependence on the various anticancer drugs is due to their respective unique benefits for treating specific cancers. Potent mainstream drugs such as DOX and 5-FU are cost efficient and exhibit a broad spectrum of anticancer activity making them an ideal model drug to target numerous cancer types. As clinical resistance and poor efficacy remain the biggest hindrance in the utilisation of such drugs, the challenge is to determine reasonable means to utilise these drugs safely and efficiently. To this end, a deeper understanding of the molecular structure, intracellular interactions and side effects of both DOX and 5-FU are essential.

2.3.1. Doxorubicin

Doxorubicin (DOX) was discovered in the 1960s from isolates of the bacterium *Streptomyces peucetius*. It is regarded as one of the greatest anticancer drugs developed, due to its broad spectrum of activity in nearly all human cancers. Currently, DOX remains one of the most effective drugs for the treatment of hepatocellular, lung, ovarian, thyroid carcinomas, lymphomas, leukaemias and solid tumours (Durmus *et al.*, 2014, Zhao *et al.*, 2017). The potency of DOX is closely related to its chemical structure (Figure 2.2). Essentially, DOX is an anthracycline containing a planar anthraquinone chromophore (A-D) linked to a sugar moiety, known as daunosamine, by a glycosidic bond. (Tan *et al.*, 2009).

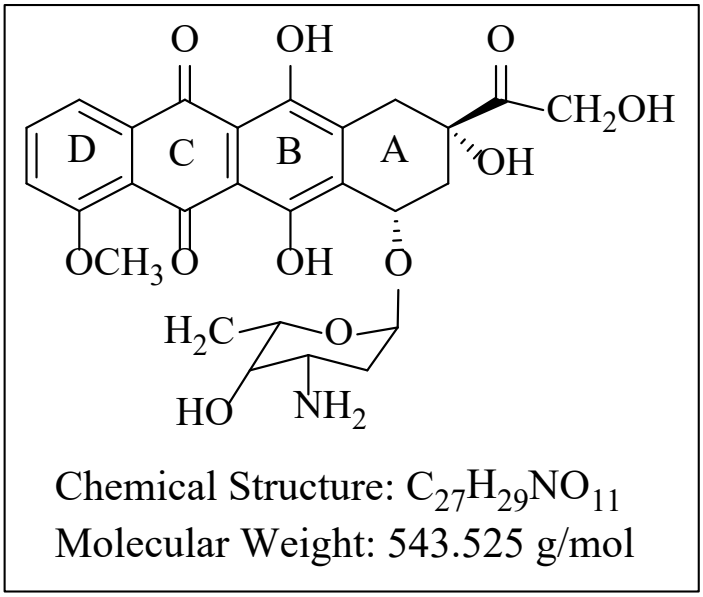

Figure 2.2: Molecular structure of doxorubicin, showing planar tetracycline rings (A-D), chemical structure and molecular weight.

Despite the extensive clinical use of DOX, a consensus on the molecular mechanism(s) by which the drug causes cell death has yet to be reached. In brief, DOX enters cells via passive diffusion and localises mainly in the nucleus by binding to proteasomes. It has been reported that a combination of interactions with nuclear DNA and bioreductive metabolism by various enzymes in cancer cells, are responsible for the observed cytotoxic effects (Kostrzewa-Nowak *et al.*, 2005, Sinha and Mason, 2015). One of the primary mechanisms of action exhibited by DOX, is the poisoning of the nuclear enzyme topoisomerase II (TOPII). Effectively, DOX intercalates into DNA, resulting in the formation of ternary DOX-DNA-TOPII cleavable complexes. An accumulation of these covalent cleavable complexes, impedes TOPII activity, prevents DNA resealing, disrupts cell replication and ultimately induces apoptosis (Chen *et al.*, 2007, Nitiss, 2009).

The second mechanism implicated in DOX-mediated cell death is through DOX induced covalent adduct formation with DNA. Effectively, the chromophore of DOX intercalates between the C and N of the 5'-GCN-3' sequence as seen in Figure 2.3. Cellular formaldehyde catalyses adduct formation by reacting with DOX to produce an activated Schiff base that creates an aminal linkage (N-C-N, covalent bond) between the daunosamine moiety and guanine on the DNA strand I. The structure is stabilised by hydrogen bonds between the drug and the complementary DNA strand producing a virtual DNA cross-link (Cutts *et al.*, 2005).

The generation of DOX-DNA adducts has been shown to activate DNA damage and induce apoptosis independent of the topoisomerase II poisoning (Swift *et al.*, 2006).

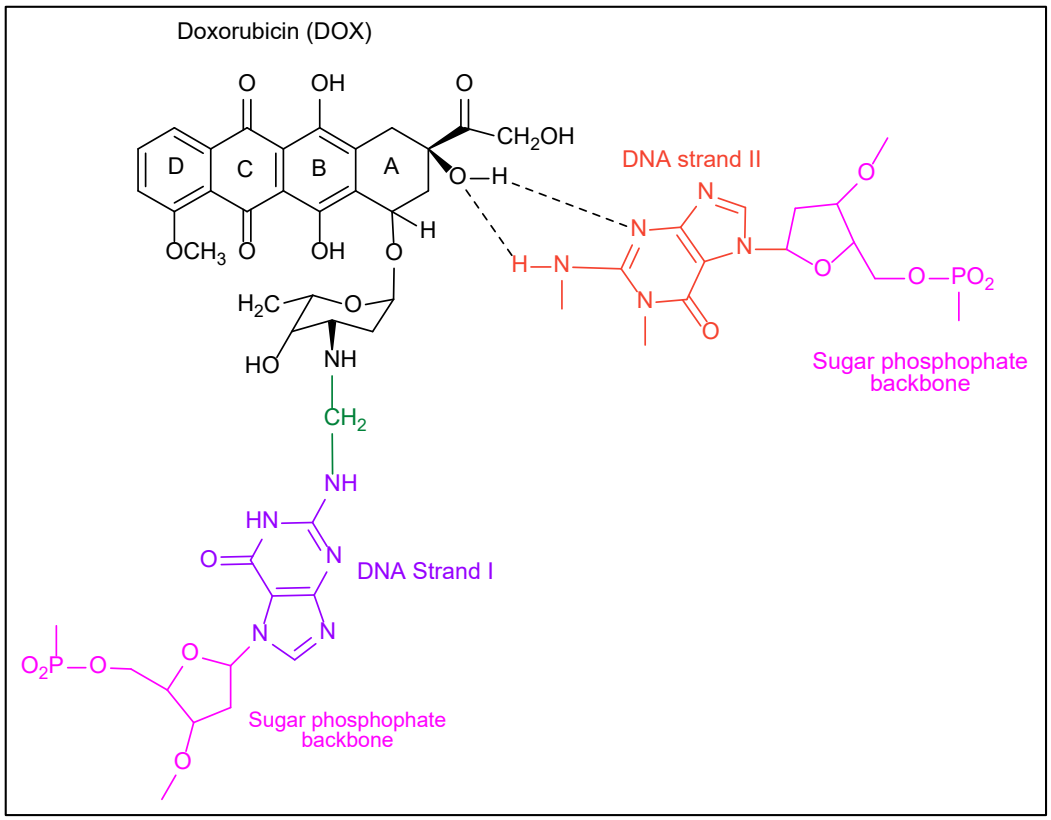

Figure 2.3: Schematic illustration of DOX-DNA adduct formation. DOX is covalently bound to guanine on the DNA strand I through a methylene linkage (N-C-N), derived from formaldehyde. Adduct formation is stabilised by hydrogen bonding (dotted lines) to guanine on the complementary DNA strand (redrawn from Parker *et al.*, 2004).

Furthermore, the generation of free radicals has been implicated in DOX-mediated cell death. The quinone moiety of doxorubicin (Ring C) is oxidised to form a DOX-semiquinone free radical, as seen in Figure 2.4. This reaction is catalysed by the several NAD(P)H oxidoreductase enzymes viz. cytochrome P450 reductase, endothelial nitric oxide synthase, mitochondrial NADH dehydrogenase and xanthine dehydrogenase. The generated DOX-semiquinone free radical is oxidised further leading to the formation of superoxides, peroxides and hydroxyl radicals (Kostrzewa-Nowak et al., 2005, Pawłowska et al., 2003). After free radical generation, redox cycling occurs, and electrons are donated to regenerate the DOX structure. Redox cycling is particularly destructive, since only a small amount of DOX is required to generate large amounts of superoxide radicals. The consequences of DOX induced free radical production include increased oxidative stress, that triggers a series of events

including DNA cleavage, cell membrane damage, increased production of ceramide and ultimately apoptosis (Tokarska-Schlattner *et al.*, 2006).

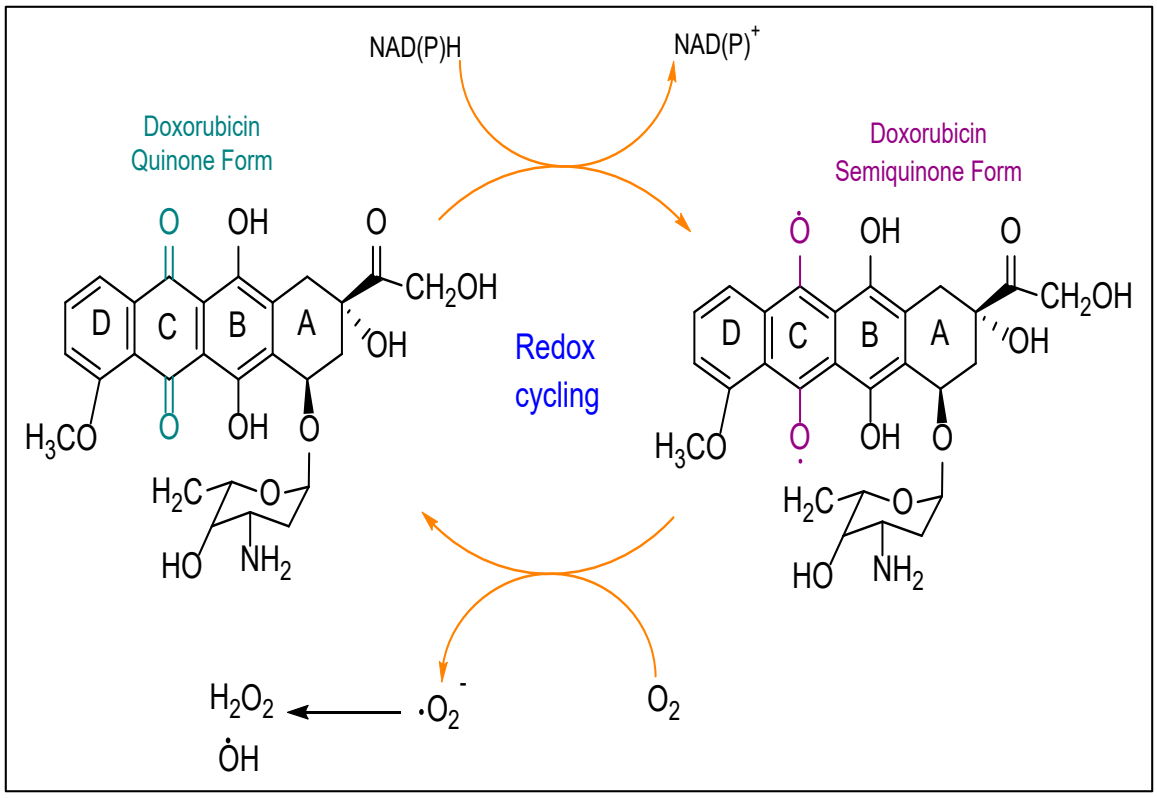

Figure 2.4: Schematic illustration of DOX induced free radical production (redrawn from Keizer *et al.*, 1990).

2.3.2. 5-Fluorouracil

Anticancer drug, 5-fluorouracil (5-FU), is a fluoropyrimidine nucleoside (Figure 2.5), with a fluorine atom covalently bound to the heterocyclic aromatic ring of uracil. This drug was rationally designed by Heidelberger and colleagues in 1957, based on the premise that cultured rat hepatoma cells incorporate radiolabelled uracil more avidly than non-malignant tissue, implicating different enzymatic pathways responsible for uracil metabolism (Heidelberger *et al.*, 1957). These findings stimulated the synthesis and subsequent implementation of 5-FU as targets for antimetabolite chemotherapy, against diverse cancer types viz. breast, prostate, liver, stomach, pancreas, head and neck cancers (Longley *et al.*, 2003). Principally, 5-FU has been used either alone or in conjunction with modulators such as oxaliplatin as well as leucovorin and represents one of the most efficient regime for treatment of metastatic colorectal cancer (Shim *et al.*, 2005).

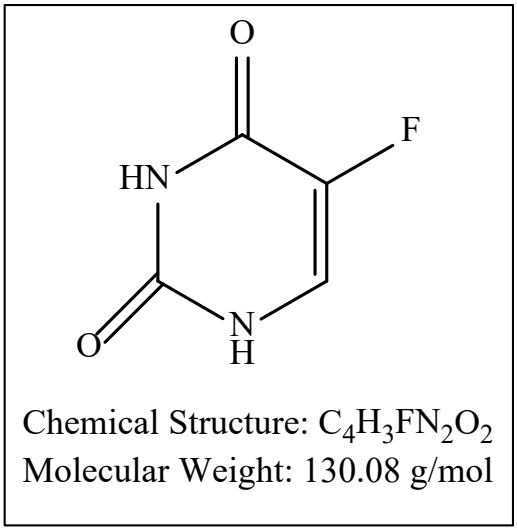

Figure 2.5: Molecular structure of 5-fluorouracil, showing planar tetracycline rings (A-D), chemical structure and molecular weight.

Essentially, 5-FU is inactive, and requires intracellular metabolism to exert its pharmacological action (Figure 2.6) (Grem, 2000). By virtue of its closely related chemical structure, 5-FU mimics uracil and thymine, and will inextricably be integrated into the same transport processes and enzymes partaking in the anabolism and catabolism of pyrimidines (Dias *et al.*, 2010). Intracellularly, 5-FU is converted into cytotoxic fraudulent nucleotides that serve as inhibitors of enzymes involved in the biosynthesis of RNA and DNA. It is converted into ribonucleotides by two pathways. Firstly, the enzyme orotate phosphoribosyltransferase directly converts 5-FU into 5-fluorouridine-5'-monophosphate (5-FUMP). The second pathway involves the conversion of 5-FU to 5-fluorouridine (5-FUrd) by uridine phosphorylase, followed by uridine kinase which catalyses the formation of 5-FUMP (Thorn *et al.*, 2011).

The 5-FUMP is subsequently phosphorylated to 5-fluorouridine diphosphate and finally to 5-fluorouridine triphosphate (5-FUTP), by the intracellular enzymes nucleoside monophosphate and nucleoside diphosphate kinases. The fraudulent nucleotide 5-FUTP mimics uridine-5'-triphosphate (UTP) and is incorporated into all classes of RNA, disrupting normal RNA function. The consequences include the ceasing of ribosomal RNA maturation, the modification of tRNAs, and the splicing of mRNA, leading to profound effects on cellular metabolism and viability (Beumer *et al.*, 2006, Ma *et al.*, 2004).

The 5-FdUrd is subsequently phosphorylated by thymidine kinase to form 5-fluoro-2'-deoxyuridine-5'-monophosphate (5-FdUMP). Finally, the enzyme thymidylate synthase mediates the transfer of a methyl group from 5,10-methylenetetrahydrofolate to 5-FdUMP forming 5-fluoro-2'-deoxyuridine-5'- triphosphate (5-FdUTP). The nucleotide 5-FdUTP exerts cytotoxic effects through competitive binding with thymidylate synthase (TS), in place of the conventional substrate 2'-deoxyuridine-5'-monophosphate (dUMP), thus halting thymidine-5'-monophosphate (dTMP) synthesis and inducing an imbalance in the deoxynucleotide pool. This ceases DNA synthesis and repair, leading to lethal DNA damage (Beumer *et al.*, 2006, Ma *et al.*, 2004).

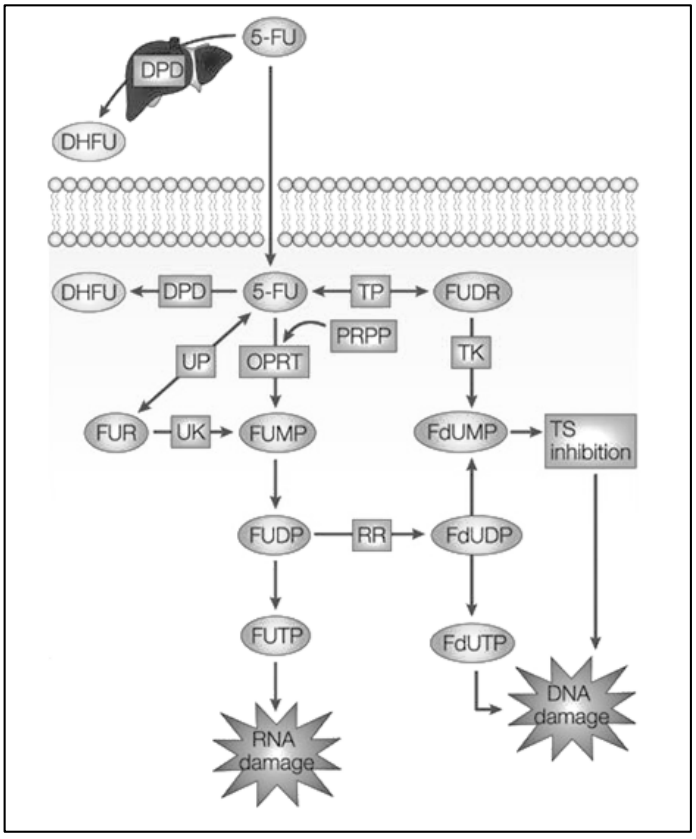

Figure 2.6: Metabolic activation and mechanism of action of 5-FU (adapted from Longley *et al.*, 2003).

Mainstream chemotherapeutic drugs such as DOX and 5-FU form a cornerstone of cancer therapy owing to their effectiveness. However, they are associated with narrow therapeutic windows and debilitating effects which need urgent attention. Modern chemotherapy has seen a paradigm shift from the exclusive use of free drugs that are in essence intracellular poisons, to targeted drug delivery regimes operating at the nanoscale.

2.4. Drug delivery

Drug delivery is a multidisciplinary scientific undertaking, aimed at optimising and developing methods to administer and release therapeutic agents in a safe and controlled manner (Chien and Lin, 2002). Such strategies are necessitated as many conventional drugs are unstable in biological milieu, have poor biodistribution, are rapidly metabolised, have limited circulation time and short biological half-lives (Hu *et al.*, 2010, Sakhrani and Padh, 2013). These underlying bottlenecks, contribute to the high attrition rates of many drugs across all therapeutic areas. Thus, the growing desire of supplementing drug molecules with innovative delivery systems arises.

Current drug formulations have proven exorbitant, time-consuming, and rather futile if not coupled with efficient delivery systems. Moreover, their therapeutic efficiency depends not only on their molecular structure and biological activity, but also on the physiochemical and surface properties of the carrier (Blanco *et al.*, 2015, Ragelle *et al.*, 2017). Most anticancer drugs work by impairing the ability of malignant cells to undergo rapid cellular proliferation, a fundamental trait of cancer (Lohse *et al.*, 2016). While this strategy does provide some primary benefits, these drugs indiscriminate between neoplastic and proliferating healthy cells. The common off-targets include the GI tract, bone marrow, intestinal mucosa and hair follicles manifesting severe effects including gastrointestinal tract ulceration, myelosuppression, mucositis, alopecia and cardiotoxicity (Huang *et al.*, 2009b).

During therapy, cancer cells within the tumour microenvironment adapt to intrinsic stress and become insensitive to programmed cell death by altering their energetics and expressing P-glycoproteins (P-gp) in abundance on their membrane (Gillies *et al.*, 2012, Hanahan and Weinberg, 2011). Effectively, P-gp, an ATP-dependent drug efflux pump actively extrudes the internalisation of many conventional drugs, causing multidrug resistance. This multidrug resistant protein together with variable vascular density, hypoxia, acidosis and different intratumoural blood pressure impede drug penetration and dispersion within the tumour core. These underlying issues, lead to low drug dosage reaching the quiescent cells at the tumour core, compared to cells at the periphery and close to the vascular surface (Ernsting *et al.*, 2013). Thus, cells in quiescence are likely to survive treatment, re-establish and unleash a powerful wave of drug resistance, deteriorating the patient's health and response to therapy.

Scientists are challenged to develop “magic bullets”, a concept postulated by Paul Ehrlich with deep tumour penetrating capabilities (Bae and Park, 2011). This concept is being realised

with the development of nanosized drug delivery systems encapsulating anticancer agents or conjugation via absorption of the drug after nanoparticle formation. An ideal drug delivery vehicle, should bind to the therapeutic agent with high efficiency, decrease the required dose concentrations, all while inducing site-specific toxicity, conferring protection to the bound cargo from degradation *in vivo*, and having sustained release under the appropriate conditions; independent of the route of administration (Freitas, 2006, Malam *et al.*, 2009).

There are several drug delivery routes viz. oral, parenteral, pulmonary, transdermal and systemic, which are dependent on the properties of the drug, patient compliance, access to the disease location, and effectiveness in dealing with the specific disease (Verma and Garg, 2001). Oral administration through the gastrointestinal tract (GIT), is the most convenient route for systemic drug delivery, due to ease of administration, mild fabrication conditions, lower manufacturing costs, slower release of the active drug for extended therapeutic effects, and favourable drug absorption (Balimane *et al.*, 2000, Scholz *et al.*, 2008, Yin *et al.*, 2006). Essentially, to safely pass the stomach to reach the intestine, the drug delivery system needs to overcome several biological barriers, including the mucosal layer and tight epithelial junctional complexes, which impede drug adsorption and restrict systemic distribution of the drug. Further hurdles include drug degradation by digestives enzymes as well as extremities in gastric pH, which affect drug solubility and absorption (Hua *et al.*, 2015, Yin *et al.*, 2006).

Mucoadhesive drug delivery platforms have been brought forth as promising candidates, to potentiate delivery through the GIT, by prolonging the residence time of the drug at the site of application, increasing the permeability of the drug into systemic circulation and enhancing the drug bioavailability. The term mucoadhesion in drug delivery, refers to the intimate interaction between the innate positively charged species of the drug carrier and the negatively charged mucin proteins (e.g., p-glycoproteins) within the mucosal layer of the GIT (Mortazavi and Smart, 1995). The mucoadhesive propensity of a carrier is influenced by several factors, including the concentration of polymer, molecular weight, cross-linking, hydrogen bonds, pH and surface charge (Andrews *et al.*, 2009).

The use of nanotechnology in drug delivery, promises to improve treatment efficiency, administration and patient compliance, as well as to control nonspecific toxicity.

2.5. Nanotechnology: A biological domain

Nanotechnology involves the collaborated efforts from interdisciplinary fields to manipulate, control and integrate matter at the nanoscale (Bamrungsap *et al.*, 2012). This fascinating domain of research lies at the core of humanity's endeavours, in creating potentially cutting-edge breakthroughs for application in biotechnology, nanoelectronics, engineering, medicine and healthcare. In fact, nanotechnology comes with the promise to address many pressing twenty first century issues, such as global contamination, renewable energy, and the fight against devastating diseases such as cancer (Roco, 2003).

The ability to produce small synthetic structures (1-100 nm) for cellular uptake, gives nanotechnology unprecedented opportunities to probe deep subcellular structures and overcome biological barriers. Their size is what makes nanomedicines particularly attractive candidates for curing functional abnormalities at the cellular level (Lammers *et al.*, 2010). Matter at the nanoscale level, displays unique properties including physiochemical, optical, thermal and electronic properties, that distinguishes them from their bulk precursor. Increasingly, these desirable intrinsic properties are being utilised in medical applications, including tissue engineering for active tissue regeneration (Taggart *et al.*, 2016), as biosensors, as tracking agents for diagnostic monitoring and imaging (Marques *et al.*, 2016, Thanh and Green, 2010), and as drug delivery systems.

A myriad of nanosized materials have been envisioned to bind and carry bioactive agents viz. therapeutic genes, drugs, targeting ligands and RNA to reach its target destination. These nanostructures include carbon structures (nanotubes, nanodiamond), lipids (liposomes, micelles), polymers (hydrogels, dendrimers) and inorganic nanoparticles (gold, platinum) (Misra *et al.*, 2010). Well-designed nanoparticulate systems can become powerful tools to reformulate drugs with improved drug solubility and pharmacokinetics, as well as prolonged shelf life and cost-effectiveness. This is exemplified by Doxil®, a pegylated liposomal doxorubicin formulation with an optimal size (<100 nm), capable of evading clearance and opsonisation by the reticuloendothelial system (RES). This organic based nanomedicine has been reported to exhibit 6 times the circulation time of unmodified doxorubicin, emphasising the impact nanotechnology has had in medicine (Koshkaryev *et al.*, 2013).

Research endeavours have shifted from well-characterised lipid based delivery systems to inorganic nanoparticles, the latter emerging superior owing to their enhanced physical, optical and electronic capabilities. Metallic nanostructures such as noble metals (e.g., Au, Pt) have

desirable surface plasmon resonance (Amendola, 2016), semiconductors (e.g. Cds, Pbs) have quantum confinement (Sagar *et al.*, 2016), and the magnetic materials (Fe_3O_4 and FePt) exhibit superparamagnetism (Ma *et al.*, 2015). These inherent properties sparked application of metallic nanoparticles in non-invasive cancer targeted regimes including, photodynamic therapy (PDT), photothermal therapy, radiotherapy, radiofrequency therapy and theranostics (Misra *et al.*, 2010). A photothermal therapy device, Auroshell (Nanospectra Biosciences), composed of silica (core) ultra-thin gold (shell), which upon irradiation selectively destroys cancerous tissue (Pannerec-Varna *et al.*, 2013), shows tremendous potential, and is entering clinical trials.

Another characteristic of nanoparticles, is their ability to deliver therapeutic agents through physiological barriers, such as the intestinal mucosa, placental, and blood brain barrier (BBB). Coating drug delivery platforms with surfactants such as polysorbate 80 or poloxamer 188, enhance the carriers ability to cross the BBB, for the treatment of neurologic disorders such as Parkinson's and Alzheimer's disease (Braakhuis *et al.*, 2015, von Roemeling *et al.*, 2017).

Nanotechnology is proving to be a powerful tool for both imaging and therapeutic purposes, offering the potential to diagnose, treat and monitor disease progression in real time (Misra *et al.*, 2010). The challenge lies in rationally designing nanomedicines to be effective, non-toxic, feasible and multimodal. A better understanding of the inherent properties of nanostructures and their functionalisation strategies, will provide key links in developing new safe and effective nanomedicines with multifaceted applications.

2.6. History of gold and platinum in medicine

The allure of Au has captivated humankind for centuries. The sheer majestic beauty of Au is naturally associated with the radiance of the sun, and is believed to have exceptional medicinal properties due to its eternal nature. A common belief amongst ancient alchemists was to make Au drinkable to enhance skin glow and cure ailments (Yamada *et al.*, 2015). As early as 2500 BC, ancient Indians used Swarna Bhasma; the first reported Au nanoparticle based medicament to treat bronchial asthma, diabetes mellitus, sexual problems and rheumatoid arthritis (Arvizo *et al.*, 2012, Paul and Sharma, 2011). The past knowledge and use of Au for therapeutic purposes, have thrust forward the use of AuNps, and hybrid AuNps for applications in medicine and cancer therapy.

While Au has a rich and distinguishing history, the fifteenth century discovery of Pt by Spanish Conquistadors in the rivers of Ecuador is more recent. Highly coveted for its rich, white lustre and untarnishable properties, Pt was proclaimed by King Louis XVI of France to be the only metal "fit for royalty" (Munir *et al.*, 2006). The chemotherapeutic potential of the platinum complex cisplatin was discovered rather fortuitously in the 1960's, based on the observation that Pt-electrodes inhibited bacterial cellular division (Boulikas and Vougiouka, 2003). This drug exhibits a broad range of antitumour activity, ascribed to Pt coordinating to the nucleophilic N7-sites of purine bases in DNA, resulting in intra-strand cross-links, causing denaturation of the DNA chain and apoptosis (Zhu *et al.*, 2015). The discovery of cisplatin has generated extensive research into the design of alternative platinum based compounds as potential chemotherapeutic agents. Despite active research in the development of new Pt-complexes, most induce mild to severe toxicity (Dasari and Tchounwou, 2014). A necessity exists to utilise platinum as a chemotherapeutic in a manner that is safe with the desired biological activity. In this regard, PtNps are believed to be an innovative means to generate platinum ions in a biological system. Reports have demonstrated that PtNps induced strand breaks in DNA, leading to activation of the P53 signalling pathways, cell cycle arrest and finally apoptosis induction (Buchtelova *et al.*, 2017, Hashimoto *et al.*, 2016, Nejdl *et al.*, 2017).

The favourable biological attributes of AuNps together with the chemopreventive and anticancer properties of PtNps has inspired the design of a multifunctional PtAuBNps, to serve as a structural backbone, to which the biocompatible polymer chitosan, and chemotherapeutic drugs DOX and 5-FU can be conjugated.

2.7. Platinum-Gold bimetallic nanoparticles

Bimetallic nanostructures are dynamic and modern products of metallurgy advancements on the nanoscale, and are composed of two different metals in either random alloy, alloy with intermetallic compound, cluster-in-cluster or core-shell distribution (Zaleska-Medynska *et al.*, 2016). The physiochemical features of bimetallic nanoparticles are strongly dependent on several factors, such as the (1) particle homogeneity, (2) surface segregation of the particles, (3) morphology of the particulate matter and, (4) the atomic distribution (influenced by the atomic radius, surface energy and standard redox potential) (Hwang *et al.*, 2005, Ma and Balbuena, 2008). The shape of monometallic nanoparticles can be engineered either as spheres, rods, cubes, tetrahedrons or octahedrons (Huang *et al.*, 2009a). However, the combination of

two metals can produce an even greater assortment of nanostructures varying in shape, structure and core-shell thickness due to miscellaneous atomic distributions (Figure 2.7) (Bhukta *et al.*, 2017, Zaleska-Medynska *et al.*, 2016).

These bimetallic nanoparticles are fabricated to either (1) reduce synthesis costs, (2) enhance specific properties, (3) improve colloidal stability, and (4) provide biocompatibility. The BNps studied thus far have predominantly been applied as catalysts in chemical reactions such as the Hendry reaction, Suzuki-Miyaura reaction and oxidation reactions. Some of the earliest work by Toshima and co-authors revealed that bimetallic AuPd and PtAu displayed enhanced catalytic activity for hydration and hydrogenation reactions compared to their monometallic counterparts (Toshima and Yonezawa, 1998, Toshima *et al.*, 1990).

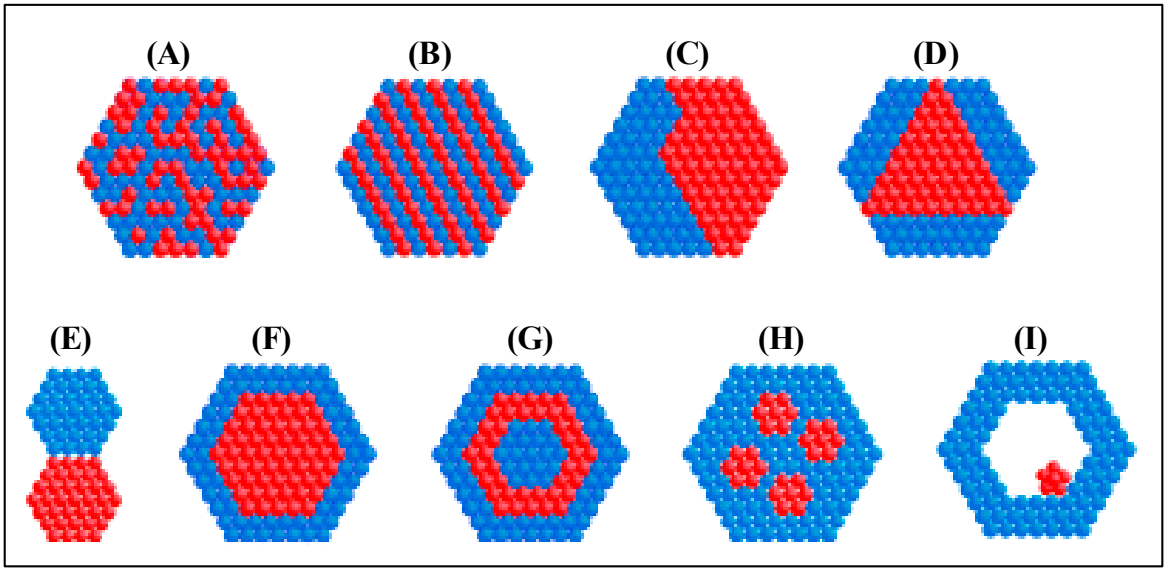

Figure 2.7: Schematic representation of the different bimetallic nanoparticle configurations (A-B) alloys; (C-E) subclusters; (F) core-shell nanoparticles; (G) multishell core-shell nanoparticles; (H) multiple small core material coated by single shell material, (I) movable core within hollow shell material (Zaleska-Medynska *et al.*, 2016).

Nanotechnology is rapidly expanding beyond the confines of standard convention with regards to chemistry, geometry and size manipulation. To truly exploit the potential of hybrid nanomaterials in biomedicine requires knowledge of how matter interacts to form core shells, and the synergistic role the core to shell ratio plays in relation to the functional properties exhibited.

2.8. Platinum-Gold bimetallic nanoparticles in medicine and drug delivery

Modern Au based core-shell nanostructures have opened new frontiers in medical advancements finding application in bio-sensing, delivery and disease diagnosis. The idea that two materials can be combined to create a single entity enriched with properties of both individual metals, as well as new ones due to synergism has attracted increased attention for fundamental and technological reasons. Metallurgy on the nanoscale produces hybrid bimetallic nanoparticles that acquire superior physicochemical, optical, magnetic, surface and structural properties compared to their precursor nanoparticle (Hwang *et al.*, 2005, Zaleska-Medynska *et al.*, 2016). Allied to that, they can be produced with a plethora of different designs varying in hydrodynamic size, shape, surface morphology, geometries and porosity with high reproducibility. BNps offer broader tailoring capabilities and versatility, far beyond monometallic systems. By merely changing the ratios of the individual precursors or their geometrical architectures, the physiochemical, catalytic, optical and electronic properties can be controlled and enhanced through quantum confinement and synergism (Chaudhuri and Paria, 2012, Fageria *et al.*, 2016).

In biomedicine, PtAuBNps have many positive attributes, their small size and high surface area to volume ratio for higher binding of therapeutic agents, deep tissue penetration and wide medical applications in diagnostics, bio-imaging and therapeutics (Erathodiyil and Ying, 2011). Research findings, highlight BNps as Raman enhancers in cellular imaging (Cui *et al.*, 2006), as radiosensitizers in radiotherapy, and photothermal ablation owing to their high atomic number (Liu *et al.*, 2016). The latter is particularly attractive due to the easy amenability of BNp's optical absorption, which can be tuned to the near infrared region (650-900 nm), where the absorption of human tissue is minimal, and penetration is optimal (Liu *et al.*, 2016, Wu *et al.*, 2012a). Recently, nanomedicine has sought carriers that offer theranostic capabilities (concurrent therapy and diagnostic imaging), with PEGylated PtAu nanodendrites showing enhanced CT imaging, while inducing photothermal destruction of cancer cells (Liu *et al.*, 2016).

Gold nanoparticles provide an inert, non-toxic, biocompatible vehicle for targeted drug delivery. These features can be further enhanced through the conjugation of multiple nanomaterials, therapeutic genes, proteins and, topical drugs. For cellular applications bimetallic carrier systems need to be stable, exhibit regulated release of bound cargo at the

target site, and improve the therapeutic efficacy of conventional bioactive agents (Papasani *et al.*, 2012).

Bimetallic nanoparticles lack functional groups to bind therapeutic agents and cannot be directed towards a specific cellular biological target. The key for successful delivery lies in modifying the periphery on PtAuBNps with cell specific ligands, stabilising agents and polymers. Current research findings have demonstrated that core-shell systems can be conjugated to complementary cellular ligands such as proteins (transferrin and growth factors), peptides (AP peptide), aptamers (A10) and small biomolecules (folic acid and galactose) (Zhong *et al.*, 2014). This targets the drug delivery system to specific cancer cells preventing unwanted interactions.

2.9. Surface plasmon resonance

The most fascinating optical property of metallic nanoparticles is undoubtedly their surface plasmon resonance (SPR). It is responsible for the mesmerising colours of colloidal gold and silver suspensions observed in the visible spectral region, that inspired archaic artisans to craft iridescent glassware (Colomban *et al.*, 2009). This phenomenon arises when metallic nanoparticles interact with light to induce a collective coherence of free electrons confined on the particles surface, which in turn, induces electronic motion in the metal, producing a dipole oscillation. Essentially, the surface plasmon resonance band is the maximum amplitude of this dipole oscillation that is reached at specific wavelengths. This resonant frequency leads to a strongly enhanced electromagnetic field on the particle surface, thus enhancing all radiative properties such as absorption and scattering. For biomedical applications, this is particularly attractive for highly sensitive diagnostic devices, Raman spectroscopy, photoablation and photothermal therapy (Huang and El-Sayed, 2010, Wiley *et al.*, 2006, Wu *et al.*, 2012b).

The SPR signal can be influenced by several factors, that adjust the particles charge density including morphology, composition, adsorbates, dielectric properties and the surrounding medium. Through modulating the nanoparticles shape, the SPR band can be finely tuned in the visible and near-infrared regions, which further strengthens their biomedical application (Huang and El-Sayed, 2010). While gold nanoparticles show strong SPR in the visible region (520 nm), platinum exhibits SPR in the ultraviolet region (215 nm) (Ungureanu *et al.*, 2011, Zhang and Toshima, 2013). The presence of AuNps in any formulation can be analysed based on its original SPR, with deviations upon PtAuBNp formation or functionalisation causing SPR

shifts and colour changes detected by UV-Vis spectroscopy. Essentially, during the formation of Pt(shell)-Au(core) bimetallic nanoparticles as Pt atoms epitaxially nucleate, and are deposited on the surface of the Au core, there is dampening of AuNps SPR, with blue shift towards the ultraviolet region (Lim *et al.*, 2008, Peng and Yang, 2009, Zhang and Toshima, 2013).

With better control over colloidal stability, size distribution and morphology the production, of hybrid nanostructures are seen as a key milestone in material advances, with further advantages being gained through the coexistence of the two metals.

2.10. Synthesis of bimetallic nanoparticles

By optimising matter at the nanoscale level, the physiochemical, biological and optical properties can be tailored precisely to meet the needs of a specific application. For biomedical applications, core-shell nanoparticles must be water soluble and have surface chemistry capable of conjugating polymers, targeting ligands, peptides and drugs. The nanoparticle synthesis procedures include physiochemical, chemical and biological synthesis.

2.10.1. Mechanochemical synthesis

The reduction of metal salts through electrochemical, photochemical and sonochemical methods is particularly attractive for biomedical applications, since it does not employ reducing agents, which may contaminate Nps. In electrochemical synthesis, the galvanic displacement technique is used to coat colloidal Au with Pt in the presence of surfactants and stabilisers at elevated temperature, to produce PtAuBNps of 5-40 nm in size (Yang *et al.*, 2016a, Zhao *et al.*, 2015). The photolytic strategies employing high-intensity femtosecond laser pulses, have been reported to produce Nps with controllable size (1 nm), composition and high purity (Nakamura *et al.*, 2012). Lastly, sonochemical synthesis using ultrasonic vibrations have been reported to mediate the formation of PtAuBNps with a size range of 5-15 nm (Mizukoshi *et al.*, 1997, Yang *et al.*, 2016b). The advantages of the mechanochemical strategies include simplicity, low cost, rapid production, high purity and excellent product yield (Sounderya and Zhang, 2008).

2.10.2. Green synthesis

A major area of research interest has been to exploit biogenic agents in plants and microorganisms, to induce competitive reduction between two monometallic nanoparticles in solution, resulting in the formation of BNps. Plant extracts in particular, tea polyphenols derived from *Camellia sinensis (L.),* have been reported to produce PtAuBNps of 10-50 nm in size (Khalil *et al.*, 2014). Polyphenol extracts containing catechins compounds are excellent scavengers of free radicals, opening an array of applications for the treatment of cancer, diabetes and cardiovascular diseases (Alshatwi *et al.*, 2015). Another promising avenue to synthesise nanoparticles and their hybrids, are through reduction aided by specific enzymes secreted by fungi such as *Schizophyllum commune*, *Aspergillus niger* and *Fusarium oxysporum*. This method has produced Nps of 50-100 nm, but with poor colloidal stability (Ahmad Siddiqui *et al.*, 2016, Arun *et al.*, 2014, Bhambure *et al.*, 2009).

Biogenic synthesis is an affordable, environmentally friendly and benign way to produce BNps, that also possess anti-oxidant and anti-microbial properties. However, this synthesis strategy is time-consuming, yields Nps that are severely aggregated with poor morphology and size distribution, and is difficult to scale up to pharmaceutical production (Narayanan and Sakthivel, 2010).

2.10.3. Chemical synthesis

For biomedical applications, chemical strategies are preferred because synthesis is facile, rapid, reproducible and yields homogeneous nanoparticles. Bimetallic nanoparticle synthesis entails two steps, the synthesis of the core followed by the growth of a shell. These growth techniques can be either a one-pot method, involving the initial growth of the core followed by deposition of the shell *in situ,* or a stepwise method involving the independent growth of the seeding material, followed by the addition of the shell material (Rodríguez-González *et al.*, 2005, Zhang and Toshima, 2013). In both strategies, metal salts are reduced in the presence of suitable reducing agents such as alcohols, hydrides, citrates and hydrazines (Nasrabadi *et al.*, 2016, Sounderya and Zhang, 2008). Typically, this reduction is assisted by suitable stabilising agents such as thiols, amines, surfactants, or polymers that act as shape directing reactants that mediate core-shell formation and prevent nanoparticle agglomeration (Chanana and Liz-Marzan, 2012, Khan *et al.*, 2012). Factors such as the lattice matching, reduction potential and band gap properties of the precursor materials as well as the pH, reaction time, temperature,

solvents, reducing and stabilising agents, all affect core to shell growth (Chaudhuri and Paria, 2012, Daniel and Astruc, 2004, Zaleska-Medynska *et al.*, 2016).

In the alcohol reduction method, metal precursors, as well as PVP, are refluxed in alcohols such as methanol, ethanol, or isopropanol. Nps are formed through the reduction of metals salts, while the alcohols are oxidised to form their respective carbonyls. This synthesis has been previously reported to produce PtAuBNps of 3.0 ± 1.0 nm in size (Zhang and Toshima, 2013).

In this study, bimetallic nanoparticles were prepared in a one-pot method by reduction of Au and Pt precursors with sodium borohydride using PVP as a protectant stabiliser. The polymer PVP was favoured because it is cheap, non-toxic and can stabilise Nps efficiently in water (Chanana and Liz-Marzan, 2012). During bimetallic nanoparticle formation, gold and platinum salts in solution are reduced to a zero valent state by sodium borohydride and can be described by the three electrochemical equations presented Table 2.1. In principle, the difference in reduction potential between Au and Pt favours core shell formation. Due to a single phase reduction hydrochloroauric acid ($HAuCl_4$) is reduced over a shorter period of time to form Au seeds, and is followed by the gradual overgrowth of Pt, resulting in the formation of a dark brown colloidal suspension. The epitaxial deposition of Pt and the formation PtAu nanostructures is mediated by the structural directing agent PVP. This syntheis statergy can produce nanostructures in the 1-10nm size range (Ataee-Esfahani *et al.*, 2010, Zhang and Toshima, 2013).

Table 2.1: Standard reduction potentials of gold and platinum salts. Adapted from (Ataee-Esfahani *et al.*, 2010).

Electrochemical equation	Standard Redox potential (eV)
$AuCl_4^- + 3e^- \rightarrow Au + 4Cl^-$	+1.00
$[PtCl_6]^{2-} + 2e^- \rightarrow [PtCl_4]^2 + 2Cl^-$	+0.68
$[PtCl_4]^{2-} + 2e^- \rightarrow Pt + 4Cl^-$	+0.76

For long term storage and therapeutic purposes PVP protected BNps are far from ideal as they have a tendency to aggregate, lack targeting specificity and the ability to bind drugs proficiently. Moreover, injection of pristine PtAuBNps are likely to, induce cytotoxicity, endoplasmic reticulum (ER) stress, cleavage of cytoskeletal protein and trigger unwanted immune responses (Luz *et al.*, 2017). Only through embracing surface functionalisation trends,

will these platforms meet stringent biological and pharmaceutical requirements, and be rendered safe and efficient. Therefore, an understanding of the surface chemistry and attributes of naturally occurring polymers such as chitosan, will provide key links in developing reinforced structures, surface amenability and stimuli responsive systems.

2.11. Surface characterisation of nanostructures

Surface chemistry plays a determining role in the physiochemistry of the bimetallic nanoparticles and their behaviour in biological environments. For biomedical applications, pristine nanoparticles require passivation with stabilising molecules such as PVP to avoid aggregation before they can be further modified (Peng and Yang, 2009). Functionalisation strategies with polymers or organic molecules are important to: (1) provide necessary functional groups to bind bioactive agents and targeting ligands, (2) stabilise the nanoparticle and prevent aggregation, (3) increase the circulation time by preventing sequestration of the nanocomposite by the reticuloendothelial system, (4) provide biocompatibility and biodegradability (Pissuwan *et al.*, 2011). The nature of the surface molecules strongly determines cellular uptake, effectiveness and the potential side effects of the nanocomposites. Hence, to fully exploit cellular functions and processes in biological systems, the surface charges and fundamental forces that govern stabilisation in aqueous media are crucial.

The zeta potential is defined as the electro-kinetic potential generated by the accumulation of ions at the surface of colloidal nanoparticles. It is often regarded as a measure of surface charge; however, it more accurately describes the magnitude of the electrical double layer repulsive forces between particles in Brownian motion (Honary and Zahir, 2013). The four types of forces that contribute to the interparticle potential in a colloidal system include van der Waals forces, electrostatic repulsive forces, magnetic dipolar forces, and steric repulsions. (Shevchenko *et al.*, 2006). In principle, colloidal nanoparticles with a high zeta potential will have a more dominant repulsive force other than an attractive force, leading to greater dispersion. On the contrary, the dominant attractive force in colloids with low zeta cause particles to clump together and coagulate as the dispersion breaks (Gibson *et al.*, 2009). Three critical parameters contribute to the zeta potential, these include pH, ionic strength and concentration. To achieve desirable colloidal stability for cellular applications, the electrostatic and steric forces can be altered through conjugation with polymers such as polyethylene glycol and chitosan (Badawy *et al.*, 2010, Gibson *et al.*, 2009).

2.12. Chitosan as a capping agent

Chitosan (CS), is a natural linear copolymer composed of alternating units of N-acetylglucosamine and D-glucosamine. It is derived through the deacetylation of chitin, primarily sourced from the exoskeleton of insects and marine animals (Cheung *et al.*, 2015). The degree of deacetylation greatly influences the intrinsic properties of CS, including the crystallinity, biodegradability, biocompatibility, mucoadhesion, purity, safety, solubility, stability, swelling and viscosity (Hsu *et al.*, 2004, Shukla *et al.*, 2013).

Chitosan is a preferred excipient for gene and drug delivery applications, as it is biodegradable, non-toxic, anti-inflammatory, immunostimulating, hemocompatible, and has permeation enhancing effects (Singla and Chawla, 2001, Szymańska and Winnicka, 2015). In humans, CS is predominantly degraded by lysozymes, chitinases and bacterial enzymes in the colon to harmless amino acids (Kean and Thanou, 2010). It has been suggested that a higher molecular weight and degree of deacetylation will result in longer degradation rates (Hsu *et al.*, 2004). Nonetheless, given adequate time CS will be degraded sufficiently for excretion. Chitosan has further demonstrated mucoadhesive capabilities to enhance and prolong drug absorption, facilitating diffusion through the mucosal epithelium. For delivery purposes, CS presences a rich density of amine (NH_2) and hydroxyl groups (OH) for binding of different therapeutic agents.

Polymeric chitosan nanoparticles (CSNps) synthesised by mild methods such as ionic gelation, coacervation, or complexation, have proved exceedingly effectual as drug delivery carriers and can retain the aforementioned benefits of CS (Pérez-Herrero and Fernández-Medarde, 2015). The ionic gelation method is the most popular method for the synthesis of CSNps as preparation conditions are mild and less time-consuming. The basic principle of this approach involves the protonation of CS in acetic acid (1-3%), followed by the addition of aqueous TPP to induce inter and intra-cross-linkages between or within CS chains, mediated through electrostatic complexation between the negatively charged phosphate groups of TPP and the amino groups of CS (Hudson and Margaritis, 2014). In general, the molecular weight of CS used, the degree of deacetylation and stoichiometry of the complexes all influence the drug delivery capabilities of the CSNps. Current literature indicates that CS with high molecular weight and a high degree of deacetylation exhibit better encapsulation efficiency, drug release, permeation enhancing properties and bioadhesiveness (Ahmed and Aljaeid, 2016, Cheung *et al.*, 2015). A study by Masarudin *et al.* (2015) demonstrated that pH 4.2 and a CS:

TPP ratio of 3:1, is best for controlling polydispersion, colloidal stability and size distribution during the protonation of CS to CSNps.

In this study, PtAuBNps, as well as DOX and 5-FU, were encased within chitosan nanoparticles as a means to (1) improve shelf life, (2) add theranostic capabilities, (3) favour cellular uptake to the negatively charged cell membrane through chitosan's positively charged moieties, (4) provide temporal control of drug release, and to (5) evoke cell specific toxicity through apoptosis.

2.13. Targeted delivery

Targeted drug delivery to solid or haematological tumours can be achieved either actively or passively. Both these targeting regimes can be supplemented with target activated drug systems to exert spatial and temporal control of drug release and thus, improve the effectiveness of active and passive targeting in non-leaky tumours. Stimuli responsive nanoparticles are designed to release their cargo in one of two ways: (1) through endogenous stimuli such as changes in pH in the target tissues, or (2) through an exogenous cue such the application of light or a magnetic field (Wicki *et al.*, 2015). In this section, the active and passive targeting approaches will be discussed briefly before highlighting pH-responsive drug release.

2.13.1. Passive targeting

Passive targeting relies on the physiochemical and functional properties of the nanomedicine to exploit the pathophysiology and anatomy of cancers. Growing tumours quickly deplete nutrients and oxygen from the normal vasculature, and become hypoxic. This upregulates several endogenous vascular mediators such as bradykinin, nitric oxide, peroxynitrite and vascular endothelial growth factor to induce angiogenesis (Samadian *et al.*, 2016, Wakaskar, 2017). Classically, solid tumours undergo extensive angiogenesis to meet high energy demands, giving rise to vascular leakiness, chaotic architecture, the lack of a smooth muscle layer lining tumour endothelial cells, and impaired functional receptors for angiotensin II (Ernsting *et al.*, 2013, Jiang *et al.*, 2013). This coupled with non-laminar blood flow and impaired lymphatic drainage leads to enhanced permeability and retention (EPR). Hence, nanomedicines can perforate by convection or diffusion through the porous vascular endothelial fenestrations, and into the tumour interstitium (Sutradhar and Amin, 2014).

Generally, it is suggested that a drug delivery system (DDS) within a threshold size range of 40-200 nm, with stealth capabilities and sufficient stability is best suited to induce the EPR effect, prolong circulation time and avoid clearance by renal filtration (Wicki *et al.*, 2015).

While passive targeting is cost efficient, increases drug bioavailability and circulation time; it fails to delineate between neoplastic and healthy tissue. Moreover, the lack of control and unpredictability of the EPR effect can contribute to multidrug resistance (MDR). Hence, an augmentation with active targeting can achieve higher payloads of the drug at the diseased site (Wicki *et al.*, 2015).

2.13.2. Active targeting

Active targeting involves the use of peripherally conjugated targeting ligands for selective binding to surface receptors that are overexpressed on cancer cells or endothelial cells in neo-vasculature (Danhier *et al.*, 2010). This targeting strategy has the edge over non-targeted strategies, as it reduces unwanted, nonspecific interaction and allows for greater uptake and localisation of the therapeutic agent at the target site, through receptor-mediated endocytosis. Ligands commonly used in targeted drug delivery systems include, folic acid, arginine-glycine-aspartic acid (RGD) peptides, transferrin and integrin (Arranja *et al.*, 2017). It is generally believed, that the higher binding efficiency of this strategy increases the targeting efficiency, but it is arguable that in solid tumours these targeting ligands anchor strongly to the cell membrane, decreasing penetration depth and uniform distribution of the drug. Thus, to successfully implement this strategy, optimisation of the targeting ligand density is needed to balance penetration depth and binding affinity, and to ensure the safe and controlled release of the encapsulated agent to its target site of action (Peer *et al.*, 2007).

2.13.3. pH-responsive drug release

The tumour microenvironment is slightly acidic (pH 5.5-6.5) compared to the physiological pH of 7.4. This acidity is induced through high glycolytic cell metabolism, hypoxia and blood perfusion leading to an accumulation of lactic acid, which in turn, increases extracellular acidification in the tumour microenvironment (Karimi *et al.*, 2016). Researchers have taken advantage of this pH variation to design smart delivery platforms that release encapsulated drugs in the presence of acidic environments, such as in the Golgi apparatus (pH 6.4),

endosomes (pH 6.0) and lysosomes (pH 5.0) (Sun *et al.*, 2014). Typically, pH-triggered release strategies encompass either (1) pH cleavable bonds such as hydrazone or oxime bonds between the drug and nanocarrier, or (2) polymers that undergo swelling/shrinkage due to protonation at specific conditions. Controlled release of the drug in the vicinity of the tumour tissue occurs either through (1) diffusion through the Np matrix, (2) desorption of drug bound to the surface, (3) erosion, or (4) a combination of erosion and diffusion (Singh and Lillard, 2009, Sun *et al.*, 2014). The drug release mechanism and factors affecting drug release can be eludicated to by kinetic mathematical models, the most common being the zero-order, first-order, Higuchi and the Korsmeyer-Peppas models (Chavda and Patel, 2011).

Targeted delivery together with controlled drug release, play a pivotal role towards developing future personalised medicine. However, many of the DDS that show immense potential *in vitro*, suffer setbacks *in vivo*. This is probably due to unpredictable interactions with blood proteins, anatomical and physiological barriers which all reduce or abrogate deep tissue penetration and subsequent release of the drug (Sun *et al.*, 2014). These need to be taken into account when developing safe and efficient targeted nanomedicines.

2.14. Physiological barriers in nanoparticle targeting

Nanomedicines encounter several barriers along their tortuous journey from their point of introduction to their accumulation at the pathological site. To achieve the desired targeting effects, the drug delivery system needs to have the necessary physicochemical attributes to avoid clearance by organs such as the liver, spleen and kidneys, as well as the immune and complement system (Longmire *et al.*, 2008). The elimination of foreign bodies, such as nanostructures in circulation is a natural process to help maintain our body in a healthy state. Upon injection, opsonisation (i.e., adsorption of opsonins) will occur immediately, to form a corona on the surface of nanoparticles. This absorption of plasma proteins occurs through hydrophobic and electrostatic interactions, together with conformational changes and associated changes in entropy (Sun *et al.*, 2014). Classical examples of opsonic molecules include complement proteins, apolipoproteins, fibronectin, serum albumin and immunoglobulins. Nanocarriers bearing these nonspecific proteins are rapidly engulfed and degraded by phagocytic cells, for example macrophages, Kupffer cells and monocytes (Misra *et al.*, 2010, Sun *et al.*, 2014). Without the presence of these opsonic molecules, phagocytes are typically not able to bind or recognise foreign particles.

It has been highlighted, that charged and hydrophobic surfaces interact avidly with plasma proteins, and to avoid immune responses, improve the pharmacokinetic profile and increase the blood residence time, the surface of nanocarriers are neutralised with hydrophilic polymers such as polyethylene glycols (PEGs), poloxamers and poloxamines. These polymers are flexible and highly hydrophilic, and can shield hydrophobic or charged blood protein interactions (Parveen *et al.*, 2012). Apart from the surface properties of nanoparticles, the hydrodynamic size is of equal importance, as Nps smaller than 10 nm are eliminated via renal filtration while Nps larger than 100 nm tend to localise in the liver, spleen and lungs. Interestingly, drug delivery systems with a hydrodynamic diameter of 10-100 nm are deemed pharmacokinetically optimum, as they can efficiently evade renal, hepatic and splenic filtration (Sun *et al.*, 2014).

In cases where a DDS escapes the immune system surveillance, it will need to interact with the vascular endothelial membrane, to reach the tumour microenvironment and face the next obstacle, the extracellular matrix (ECM). The ECM of tumours is characterised by extensive stromal components such as collagen, elastin fibres, hyaluronic acid, proteoglycans networks, as well as elevated interstitial fluid pressures (IFP) (Arranja *et al.*, 2017, Blanco *et al.*, 2015). These underlying bottlenecks cause significant resistance to the diffusion of drug laden nanoparticles through the tumour interstitium, causing premature release of the bound drug far from the intended site of action, reducing the therapeutic effect of the nanomedicine. While the extravasation of many smaller delivery systems into the tumour periphery may be favoured by increased permeability and perfusion, dispersion to distal regions of the tumour is impaired by the high IFP. Angiotensin and nitroglycerine have been used to increase system blood pressure and enhance passive targeting to tumour tissue (Bertrand *et al.*, 2014).

After the extravasation into the tumour tissue, the delivery system is internalised via endocytosis, followed by transfer to various organelles, including the endosomes, lysosomes, Golgi apparatus, mitochondria, endoplasmic reticulum, and nucleus (Sun *et al.*, 2014). Knowledge of the *in vitro* delivery capabilities of novel drug delivery systems is essential before any *in vivo* evaluation or application. An ideal DDS must be able to enhance vascular penetration as well as subcellular distribution, and upon reaching its' target site should degrade or disassemble to allow for quick release of the encapsulated cargo.

2.15. Intracellular delivery of nanomedicines

Nanomedicines empowered with active or passive targeting capabilities release their payloads either into the extracellular space or the intracellular environment, following successful cellular uptake through clathrin-mediated endocytosis, caveolae-mediated endocytosis or macropinocytosis (Sun *et al.*, 2014). As illustrated in Figure 2.8, nanoparticles are engulfed by membrane protrusions to form an endocytic vesicle, followed by spatiotemporal trafficking, mediated mainly by a network of cellular endosomes together with the Golgi apparatus, endoplasmic reticulum and lysosomes. In the early endosome, Nps are either exocytosed resulting in the release of cargo in the cytoplasm or are further transported towards the degradative endolysosomal compartment. To deliver the encapsulated drug more efficiently to the desired subcellular component (nucleus or mitochondria), endosomal escape must occur before the late endosome fuses with the lysosome (Behzadi *et al.*, 2017). Therefore, the incorporation of either fusogenic agents or cationic polymers such as polyethyleneimine, poly-l-lysine and CS can be used to facilitate endosomal escape (Sakhrani and Padh, 2013). Fusogenic agents are random structures at physiological pH, and undergo a conformational change to adopt an amphiphilic α-helical conformation in the endosome, leading to the destabilisation of the endosomal membrane and subsequent release of cargo into the cytoplasm (Varkouhi *et al.*, 2011). On the other hand, pH-sensitive drug carriers function by inducing the "proton sponge effect", whereby the surface polymers incorporated into the DDS, buffer endosomal acidification, leading to a vesicular influx of protons as well as water, which in turn causes swelling, endosomal rupture and leakage of the drug into the cytosol (Danhier *et al.*, 2010).

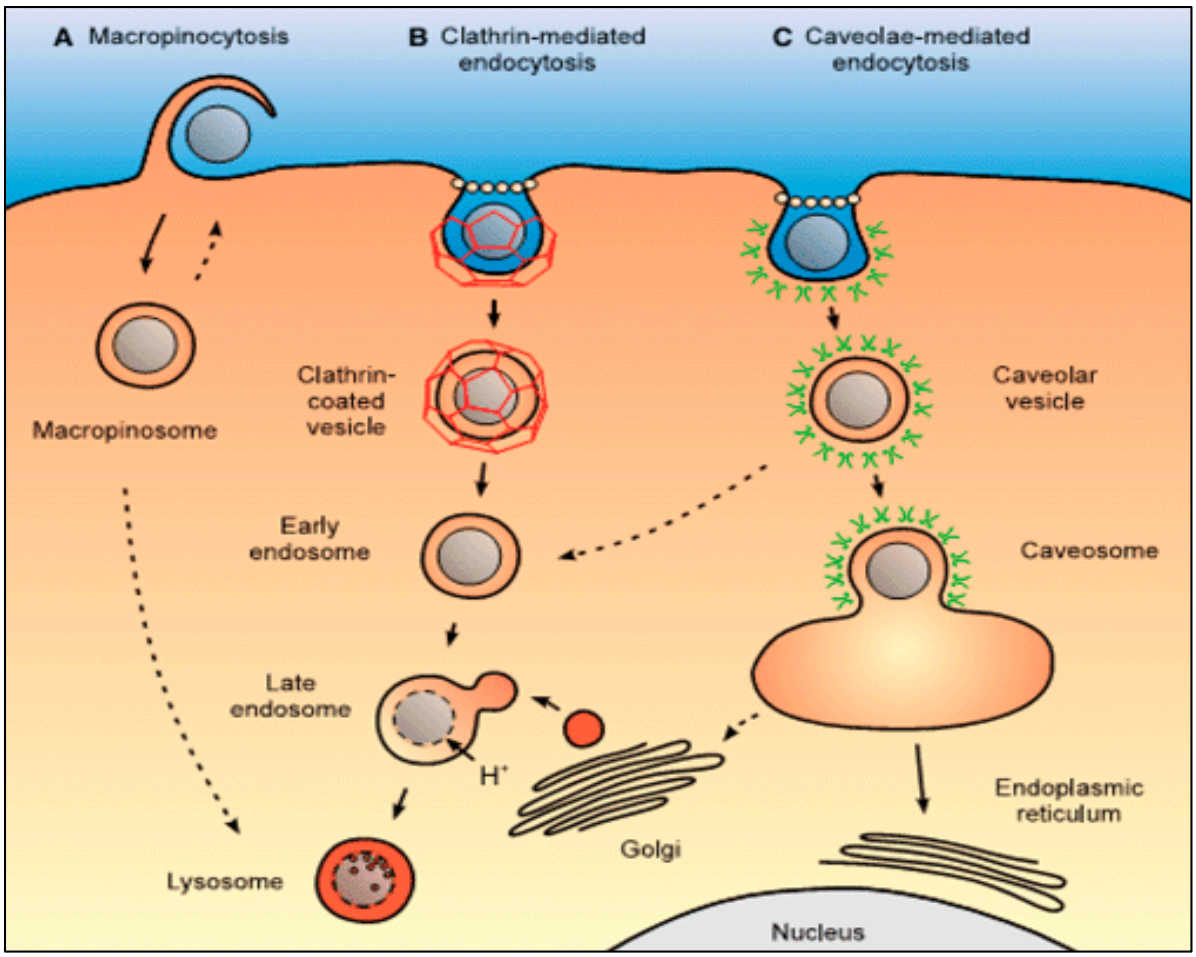

Figure 2.8: Schematic of the possible endocytosis pathways and intracellular trafficking of nanocomposites along the degradative endolysosomal network (Mao *et al.*, 2013)

References

Ahmad Siddiqui, E., Ahmad, A., Julius, A., Syed, A., Khan, S., Kharat, M., Pai, K., Kadoo, N., and Gupta, V. 2016. Biosynthesis of Anti-Proliferative Gold Nanoparticles Using Endophytic *Fusarium oxysporum* Strain Isolated from Neem (A. indica) Leaves. *Current Topics in Medicinal Chemistry,* 16, 2036-2042.

Ahmed, T. A., and Aljaeid, B. M. 2016. Preparation, characterization, and potential application of chitosan, chitosan derivatives, and chitosan metal nanoparticles in pharmaceutical drug delivery. *Drug design, development and therapy,* 10, 483-507.

Albain, K. S., Swann, R. S., Rusch, V. W., Turrisi, A. T., Shepherd, F. A., Smith, C., Chen, Y., Livingston, R. B., Feins, R. H., Gandara, D. R., Fry, W. A., Darling, G., Johnson, D. H., Green, M. R., Miller, R. C., Ley, J., Sause, W. T., and Cox, J. D. 2009. Radiotherapy plus chemotherapy with or without surgical resection for stage III non-small-cell lung cancer: a phase III randomised controlled trial. *Lancet,* 374, 379-386.

Alshatwi, A. A., Athinarayanan, J., and Periasamy, V. S. 2015. Green synthesis of bimetallic Au@ Pt nanostructures and their application for proliferation inhibition and apoptosis induction in human cervical cancer cell. *Journal of Materials Science: Materials in Medicine,* 26, 148-151.

Amendola, V. 2016. Surface plasmon resonance of silver and gold nanoparticles in the proximity of graphene studied using the discrete dipole approximation method. *Physical Chemistry Chemical Physics,* 18, 2230-2241.

Andrews, G. P., Laverty, T. P., and Jones, D. S. 2009. Mucoadhesive polymeric platforms for controlled drug delivery. *European Journal of Pharmaceutics and Biopharmaceutics,* 71, 505-518.

Arranja, A. G., Pathak, V., Lammers, T., and Shi, Y. 2017. Tumor-targeted nanomedicines for cancer theranostics. *Pharmacological Research,* 115, 87-95.

Arun, G., Eyini, M., and Gunasekaran, P. 2014. Green synthesis of silver nanoparticles using the mushroom fungus *Schizophyllum commune* and its biomedical applications. *Biotechnology and Bioprocess Engineering: BBE,* 19, 1083-1086.

Arvizo, R. R., Bhattacharyya, S., Kudgus, R. A., Giri, K., Bhattacharya, R., and Mukherjee, P. 2012. Intrinsic therapeutic applications of noble metal nanoparticles: past, present and future. *Chemical Society Reviews,* 41, 2943-2970.

Ataee-Esfahani, H., Wang, L., Nemoto, Y., and Yamauchi, Y. 2010. Synthesis of bimetallic Au@ Pt nanoparticles with Au core and nanostructured Pt shell toward highly active electrocatalysts. *Chemistry of Materials,* 22, 6310-6318.

Badawy, A. M. E., Luxton, T. P., Silva, R. G., Scheckel, K. G., Suidan, M. T., and Tolaymat, T. M. 2010. Impact of environmental conditions (pH, ionic strength, and electrolyte type) on the surface charge and aggregation of silver nanoparticles suspensions. *Environmental Science & Technology,* 44, 1260-1266.

Bae, Y. H., and Park, K. 2011. Targeted drug delivery to tumors: myths, reality and possibility. *Journal of Controlled Release,* 153, 198-205.

Balimane, P. V., Chong, S., and Morrison, R. A. 2000. Current methodologies used for evaluation of intestinal permeability and absorption. *Journal of Pharmacological and Toxicological Methods,* 44, 301-312.

Bamrungsap, S., Zhao, Z., Chen, T., Wang, L., Li, C., Fu, T., and Tan, W. 2012. Nanotechnology in therapeutics: a focus on nanoparticles as a drug delivery system. *Nanomedicine,* 7, 1253-1271.

Behzadi, S., Serpooshan, V., Tao, W., Hamaly, M. A., Alkawareek, M. Y., Dreaden, E. C., Brown, D., Alkilany, A. M., Farokhzad, O. C., and Mahmoudi, M. 2017. Cellular uptake of nanoparticles: journey inside the cell. *Chemical Society Reviews,* 46, 4218-4244.

Bertrand, N., Wu, J., Xu, X., Kamaly, N., and Farokhzad, O. C. 2014. Cancer nanotechnology: the impact of passive and active targeting in the era of modern cancer biology. *Advanced Drug Delivery Reviews,* 66, 2-25.

Beumer, J. H., Eiseman, J. L., Parise, R. A., Joseph, E., Holleran, J. L., Covey, J. M., and Egorin, M. J. 2006. Pharmacokinetics, metabolism, and oral bioavailability of the DNA methyltransferase inhibitor 5-fluoro-2′-deoxycytidine in mice. *Clinical Cancer Research,* 12, 7483-7491.

Bhambure, R., Bule, M., Shaligram, N., Kamat, M., and Singhal, R. 2009. Extracellular biosynthesis of gold nanoparticles using *Aspergillus niger*-its characterization and stability. *Chemical Engineering & Technology,* 32, 1036-1041.

Bhukta, A., Bagarti, T., Guha, P., Sathyavathi, R., Satpati, B., Rakshit, B., Maiti, P., and Satyam, P. V. 2017. Study of Ag induced bimetallic (Au-Ag) nanowires on Silicon (5 5 12) surfaces: Experiment and theoretical aspects. *Surface Science,* 664, 29-37.

Blanco, E., Shen, H., and Ferrari, M. 2015. Principles of nanoparticle design for overcoming biological barriers to drug delivery. *Nature Biotechnology,* 33, 941-951.

Boroughs, L. K., and Deberardinis, R. J. 2015. Metabolic pathways promoting cancer cell survival and growth. *Nature Cell Biology,* 17, 351-359.

Boulikas, T., and Vougiouka, M. 2003. Cisplatin and platinum drugs at the molecular level. *Oncology Reports,* 10, 1663-1682.

Braakhuis, H. M., Kloet, S. K., Kezic, S., Kuper, F., Park, M. V., Bellmann, S., Van Der Zande, M., Le Gac, S., Krystek, P., and Peters, R. J. 2015. Progress and future of *in vitro* models to study translocation of nanoparticles. *Archives of Toxicology,* 89, 1469-1495.

Buchtelova, H., Dostalova, S., Michalek, P., Krizkova, S., Strmiska, V., Kopel, P., Hynek, D., Richtera, L., Ridoskova, A., and Adam, P. 2017. Size-related cytotoxicological aspects of polyvinylpyrrolidone-capped platinum nanoparticles. *Food and Chemical Toxicology,* 105, 337-346.

Chanana, M., and Liz-Marzan, L. M. 2012. Coating matters: the influence of coating materials on the optical properties of gold nanoparticles. *Nanophotonics,* 1, 199-220.

Chaudhuri, R. G., and Paria, S. 2012. Core/shell nanoparticles: classes, properties, synthesis mechanisms, characterization, and applications. *Chemical Reviews,* 112, 2373-2433.

Chavda, H., and Patel, C. 2011. Preparation and *in vitro* evaluation of a stomach specific drug delivery system based on superporous hydrogel composite. *Indian Journal of Pharmaceutical Sciences,* 73, 30-37.

Chen, B., Peng, X., Pentassuglia, L., Lim, C. C., and Sawyer, D. B. 2007. Molecular and cellular mechanisms of anthracycline cardiotoxicity. *Cardiovascular Toxicology,* 7, 114-121.

Cheung, R. C. F., Ng, T. B., Wong, J. H., and Chan, W. Y. 2015. Chitosan: an update on potential biomedical and pharmaceutical applications. *Marine drugs,* 13, 5156-5186.

Chien, Y. W., and Lin, S. 2002. Drug delivery: Controlled release. *Encyclopedia of Pharmaceutical Technology,* 1, 811-833.

Coffey, J. C., Wang, J., Smith, M., Bouchier-Hayes, D., Cotter, T., and Redmond, H. 2003. Excisional surgery for cancer cure: therapy at a cost. *The Lancet Oncology,* 4, 760-768.

Colomban, P., Tournie, A., and Ricciardi, P. 2009. Raman spectroscopy of copper nanoparticle-containing glass matrices: Ancient red stained-glass windows. *Journal of Raman Spectroscopy,* 40, 1949-1955.

Cui, Y., Ren, B., Yao, J. L., Gu, R. A., and Tian, Z. Q. 2006. Synthesis of AgcoreAushell bimetallic nanoparticles for immunoassay based on surface-enhanced Raman spectroscopy. *The Journal of Physical Chemistry B,* 110, 4002-4006.

Cutts, S. M., Nudelman, A., Rephaeli, A., and Phillips, D. R. 2005. The power and potential of doxorubicin-DNA adducts. *IUBMB Life,* 57, 73-81.

Danhier, F., Feron, O., and Préat, V. 2010. To exploit the tumor microenvironment: passive and active tumor targeting of nanocarriers for anti-cancer drug delivery. *Journal of Controlled Release,* 148, 135-146.

Daniel, M. C., and Astruc, D. 2004. Gold nanoparticles: assembly, supramolecular chemistry, quantum-size-related properties, and applications toward biology, catalysis, and nanotechnology. *Chemical Reviews,* 104, 293-346.

Dasari, S., and Tchounwou, P. B. 2014. Cisplatin in cancer therapy: molecular mechanisms of action. *European Journal of Pharmacology,* 740, 364-378.

Dias, J. D., Liikanen, I., Guse, K., Foloppe, J., Sloniecka, M., Diaconu, I., Rantanen, V., Eriksson, M., Hakkarainen, T., and Lusky, M. 2010. Targeted chemotherapy for head

and neck cancer with a chimeric oncolytic adenovirus coding for bifunctional suicide protein FCU1. *Clinical Cancer Research,* 16, 2540-2549.

Durmus, S., Naik, J., Buil, L., Wagenaar, E., Tellingen, O., and Schinkel, A. H. 2014. *In vivo* disposition of doxorubicin is affected by mouse Oatp1a/1b and human OATP1A/1B transporters. *International Journal of Cancer,* 135, 1700-1710.

Eckhardt, S. 2002. Recent progress in the development of anticancer agents. *Current Medicinal Chemistry-Anti-Cancer Agents,* 2, 419-439.

Erathodiyil, N., and Ying, J. Y. 2011. Functionalization of inorganic nanoparticles for bioimaging applications. *Accounts of Chemical Research,* 44, 925-935.

Ernsting, M. J., Murakami, M., Roy, A., and Li, S.-D. 2013. Factors controlling the pharmacokinetics, biodistribution and intratumoral penetration of nanoparticles. *Journal of Controlled Release,* 172, 782-794.

Fageria, P., Uppala, S., Nazir, R., Gangopadhyay, S., Chang, C. H., Basu, M., and Pande, S. 2016. Synthesis of Monometallic (Au and Pd) and Bimetallic (AuPd) Nanoparticles Using Carbon Nitride (C3N4) Quantum Dots via the Photochemical Route for Nitrophenol Reduction. *Langmuir,* 32, 10054-10064.

Freitas, R. A. 2006. Pharmacytes: An ideal vehicle for targeted drug delivery. *Journal of Nanoscience and Nanotechnology,* 6, 2769-2775.

Gibson, N., Shenderova, O., Luo, T., Moseenkov, S., Bondar, V., Puzyr, A., Purtov, K., Fitzgerald, Z., and Brenner, D. 2009. Colloidal stability of modified nanodiamond particles. *Diamond and Related Materials,* 18, 620-626.

Gillies, R. J., Verduzco, D., and Gatenby, R. A. 2012. Evolutionary dynamics unifies carcinogenesis and cancer therapy. *Nature Reviews Cancer,* 12, 487-493.

Gomez, D. R., Estilo, C. L., Wolden, S. L., Zelefsky, M. J., Kraus, D. H., Wong, R. J., Shaha, A. R., Shah, J. P., Mechalakos, J. G., and Lee, N. Y. 2011. Correlation of osteoradionecrosis and dental events with dosimetric parameters in intensity-modulated radiation therapy for head-and-neck cancer. *International Journal of Radiation Oncology* Biology* Physics,* 81, e207-e213.

Grem, J. L. 2000. 5-Fluorouracil: forty-plus and still ticking. A review of its preclinical and clinical development. *Investigational New Drugs,* 18, 299-313.

Hanahan, D., and Weinberg, R. A. 2011. Hallmarks of cancer: the next generation. *Cell,* 144, 646-674.

Hashimoto, M., Kawai, K., Kawakami, H., and Imazato, S. 2016. Matrix metalloproteases inhibition and biocompatibility of gold and platinum nanoparticles. *Journal of Biomedical Materials Research Part A,* 104, 209-217.

Heidelberger, C., Chaudhuri, N., Danneberg, P., Mooren, D., Griesbach, L., Duschinsky, R., Schnitzer, R., Pleven, E., and Scheiner, J. 1957. Fluorinated pyrimidines, a new class of tumour-inhibitory compounds. *Nature,* 179, 663-666.

Honary, S., and Zahir, F. 2013. Effect of zeta potential on the properties of nano-drug delivery systems-a review (Part 1). *Tropical Journal of Pharmaceutical Research,* 12, 255-264.

Hsu, S. H., Whu, S. W., Tsai, C. L., Wu, Y. H., Chen, H. W., and Hsieh, K. H. 2004. Chitosan as scaffold materials: effects of molecular weight and degree of deacetylation. *Journal of Polymer Research,* 11, 141-147.

Hu, C. M. J., Aryal, S., and Zhang, L. 2010. Nanoparticle-assisted combination therapies for effective cancer treatment. *Therapeutic Delivery,* 1, 323-334.

Hua, S., Marks, E., Schneider, J. J., and Keely, S. 2015. Advances in oral nano-delivery systems for colon targeted drug delivery in inflammatory bowel disease: selective targeting to diseased versus healthy tissue. *Nanomedicine: Nanotechnology, Biology and Medicine,* 11, 1117-1132.

Huang, X., and El-Sayed, M. A. 2010. Gold nanoparticles: optical properties and implementations in cancer diagnosis and photothermal therapy. *Journal of Advanced Research,* 1, 13-28.

Huang, X., Tang, S., Zhang, H., Zhou, Z., and Zheng, N. 2009a. Controlled formation of concave tetrahedral/trigonal bipyramidal palladium nanocrystals. *Journal of the American Chemical Society,* 131, 13916-13917.

Huang, Y. F., Shangguan, D., Liu, H., Phillips, J. A., Zhang, X., Chen, Y., and Tan, W. 2009b. Molecular assembly of an aptamer-drug conjugate for targeted drug delivery to tumor cells. *ChemBioChem,* 10, 862-868.

Hudson, D., and Margaritis, A. 2014. Biopolymer nanoparticle production for controlled release of biopharmaceuticals. *Critical Reviews in Biotechnology,* 34, 161-179.

Hwang, B. J., Sarma, L. S., Chen, J. M., Chen, C. H., Shih, S. C., Wang, G. R., Liu, D. G., Lee, J. F., and Tang, M. T. 2005. Structural models and atomic distribution of bimetallic nanoparticles as investigated by X-ray absorption spectroscopy. *Journal of the American Chemical Society,* 127, 11140-11145.

Jiang, S. P., He, S. N., Li, Y. L., Feng, D. L., Lu, X. Y., Du, Y. Z., Yu, H. Y., Hu, F. Q., and Yuan, H. 2013. Preparation and characteristics of lipid nanoemulsion formulations loaded with doxorubicin. *International Journal of Nanomedicine,* 8, 3141-3150.

Karimi, M., Eslami, M., Sahandi-Zangabad, P., Mirab, F., Farajisafiloo, N., Shafaei, Z., Ghosh, D., Bozorgomid, M., Dashkhaneh, F., and Hamblin, M. R. 2016. pH-Sensitive stimulus-responsive nanocarriers for targeted delivery of therapeutic agents. *Wiley Interdisciplinary Reviews: Nanomedicine and Nanobiotechnology,* 8, 696-716.

Kean, T., and Thanou, M. 2010. Biodegradation, biodistribution and toxicity of chitosan. *Advanced drug delivery reviews,* 62, 3-11.

Keizer, H., Pinedo, H. M., Schuurhuis, G. J., and Joenje, H. 1990. Doxorubicin (adriamycin): a critical review of free radical-dependent mechanisms of cytotoxicity. *Pharmacology & therapeutics,* 47, 219-231.

Khalil, M., M. Mostafa, Y., and Torad, E. 2014. Biosynthesis and characterization of Pt and Au-Pt nanoparticles and their photo catalytic degradation of methylene blue. *International Journal of Advanced Research,* 2, 694-703.

Khan, Z., Al-Thabaiti, S. A., Obaid, A. Y., Khan, Z. A., and Al-Youbi, A. A. 2012. Shape-directing role of cetyltrimethylammonium bromide in the preparation of silver nanoparticles. *Journal of Colloid and Interface Science,* 367, 101-108.

Koshkaryev, A., Sawant, R., Deshpande, M., and Torchilin, V. 2013. Immunoconjugates and long circulating systems: origins, current state of the art and future directions. *Advanced Drug Delivery Reviews,* 65, 24-35.

Kostrzewa-Nowak, D., Paine, M., Wolf, C., and Tarasiuk, J. 2005. The role of bioreductive activation of doxorubicin in cytotoxic activity against leukaemia HL60-sensitive cell line and its multidrug-resistant sublines. *The British Journal of Cancer,* 93, 89-97.

Lammers, T., Kiessling, F., Hennink, W. E., and Storm, G. 2010. Nanotheranostics and image-guided drug delivery: current concepts and future directions. *Molecular Pharmaceutics,* 7, 1899-1912.

Lim, B., Wang, J., Camargo, P. H., Jiang, M., Kim, M. J., and Xia, Y. 2008. Facile synthesis of bimetallic nanoplates consisting of Pd cores and Pt shells through seeded epitaxial growth. *Nano Letters,* 8, 2535-2540.

Liu, M., Jiang, L., and Guan, X. Y. 2014. The genetic and epigenetic alterations in human hepatocellular carcinoma: a recent update. *Protein & Cell,* 5, 673-691.

Liu, X., Zhang, X., Zhu, M., Lin, G., Liu, J., Zhou, Z., Tian, X., and Pan, Y. 2016. PEGylated Au@ Pt nanodendrites as novel theranostic agents for computed tomography imaging and photothermal/radiation synergistic therapy. *ACS Applied Materials & Interfaces,* 9, 279-285.

Lohse, I., Rasowski, J., Cao, P., Pintilie, M., Do, T., Tsao, M.-S., Hill, R. P., and Hedley, D. W. 2016. Targeting hypoxic microenvironment of pancreatic xenografts with the hypoxia-activated prodrug TH-302. *Oncotarget,* 7, 33571-33580.

Longley, D. B., Harkin, D. P., and Johnston, P. G. 2003. 5-fluorouracil: mechanisms of action and clinical strategies. *Nature Reviews Cancer,* 3, 330-338.

Longmire, M., Choyke, P. L., and Kobayashi, H. 2008. Clearance properties of nano-sized particles and molecules as imaging agents: considerations and caveats. *Nanomedicine,* 3, 703-717.

Lukong, K. E. 2017. Understanding breast cancer-The long and winding road. *BBA Clinical,* 7, 64-77.

Luz, C. M., Boyles, M. S. P., Falagan-Lotsch, P., Pereira, M. R., Tutumi, H. R., Santos, E. O., Martins, N. B., Himly, M., Sommer, A., and Foissner, I. 2017. Poly-lactic acid nanoparticles (PLA-NP) promote physiological modifications in lung epithelial cells and are internalized by clathrin-coated pits and lipid rafts. *Journal of Nanobiotechnology,* 15, 11-26.

Ma, J., Sun, S., Wang, T., and Chen, K. 2015. Discovery of hard-magnetic domains in two-dimensional arrays of soft-magnetic Fe_3O_4 nanocubes. *Journal of Applied Physics,* 118, 073901.

Ma, T., Zhu, Z. G., Ji, Y.-B., Zhang, Y., Yu, Y. Y., Liu, B. Y., Yin, H. R., and Lin, Y. Z. 2004. Correlation of thymidylate synthase, thymidine phosphorylase and dihydropyrimidine dehydrogenase with sensitivity of gastrointestinal cancer cells to 5-fluorouracil and 5-fluoro-2'-deoxyuridine. *World Journal of Gastroenterology,* 10, 172-176.

Ma, Y., and Balbuena, P. B. 2008. Pt surface segregation in bimetallic Pt 3 M alloys: a density functional theory study. *Surface Science,* 602, 107-113.

Malam, Y., Loizidou, M., and Seifalian, A. M. 2009. Liposomes and nanoparticles: nanosized vehicles for drug delivery in cancer. *Trends in Pharmacological Sciences,* 30, 592-599.

Mao, Z., Zhou, X., and Gao, C. 2013. Influence of structure and properties of colloidal biomaterials on cellular uptake and cell functions. *Biomaterials Science,* 1, 896-911.

Marques, L., Hernandez, F., James, S. W., Morgan, S., Clark, M., Tatam, R. P., and Korposh, S. 2016. Highly sensitive optical fibre long period grating biosensor anchored with silica core gold shell nanoparticles. *Biosensors and Bioelectronics,* 75, 222-231.

Masarudin, M. J., Cutts, S. M., Evison, B. J., Phillips, D. R., and Pigram, P. J. 2015. Factors determining the stability, size distribution, and cellular accumulation of small, monodisperse chitosan nanoparticles as candidate vectors for anticancer drug delivery: application to the passive encapsulation of [14C]-doxorubicin. *Nanotechnology, Science and Applications,* 8, 67-80.

Misra, R., Acharya, S., and Sahoo, S. K. 2010. Cancer nanotechnology: application of nanotechnology in cancer therapy. *Drug Discovery Today,* 15, 842-850.

Mizukoshi, Y., Okitsu, K., Maeda, Y., Yamamoto, T. A., Oshima, R., and Nagata, Y. 1997. Sonochemical preparation of bimetallic nanoparticles of gold/palladium in aqueous solution. *The Journal of Physical Chemistry B,* 101, 7033-7037.

Mortazavi, S., and Smart, J. 1995. An investigation of some factors influencing the *in vitro* assessment of mucoadhesion. *International Journal of Pharmaceutics,* 116, 223-230.

Munir, Z., Anselmi-Tamburini, U., and Ohyanagi, M. 2006. The effect of electric field and pressure on the synthesis and consolidation of materials: a review of the spark plasma sintering method. *Journal of Materials Science,* 41, 763-777.

Nakamura, T., Herbani, Y., and Sato, S. 2012. Fabrication of solid-solution gold-platinum nanoparticles with controllable compositions by high-intensity laser irradiation of solution. *Journal of Nanoparticle Research,* 14, 785.

Narayanan, K. B., and Sakthivel, N. 2010. Biological synthesis of metal nanoparticles by microbes. *Advances in Colloid and Interface Science,* 156, 1-13.

Nasrabadi, H. T., Abbasi, E., Davaran, S., Kouhi, M., and Akbarzadeh, A. 2016. Bimetallic nanoparticles: Preparation, properties, and biomedical applications. *Artificial cells, Nanomedicine, and Biotechnology,* 44, 376-380.

Nejdl, L., Kudr, J., Moulick, A., Hegerova, D., Ruttkay-Nedecky, B., Gumulec, J., Cihalova, K., Smerkova, K., Dostalova, S., and Krizkova, S. 2017. Platinum nanoparticles induce damage to DNA and inhibit DNA replication. *PLOS One,* 12, e0180798.

Nitiss, J. L. 2009. Targeting DNA topoisomerase II in cancer chemotherapy. *Nature Reviews Cancer,* 9, 338.

Odes, E. J., Randolph-Quinney, P. S., Steyn, M., Throckmorton, Z., Smilg, J. S., Zipfel, B., Augustine, T. N., De Beer, F., Hoffman, J. W., and Franklin, R. D. 2016. Earliest hominin cancer: 1.7-million-year-old osteosarcoma from Swartkrans Cave, South Africa. *South African Journal of Science,* 112, 1-5.

Osborne, C., Wilson, P., and Tripathy, D. 2004. Oncogenes and tumor suppressor genes in breast cancer: potential diagnostic and therapeutic applications. *The Oncologist,* 9, 361-377.

Pannerec-Varna, M., Ratajczak, P., Bousquet, G., Ferreira, I., Leboeuf, C., Boisgard, R., Gapihan, G., Verine, J., Palpant, B., and Bossy, E. 2013. *In vivo* uptake and cellular distribution of gold nanoshells in a preclinical model of xenografted human renal cancer. *Gold Bulletin,* 46, 257-265.

Papasani, M. R., Wang, G., and Hill, R. A. 2012. Gold nanoparticles: the importance of physiological principles to devise strategies for targeted drug delivery. *Nanomedicine: Nanotechnology, Biology and Medicine,* 8, 804-814.

Parker, B. S., Buley, T., Evison, B. J., Cutts, S. M., Neumann, G. M., Iskander, M. N., and Phillips, D. R. 2004. A Molecular Understanding of Mitoxantrone-DNA Adduct Formation Effect of Cytosine Methylation And Flanking Sequences. *Journal of Biological Chemistry,* 279, 18814-18823.

Parveen, S., Misra, R., and Sahoo, S. K. 2012. Nanoparticles: a boon to drug delivery, therapeutics, diagnostics and imaging. *Nanomedicine: Nanotechnology, Biology and Medicine,* 8, 147-166.

Paul, W., and Sharma, C. 2011. Blood compatibility studies of Swarna bhasma (gold bhasma), an Ayurvedic drug. *International Journal of Ayurveda Research,* 2, 14.

Pawłowska, J., Tarasiuk, J., Wolf, C. R., Paine, M. J., and Borowski, E. 2003. Differential ability of cytostatics from anthraquinone group to generate free radicals in three enzymatic systems: NADH dehydrogenase, NADPH cytochrome P450 reductase, and xanthine oxidase. *Oncology Research Featuring Preclinical and Clinical Cancer Therapeutics,* 13, 245-252.

Peer, D., Karp, J. M., Hong, S., Farokhzad, O. C., Margalit, R., and Langer, R. 2007. Nanocarriers as an emerging platform for cancer therapy. *Nature Nanotechnology,* 2, 751-760.

Peng, Z., and Yang, H. 2009. PtAu bimetallic heteronanostructures made by post-synthesis modification of Pt-on-Au nanoparticles. *Nano Research,* 2, 406-415.

Pérez-Herrero, E., and Fernández-Medarde, A. 2015. Advanced targeted therapies in cancer: drug nanocarriers, the future of chemotherapy. *European Journal of Pharmaceutics and Biopharmaceutics,* 93, 52-79.

Pissuwan, D., Niidome, T., and Cortie, M. B. 2011. The forthcoming applications of gold nanoparticles in drug and gene delivery systems. *Journal of controlled release,* 149, 65-71.

Ragelle, H., Danhier, F., Préat, V., Langer, R., and Anderson, D. G. 2017. Nanoparticle-based drug delivery systems: a commercial and regulatory outlook as the field matures. *Expert Opinion on Drug Delivery,* 14, 851-864.

Roco, M. C. 2003. Nanotechnology: convergence with modern biology and medicine. *Current Opinion in Biotechnology,* 14, 337-346.

Rodríguez-González, B., Burrows, A., Watanabe, M., Kiely, C. J., and Marzán, L. M. L. 2005. Multishell bimetallic AuAg nanoparticles: synthesis, structure and optical properties. *Journal of Materials Chemistry,* 15, 1755-1759.

Rosenblum, D., and Peer, D. 2014. Omics-based nanomedicine: the future of personalized oncology. *Cancer Letters,* 352, 126-136.

Ross, C. R., Brennan-Laun, S. E., and Wilson, G. M. 2012. Tristetraprolin: Roles in Cancer and Senescence. *Ageing Research Reviews,* 11, 473-484.

Sagar, L. K., Walravens, W., Zhao, Q., Vantomme, A., Geiregat, P., and Hens, Z. 2016. PbS/CdS Core/Shell Quantum Dots by Additive, Layer-by-Layer Shell Growth. *Chemistry of Materials,* 28, 6953-6959.

Sakhrani, N. M., and Padh, H. 2013. Organelle targeting: third level of drug targeting. *Drug Design, Development and Therapy,* 7, 585-599.

Samadian, H., Hosseini-Nami, S., Kamrava, S. K., Ghaznavi, H., and Shakeri-Zadeh, A. 2016. Folate-conjugated gold nanoparticle as a new nanoplatform for targeted cancer therapy. *Journal of Cancer Research and Clinical Oncology,* 142, 2217-2229.

Savage, P., Stebbing, J., Bower, M., and Crook, T. 2009. Why does cytotoxic chemotherapy cure only some cancers? *Nature Reviews Clinical Oncology,* 6, 43-52.

Scholz, O. A., Wolff, A., Schumacher, A., Giannola, L. I., Campisi, G., Ciach, T., and Velten, T. 2008. Drug delivery from the oral cavity: focus on a novel mechatronic delivery device. *Drug Discovery Today,* 13, 247-253.

Shevchenko, E. V., Talapin, D. V., Kotov, N. A., O'brien, S., and Murray, C. B. 2006. Structural diversity in binary nanoparticle superlattices. *Nature,* 439, 55-59.

Shim, B. Y., Lee, K. M., Cho, H. M., Kim, H. J., Cho, H. J., Yang, J., Kim, J. G., and Kim, H. K. 2005. Oxaliplatin/5-FU without Leucovorin Chemotherapy in Metastatic Colorectal Cancer. *Cancer Research and Treatment : Official Journal of Korean Cancer Association,* 37, 212-215.

Shukla, S. K., Mishra, A. K., Arotiba, O. A., and Mamba, B. B. 2013. Chitosan-based nanomaterials: A state-of-the-art review. *International Journal of Biological Macromolecules,* 59, 46-58.

Siegel, R. L., Miller, K. D., and Jemal, A. 2017. Cancer statistics, 2017. *CA: A Cancer Journal for Clinicians,* 67, 7-30.

Singh, R., and Lillard, J. W. 2009. Nanoparticle-based targeted drug delivery. *Experimental and Molecular Pathology,* 86, 215-223.

Singla, A., and Chawla, M. 2001. Chitosan: Some pharmaceutical and biological aspects-an update. *Journal of Pharmacy and Pharmacology,* 53, 1047-1067.

Sinha, B., and Mason, R. 2015. Is Metabolic Activation of Topoisomerase II Poisons Important In The Mechanism Of Cytotoxicity. *Journal of Drug Metabolism & Toxicology,* 6, 2-8.

Sounderya, N., and Zhang, Y. 2008. Use of core/shell structured nanoparticles for biomedical applications. *Recent Patents on Biomedical Engineering,* 1, 34-42.

Spano, D., Heck, C., De Antonellis, P., Christofori, G., and Zollo, M. 2012. Molecular networks that regulate cancer metastasis. *Seminars in Cancer Biology,* 22, 234-249.

Sun, T., Zhang, Y. S., Pang, B., Hyun, D. C., Yang, M., and Xia, Y. 2014. Engineered nanoparticles for drug delivery in cancer therapy. *Angewandte Chemie International Edition,* 53, 12320-12364.

Sutradhar, K. B., and Amin, M. L. 2014. Nanotechnology in cancer drug delivery and selective targeting. *ISRN Nanotechnology,* 2014, 1-12.

Swift, L. P., Rephaeli, A., Nudelman, A., Phillips, D. R., and Cutts, S. M. 2006. Doxorubicin-DNA adducts induce a non-topoisomerase II-mediated form of cell death. *Cancer Research,* 66, 4863-4871.

Szymańska, E., and Winnicka, K. 2015. Stability of chitosan-a challenge for pharmaceutical and biomedical applications. *Marine drugs,* 13, 1819-1846.

Taggart, L., Mcmahon, S., Butterworth, K., Currell, F., Schettino, G., and Prise, K. 2016. Protein disulphide isomerase as a target for nanoparticle-mediated sensitisation of cancer cells to radiation. *Nanotechnology,* 27, 215101.

Tan, M. L., Choong, P. F., and Dass, C. R. 2009. Doxorubicin delivery systems based on chitosan for cancer therapy. *Journal of Pharmacy and Pharmacology,* 61, 131-142.

Thanh, N. T., and Green, L. A. 2010. Functionalisation of nanoparticles for biomedical applications. *Nano Today,* 5, 213-230.

Thorn, C. F., Marsh, S., Carrillo, M. W., Mcleod, H. L., Klein, T. E., and Altman, R. B. 2011. PharmGKB summary: fluoropyrimidine pathways. *Pharmacogenetics and Genomics,* 21, 237-242.

Tokarska-Schlattner, M., Zaugg, M., Zuppinger, C., Wallimann, T., and Schlattner, U. 2006. New insights into doxorubicin-induced cardiotoxicity: the critical role of cellular energetics. *Journal of Molecular and Cellular Cardiology,* 41, 389-405.

Toshima, N., and Yonezawa, T. 1998. Bimetallic nanoparticles-novel materials for chemical and physical applications. *New Journal of Chemistry,* 22, 1179-1201.

Toshima, N., Yonezawa, T., Harada, M., Asakura, K., and Iwasawa, Y. 1990. The polymer-protected Pd-Pt bimetallic clusters having catalytic activity for selective hydrogenation of diene. Preparation and EXAFS investigation on the structure. *Chemistry Letters,* 19, 815-818.

Ungureanu, C., Kroes, R., Petersen, W., Groothuis, T. A., Ungureanu, F., Janssen, H., Van Leeuwen, F. W., Kooyman, R. P., Manohar, S., and Van Leeuwen, T. G. 2011. Light interactions with gold nanorods and cells: implications for photothermal nanotherapeutics. *Nano Letters,* 11, 1887-1894.

Varkouhi, A. K., Scholte, M., Storm, G., and Haisma, H. J. 2011. Endosomal escape pathways for delivery of biologicals. *Journal of Controlled Release,* 151, 220-228.

Verma, R. K., and Garg, S. 2001. Drug delivery technologies and future directions. *Pharmaceutical Technology,* 25, 1-14.

Von Roemeling, C., Jiang, W., Chan, C. K., Weissman, I. L., and Kim, B. Y. 2017. Breaking down the barriers to precision cancer nanomedicine. *Trends in Biotechnology,* 35, 159-171.

Wakaskar, R. R. 2017. Passive and Active Targeting in Tumor Microenvironment. *International Journal of Drug Development and Research,* 9, 37-41.

Wicki, A., Witzigmann, D., Balasubramanian, V., and Huwyler, J. 2015. Nanomedicine in cancer therapy: challenges, opportunities, and clinical applications. *Journal of Controlled Release,* 200, 138-157.

Wiley, B. J., Im, S. H., Li, Z. Y., Mclellan, J., Siekkinen, A., and Xia, Y. 2006. Maneuvering the surface plasmon resonance of silver nanostructures through shape-controlled synthesis. *The Journal of Physical Chemistry B,* 110, 15666-15675.

Wu, H., Wang, P., He, H., and Jin, Y. 2012a. Controlled synthesis of porous Ag/Au bimetallic hollow nanoshells with tunable plasmonic and catalytic properties. *Nano Research,* 5, 135-144.

Wu, P., Gao, Y., Zhang, H., and Cai, C. 2012b. Aptamer-guided silver-gold bimetallic nanostructures with highly active surface-enhanced raman scattering for specific detection and near-infrared photothermal therapy of human breast cancer cells. *Analytical Chemistry,* 84, 7692-7699.

Yamada, M., Foote, M., and Prow, T. W. 2015. Therapeutic gold, silver, and platinum nanoparticles. *Wiley Interdisciplinary Reviews: Nanomedicine and Nanobiotechnology,* 7, 428-445.

Yang, C. Y., Chen, S. M., Palanisamy, S., Thirumalraj, B., and Liu, X. 2016a. Electrochemical synthesis of PtAu bimetallic nanoparticles on multiwalled carbon nanotubes and

application for amperometric determination of nitrite. *International Journal of Electrochemical Science,* 11, 4027-4036.

Yang, G., Zhou, Y., Pan, H. B., Zhu, C., Fu, S., Wai, C. M., Du, D., Zhu, J. J., and Lin, Y. 2016b. Ultrasonic-assisted synthesis of Pd-Pt/carbon nanotubes nanocomposites for enhanced electro-oxidation of ethanol and methanol in alkaline medium. *Ultrasonics Sonochemistry,* 28, 192-198.

Yin, Y., Chen, D., Qiao, M., Lu, Z., and Hu, H. 2006. Preparation and evaluation of lectin-conjugated PLGA nanoparticles for oral delivery of thymopentin. *Journal of Controlled Release,* 116, 337-345.

Zaleska-Medynska, A., Marchelek, M., Diak, M., and Grabowska, E. 2016. Noble metal-based bimetallic nanoparticles: the effect of the structure on the optical, catalytic and photocatalytic properties. *Advances in Colloid and Interface Science,* 229, 80-107.

Zhang, H., and Toshima, N. 2013. Synthesis of Au/Pt bimetallic nanoparticles with a Pt-rich shell and their high catalytic activities for aerobic glucose oxidation. *Journal of Colloid and Interface Science,* 394, 166-176.

Zhao, P., Wu, S., Cheng, Y., You, J., Chen, Y., Li, M., He, C., Zhang, X., Yang, T., and Lu, Y. 2017. MiR-375 Delivered by Lipid-coated Doxorubicin-Calcium Carbonate Nanoparticles Overcomes Chemoresistance in Hepatocellular Carcinoma. *Nanomedicine: Nanotechnology, Biology and Medicine,* 13, 2507-2516.

Zhao, Z., Zhang, M., Chen, X., Li, Y., and Wang, J. 2015. Electrochemical co-reduction synthesis of aupt bimetallic nanoparticles-graphene nanocomposites for selective detection of dopamine in the presence of ascorbic acid and uric acid. *Sensors,* 15, 16614-16631.

Zhong, Y., Meng, F., Deng, C., and Zhong, Z. 2014. Ligand-directed active tumor-targeting polymeric nanoparticles for cancer chemotherapy. *Biomacromolecules,* 15, 1955-1969.

Zhu, S., Pabla, N., Tang, C., He, L., and Dong, Z. 2015. DNA damage response in cisplatin-induced nephrotoxicity. *Archives of Toxicology,* 89, 2197-2205.

CHAPTER THREE

AN *IN VITRO* ASSESSMENT OF NOVEL CHITOSAN/ BIMETALLIC PtAu NANOCOMPOSITES AS DELIVERY VEHICLES FOR DOXORUBICIN

Published in Nanomedicine

Maney, V. and Singh,M*. (2017). An *in vitro* assessment of novel chitosan/ bimetallic PtAu nanocomposites as delivery vehicles for doxorubicin". Nanomedicine.12(22): 2625-2640. DOI: 10.2217/nnm-2017-0024. ***Impact factor = 4.727.***

Abstract

Modern bimetallic nanostructures have recently garnered widespread attention as potential carriers for therapeutic payloads due to their extraordinary chemical, biological, optical, surface and mechanical properties. Cancer is a tremendous burden to health care systems and requires innovative strategies to safely ferry encapsulated therapeutic agents to a pathological site against tedious biological barriers. In this study, platinum (core)-gold (shell) bimetallic nanoparticles was synthesised and functionalised with chitosan and doxorubicin (DOX) to display favourable pharmacokinetics, biodegradability, biological activity and safety *in vitro*. All PtAuBNps and their drug nanocomposites were morphologically and physicochemically characterised through UV-Vis spectroscopy, TEM, ATR-FTIR and NTA. Binding studies were performed to determine the efficiency and bio-adhesiveness of platforms. *In vitro* release kinetics were evaluated under simulated environments, cytotoxicity profiles through MTT and SRB assays and apoptosis induction using the dual EtBr/AO staining. The results obtained indicate that functionalised PtAuBNps displayed favourable physiochemical attributes such as small size (<150 nm), excellent colloidal stability (>24 mV) and high binding capabilities (≥ 10% loading content and 70% encapsulation efficiency), pH-triggered drug release through zero-order release kinetics and cell specific cytotoxicity (≤ 50 % cell death recorded in all cancerous cell lines). Overall the positive attributes of this novel delivery system bodes well for future *in vivo* studies.

Keywords: bimetallic nanoparticles, gold, platinum, cancer, cytotoxicity, doxorubicin

3.1. Introduction

The use of nanosized materials has become increasingly popular in diverse nanomedical fields as biosensors, drug delivery systems, imaging and tracking agents (Daraee *et al.*, 2016, Thanh and Green, 2010). The arsenal of nanoparticles used in cancer therapeutics includes liposomes, metal and polymeric nanoparticles, polymeric micelles, dendrimers, nanocantilevers, carbon nanotubes and quantum dots (Misra *et al.*, 2010). Nanoscale materials are expected to revolutionise cancer therapy through advances in early detection, diagnosis and treatment. Drug loaded nanoparticles (10-200 nm in diameter) offer the prospects of site-specific delivery, improved potency of bound therapeutic agents, improved delivery of infective drugs, prevention of early degradation, and the ability to overcome multidrug resistance (Anselmo and Mitragotri, 2014, Mousa and Bharali, 2011, Robert *et al.*, 1985, Singh and Lillard, 2009). Moreover, nanoparticle drug delivery vehicles can penetrate various biological barriers including the tumour vasculature and the mucosal membrane, and may further facilitate transport across the blood brain barrier (von Roemeling *et al.*, 2017, Yin *et al.*, 2006).

To date, doxorubicin (DOX) is one of the most potent anticancer drug available and exhibits a broad spectrum of activity towards nearly all human cancers (González-Fernández *et al.*, 2017). The antineoplastic activity of DOX is mainly believed to be attributed to DOX acting as a topoisomerase II poison, DNA cross-linking, mitochondrial dysfunction, generation of free radicals and induction of apoptosis (Green and Leeuwenburgh, 2002, Yang *et al.*, 2014). DOX administration has been known to induce life threatening side effects including cardiotoxicity, myelosuppression and mucositis (Kamba *et al.*, 2013). The unendurable toxicity caused due to the accumulation of DOX within healthy organs can lead to patient fatality rather than from the disease itself.

With the hope to ameliorate these potent side effects, nano-platforms synthesised of noble metals (Au and Pt) were preferred owing to their physiochemical, biological and photonic properties. The use of gold nanoparticles (AuNps) as drug delivery agents is the most prominent in literature, since they are inert, non-toxic, easily synthesised and amenable to surface functionalisation with targeting molecules (Dhamecha *et al.*, 2015). Platinum nanoparticles (PtNps) share similar chemical, physical and optical properties, however unlike AuNps, the emergence of PtNps for therapeutic purposes is recent. Topical platinum-based chemotherapeutic drugs (cisplatin and derivatives) are known to kill cancer cells through

inducing DNA damage resulting in apoptosis (Vigderman and Zubarev, 2013, Yamada *et al.*, 2015). It is believed that the use of PtNps will serve as a reservoir for generating platinum ions, and will have the same mode of action as platinum based drugs (Yamada *et al.*, 2015). In addition, PtNps are potent antioxidants that quench free radical production when oxidative stress levels are high (Khalil *et al.*, 2014). The synthesis of bimetallic nanoparticles using these two physicochemically favourable metals, would incorporate their individual metal properties as well as any novel properties obtained through synergistic effects between the two metals. Typically, these hybrid nanostructures boast higher surface porosity, enhanced chemical, physical, electronic and optic properties compared to monometallic systems which have propelled their applications as delivery vectors and theranostic agents (Dutta *et al.*, 2016, Feng *et al.*, 2016).

Chitosan (CS) being non-toxic, biocompatible and bioadhesive is an attractive excipient for use in nanomedical drug formulations (Singla and Chawla, 2001). CS is a cationic polymer that has amino groups capable of interacting with the negatively charged glycoproteins of the mucosal layer. CS has penetration enhancement properties by facilitating drug transport through the tight junctions of the epithelial layer, and protecting the encapsulated drug from degradation by lumen enzymes of the gastrointestinal tract (Kamba *et al.*, 2013, Szymańska and Winnicka, 2015). In addition, CS provides amine (NH_2) and hydroxyl groups (OH) for binding to drugs, as well as to enable site-specific targeting (Nivethaa *et al.*, 2015). The latter is due to chitosan's amine groups that have a pKa of 6.2 at acidic pH, which mimics that of tumour cells, allowing the CS nanocomposites to interact favourably with the cell membrane (Suarato *et al.*, 2016). It is anticipated that the combination of pH-triggered release, as well as good bioadhesiveness, will facilitate the uptake of active DOX through the mucosal membrane, improving the absorption of DOX, prolonging its' residence time at the application site, and improving the biological efficacy after local administration

Chitosan nanoparticles prepared by the ionic gelation method using non-toxic TPP has been reported to encapsulate many anticancer drugs such as doxorubicin and 5-fluorouracil (Masarudin *et al.*, 2015, Nivethaa *et al.*, 2015). Due to DOX being hydrophilic and cationic, high encapsulation within the PtAuCS nanocomposite occurs when DOX is pre-complexed to anionic TPP (Masarudin *et al.*, 2015). Essentially, TPP acts as a cross-linker between the ionic cross-links of the tertiary amines of DOX and CS (Yang *et al.*, 2017). The objectives of the present work were to (1) synthesise Pt(shell)-Au(Core) bimetallic nanoparticles, (2) to create novel chitosan/PtAu nanoconjugates through ionic gelation with TPP and determine drug

encapsulation efficiency, (3) to fully characterise the BNps with respect to it's particle size, zeta (ζ) potential, ultrastructural morphology using TEM and chemical composition using UV spectroscopy and FTIR, (4) to investigate drug release kinetics under various simulated conditions, and, (5) to assess *in vitro* cytotoxicity and apoptosis. Figure 3.1, schematically represents the research undertakings.

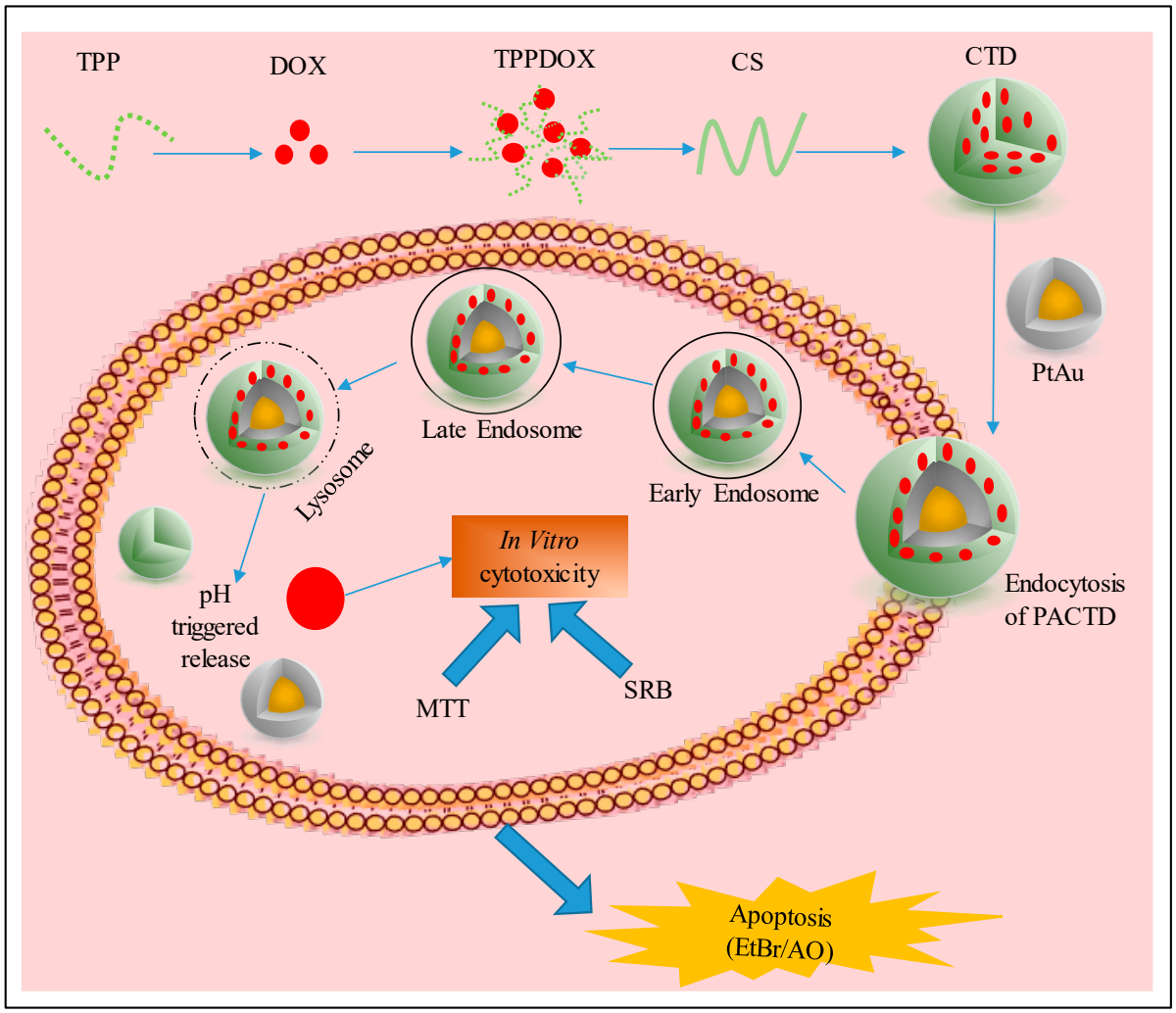

Figure 3.1: Schematic illustration of doxorubicin encapsulated platinum-gold/chitosan bimetallic nanoparticles for sustained pH-responsive release leading to site-specific *in vitro* biological activity and apoptosis.

3.2. Methods and materials

3.2.1. Materials

Hydrogen hexachloroplatinate (IV) hexahydrate ($H_2PtCl_6.6H_2O$, 517.90 g mol^{-1}), gold (III) chloride trihydrate ($HAuCL_4.3H_2O$, Mw: 393.83 g mol^{-1}), polyvinylpyrrolidone (PVP, Mw 40,000), sodium borohydride ($NaBH_4$, Mw 37.83 g mol^{-1}), sodium triphosphate ($Na_5P_3O_{10}$, Mw: 367.86 g mol^{-1}), Sulforodhamine B (SRB Dye, $C_{27}H_{30}N_2O_7S_2$, Mw: 558.67 g mol^{-1}), Doxorubicin hydrochloride (DOX, $C_{27}H_{29}NO_{11}$. HCl, Mw: 579.98 g mol^{-1}), acridine orange hemi (zinc chloride) salt [3,6-Bis(dimethylamino) acridine hydrochloride zinc chloride double salt] ($C_{17}H_{19}N_3$, Mw: 265.36, g mol^{-1}), chitosan (75% deacetylation) and dialysis tubing (MWCO= 12000 Daltons) was purchased from Sigma-Aldrich (St. Louis, USA). Ethidium bromide, glacial acetic acid, dimethyl sulfoxide [DMSO], 3- [(4,5-dimethylthiazol-2-yl)-2,5-diphenyl-2H-tetrazolium bromide] (MTT) and phosphate buffered saline tablets [PBS, (140 mM NaCl, 10 mM phosphate buffer, 3 mM KCl)] were sourced from Merck (Darmstadt, Germany). Eagle's Minimum Essential Medium (EMEM) along with L-glutamine (4.5gL^{-1}), trypsin-versene-EDTA and antibiotic mixture [(penicillin (10000 U/mL) streptomycin (10000 µg/mL), amphotericin B (25 µg/mL)] were purchased from Lonza Bio-Whittaker (Verviers, Belgium). Sterile foetal bovine serum (FBS) was purchased from Hyclone GE Healthcare (Utah, USA). Human embryonic kidney cells (HEK293), breast adenocarcinoma (MCF-7), epithelial colorectal adenocarcinoma cells (Caco-2), and hepatocellular carcinoma cells (HepG2) was obtained from the ATCC (Pty) Ltd, Manassas, Virginia, USA. All sterile tissue culture plasticware were obtained from Corning Inc., (New York, USA). All chemical reagents were of analytical quality and were used without further purification. Ultrapure (18 MOhm) water (milli-Q50, Millipore, France) was used throughout.

3.2.2. Preparation of bimetallic $Pt_{50}Au_{50}$ nanoparticles (PtAuBNps)

Bimetallic nanoparticles with platinum shell gold core were prepared using PVP as a protecting agent, followed by rapid injection of $NaBH_4$ (Zhang and Toshima, 2013). Briefly, to 25 mL of $HAuCl_4.4H_2O$ (0.44 mM) was added approximately 50 mL of PVP (0.44 mM) with gentle stirring at 0°C for 15 min. Thereafter, the solution was mixed with $H_2PtCl_6.6H_2O$ (25 mL, 0.44 mM) and stirred for a further 30 min at 0°C. Subsequently, $NaBH_4$ (6.67 mL, 16.5 mM, 0°C), was rapidly injected into the above-mentioned solution under vigorous stirring,

until a brownish colloidal dispersion was formed. The final concentration of prepared PtAuBNps was 0.18 mg/mL.

3.2.3. Preparation of nanocomposites

To 1 mM DOX-HCL solution (in 18 Mohm water) was added 0.35 mg/mL TPP solution (pH 2.0) in a 1:1 ratio ($^{v}/_{v}$). The DOX-TPP solution was stirred for 30 min and the complex allowed to settle for 10 min. Thereafter, 3 mL chitosan (CS) (0.25 mg/mL, pH 4.0) followed by PtAuBNps (0.18 mg/mL) were added dropwise with constant stirring for 2 h, and then subjected to centrifugation at 2.1×10^3 rpm for 15 min at 10°C. The supernatant containing unbound drug, CS and TPP was discarded, and the pellet resuspended in 1 mL ultrapure water. The final ratio of the nanocomposite PtAu-CS-TPP-DOX (PACTD) was 1:3:1:1 ($^{v}/_{v}$). Similarly, the nanocomposite CS-TPP-DOX (CTD), used as an encapsulation control, was prepared by initially complexing DOX with TPP, followed by dropwise addition of CS. The final selective ratio of the nanocomposite CS-TPP-DOX was 3:1:1 ($^{v}/_{v}$). The theoretical DOX concentrations are reflected in Table 3.3.

3.2.4. UV-Vis spectroscopy

The conformation of polymer binding and drug entrapment by the PtAuBNps was evaluated using the absorption spectra of the individual samples against known literature. Approximately 10 µL of each sample was analysed over a wavelength range of 200-800 nm using a UV-Vis spectrophotometer (Nanodrop oneC, Thermo-Fischer Scientific Inc., Waltham, Massachusetts, USA).

3.2.5. ATR-FTIR

ATR-FTIR is an appropriate technique to identify functional groups bound to the surface of the nanoparticle and characterise carrier-drug interactions. Sample analysis was performed on a Perkin Elmer spectrum 100 FTIR spectrometer fitted with a universal ATR accessory (diamond crystal) in the wave number range of 400-4000 cm^{-1} at a 1 cm^{-1} resolution. The spectra requisition was carried out using the Spectrum 10 analysis software (Perkin Elmer).

3.2.6. TEM

The ultrastructural morphology of the bimetallic nano-suspensions was analysed using TEM (Jeol JEM 1010, Tokyo, Japan, operating at 100 kV). Briefly, one drop of nanoparticle/nanoconjugate suspension was placed onto carbon coated copper grids and air dried at room temperature, prior to obtaining images. Images were captured using the iTEM Soft Imaging Systems (SIS) Megaview III fitted with a side-mounted 3-megapixel digital camera.

3.2.7. Nanoparticle tracking analysis (NTA)

Size, particle distribution, ζ potential and stability was determined using NTA (Nanosight NS500; Malvern Instruments, Worcestershire, UK). All PtAuBNps and their nanocomplexes were diluted 1:1000 in ultrapure water, and 1 mL of each sample was evaluated, after the instrument was primed, flushed and the camera zero position set. All samples were run in triplicates. The Stokes-Einstein equation was used to determine particle size distribution based on tracking the trajectories of particles in Brownian motion within the laser scatter volume. zeta potentials were calculated from the mean electrophoretic mobility using Smoluchowski approximation based on Laser-Doppler microelectrophoresis. All measurements were performed at 25°C and 24V.

3.2.8. Encapsulation efficiency

The encapsulation efficiency (%) of DOX in the nanoconjugates was determined by separating unbound DOX by centrifugation at 2.1×10^3 rpm for 15 min at 10°C (Beckman Ultracentrifuge). Analysis of DOX content present in samples was determined by UV-Vis spectroscopy (Nanodrop oneC, Thermo-Fischer Scientific Inc., Waltham, Massachusetts, USA) at a wavelength 481 nm. All the samples were measured in triplicates. The theoretical drug content (TDC), entrapment efficiency (EE), actual drug content and loading capacity (LC) were calculated using Equations (3.1-3.4).

$$\text{TDC } (\mu g) = \frac{\text{Weight of DOX}}{\text{Weight of nanocomposite}} \tag{3.1}$$

$$\text{EE (\%)} = \frac{\text{Total DOX added - Free DOX}}{\text{Total DOX added}} \times 100 \quad (3.2)$$

$$\text{ADC (μg)} = \text{TDC} \times \text{EE (\%)} \quad (3.3)$$

$$\text{LC (\%)} = \frac{\text{Total DOX added - Free DOX}}{\text{weight of nanocomposite}} \times 100 \quad (3.4)$$

3.2.9. Pharmacokinetic studies

Prepared nanocomposites (5 mL, 20 μg/mL) were dialysed (MWCO 12000 Da) against 25 mL of phosphate buffered saline (PBS, pH 7.4, pH 6.5, pH 5.0, pH 4.5), with stirring at 37°C. At designated time intervals, 10 μL of dialysate was removed and analysed. The amount of doxorubicin released was determined by UV-Vis spectroscopy, at a wavelength 480 nm. The cumulative drug release percent was calculated relative to the total absorbance of DOX loaded onto nanocomposites using Equation (3.5).

$$\text{Cumulative (\%)} = \frac{\text{Abs free DOX}}{\text{Abs total DOX loaded}} \times 100 \quad (3.5)$$

In order to describe the mechanism of drug release for PACTD and CTD and to elucidate possible factors affecting release at different simulated environments, the dissolution data was fitted onto several selected kinetic models commonly used in literature (Chavda and Patel, 2011) as shown in Table 3.1.

Table 3.1: Time-dependent pharmacokinetic modelling of dissolution data to ascertain drug release mechanisms at acidic and physiological pH conditions.

Kinetic model	**Equation**
Zero-order	$R_t = R_0 + K_0 t$
First-order	$\text{Ln } R_t = \ln R_0 + K_1 t$
Higuchi	$R_t = K_H t^{1/2}$
Korsmeyer· Peppas	$R_t / R_\infty = K_k t^n$

K_0, K_1, K_H, K_k: Release rate constants; n: Release exponent (indicative of drug release mechanism); R_0: initial amount of DOX in the nanocomposite; R_∞: Total amount of drug dissolved when the dosage form is exhausted; Rt: Amount of DOX released at time t.

3.2.10. Mucoadhesion assay

The mucoadhesive properties of the nanoparticles and nanocomposites were evaluated *in vitro,* based on their ability to adhere to the intestinal mucosa resulting in rheological synergism. Briefly, porcine mucin (PM, 400 µg/mL) was hydrated in intestinal fluid (25% $^{v}/_{v}$, pH 6.8), and added (1:1 $^{v}/_{v}$) with the nanocomposite suspensions (20 µg/mL) and gently shaken (50 rpm) for 6 h at 37°C. Thereafter, the bound PM was obtained by centrifugation at 2.1x 10^3 rpm for 30 min at 10°C (Eppendorf 5424R). Analysis of the extent of cross-linking between the mucin and the nanocomposites was determined by measuring the absorbance in a Jasco V-730 Bio-spectrophotometer set at a wavelength of 251 nm, using intestinal fluid as the blank. The mucoadhesion percentage was calculated using Equation (3.6).

$$\text{Mucoadhesion (\%)} = \frac{\text{Total Mucin before - Free Mucin after}}{\text{Total Mucin before}} \times 100 \qquad (3.6)$$

3.2.11. Routine cell culture

All cells were cultured in complete medium (EMEM supplemented with 10% FBS and 1% antibiotics) at 37°C in 5% carbon dioxide humidified air. All biological assays were conducted under aseptic conditions in an Airvolution Class II biosafety laminar flow hood. Cells at the log phase of growth were either subculture into separate cell culture flasks for routine maintenance, multiwall plates for *in vitro* assays or cryopreserved for future studies (Appendix B).

3.2.12. *In vitro* cytotoxicity assays

Two cell viability assays were employed for greater reliability and comparative assessment of the *in vitro* cytotoxicity of the BNp nano-drug formulations. The MTT and SRB *in vitro* cytotoxicity assays were investigated on HEK293, Caco-2, HepG2 and MCF-7 cell lines. For both assays, the above-mentioned cell lines were seeded in a 96-well plate at a cell density of 2.5×10^2 cells/well and incubated overnight at 37°C. Thereafter, the medium was replaced with 100 µL fresh growth medium, to which the samples were added at various concentrations (5, 10, 15 and 20 µg/mL), and incubated for 48 h at 37°C. Wells containing cells only served as

the positive control. All assays were done in triplicate. The percentage cell survival was calculated according to Equation (3.7).

$$\text{Cell survival (\%)} = \frac{\text{Abs of treated cells}}{\text{Abs of untreated cells}} \times 100 \quad (3.7)$$

3.2.12.1. MTT assay

After the 48-h incubation, the medium replaced with 100 µL of fresh medium and 100 µL MTT reagent (5 mg/mL in PBS), and incubated for 4 h at 37°C. Thereafter, the MTT-medium mixture was removed, and 100 µL of DMSO was added and the plate gently shaken until the insoluble formazan crystals were dissolved. Absorbance was read using a Mindray MR-96A microplate reader (Vacutec, Hamburg, Germany) at 570 nm with DMSO as a blank.

3.2.12.2. SRB assay

After the incubation period, the cells were fixed with 25 µL cold TCA (50% $^{w}/_{v}$) and then incubated for 1 h at 4°C. The cells were then gently washed (3x) with distilled water to remove residual TCA and serum proteins. The plate was then air dried, and 50 µL of SRB (0.4% $^{w}/_{v}$ in 1% acetic acid) was added to the cells and incubated at 37°C in 5% CO_2 for 30 min, followed by washing (3x) with acetic acid (1%) and air drying of the plate. Finally, the dried cellular bound protein dye was solubilised in 100 µL of Tris buffer (10 mM, pH 10.5), and plates read on a Mindray MR-96A microplate reader at 565 nm using Tris base as the blank.

3.2.13. Apoptosis assay

The induction of apoptosis through cytotoxic BNp drug nanoconjugates was investigated quantitatively and qualitatively using the acridine orange/ethidium bromide (AO/EB) dual staining method. Briefly, cells were seeded in 24 well plates at a cell density of 1.5×10^5/well and incubated at 37°C in 5% CO_2 for 24 h to allow cells to attach. Thereafter, spent medium was removed and replenished with 0.5 mL of complete medium. Complexes were added in triplicate at predetermined IC_{50} values (average of the two assays) and incubated at 37°C in 5% CO_2 for 24 h. Cells containing no added complexes was used a positive control. Following

incubation, the medium was aspirated, and wells washed (2x) with 100 µL of cold PBS. Cells were stained with 12 µL of dye mixture (1:1 v/v of 100 mg/mL AO and 100 mg/mL EB, in PBS) for 5 min. The stained cells were viewed under an Olympus fluorescence microscope (200x magnification), fitted with a CC12 fluorescent camera (Olympus Co., Tokyo, Japan). The apoptotic indices were calculated according to Equation (3.8).

$$\text{Apoptotic Index} = \frac{\text{Number of Apoptotic cells}}{\text{Total number of cells counted}} \tag{3.8}$$

3.2.14. Statistical analysis

Statistical analyses of data were carried out using GraphPad Prism version 5.01 (GraphPad Software Inc., La Jolla, CA, USA). All Data were presented as Mean ± SD (Standard deviation). The significance of results and differences between control and treatment were evaluated for triplicate sets of data by using one-way analysis of variance (ANOVA). The Dunnett's multiple group comparison test was used for comparisons among different means. Statistical significance between groups was considered significant at **$p<0.01$ and * $p<0.05$. Dissolution kinetics parameters were evaluated using Microsoft Excel 2016 ™ and excel Add-in DD Solver software. The parameters are indicated in Table 3.1. The best-fit dissolution profile was identified at r^2 values ≥ 0.99.

3.3. Results and discussion

3.3.1. UV-Vis spectra

The presence of gold nanoparticles in samples can be detected by their distinct surface plasmon excitation peak in the range of 522-525 nm. Platinum (IV) species have previously been reported to have absorption spectrum at 265 nm. The UV-Vis spectra of PtAuBNps, PtAuCSBNps, PCTD, CTD and DOX are shown in Figure 3.2. Analysis of PtAuBNps revealed monotonically increasing absorbance towards higher energy until an SPR peak at 214 nm was reached. The distinct plasmon peak of Au vanished, indicating that the synthesised BNps are of gold (core)-platinum (shell). These observations are supported by studies of Zhang and co-workers who showed increased suppression of the Au plasmon band and a blue shift upon addition of increased amounts of platinum to gold (Zhang and Toshima, 2013). Chitosan

functionalised PtAuBNps (Figure 2B) presented a with a slight red shift in the SPR peak to 235 nm, indicating functionalisation and an increase in particle size. In water, DOX is known to have two absorption peaks at between 480-490 nm and 232 nm. Upon encapsulation within PCTD (Figure 2D) and CTD, these two peaks showed a red shift indicative of covalent binding of DOX with TPP and encapsulation of DOX within the chitosan nanoparticle and CS/BNp nanocomposite.

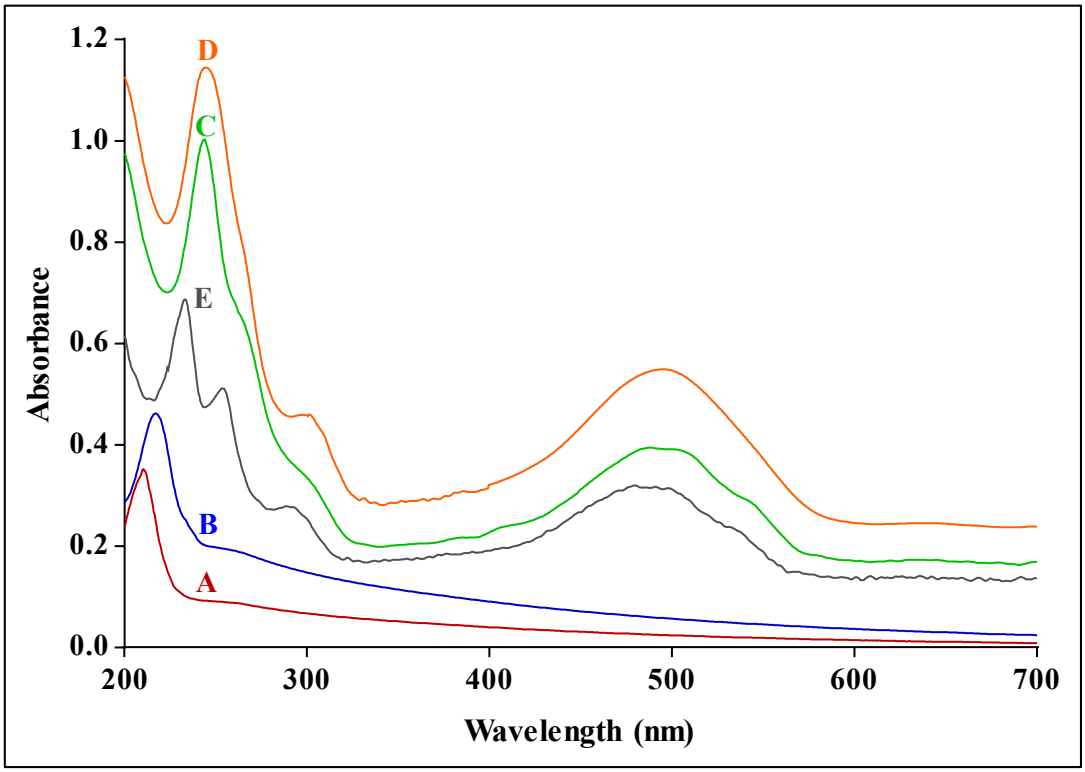

Figure 3.2: UV-Vis spectra of (A) PtAuBNps, (B) PtAuCSBNps, (C) PACTD, (D) CTD and (E) DOX in ultrapure water.
CTD: CS-TPP-DOX; DOX: Doxorubicin, PACTD: PtAu-CS-TPP-DOX.

3.3.2. ATR-FTIR spectra

Infrared spectroscopy is a useful technique to analyse the conformational structures present in a nano-formulation. The ATR-FTIR spectroscopic results confirmed the composition of CS, PACTD, CTD and DOX (Figure 3.3). The ATR-FTIR spectra of CS (Figure 3.3 A) showed distinct vibrational frequencies that include OH and N-H stretching of the amide A band near wave number 3352 cm^{-1}, stretching vibrations of C-H bond at ~ 2935 cm^{-1} and C=O stretching of the amide I band at ~ 1647 cm^{-1}. Furthermore, a peak at ~ 1573 cm^{-1} is descriptive of N-H bending vibrations of the amide II band, a peak at ~ 1150 cm^{-1} corresponds to anti-symmetric

stretching of the (C-O-C) bridge and finally, a peak at ~ 895 cm^{-1} is attributed to NH_2 twisting. The vibrational frequencies displayed by pure CS correlated with the previous literature (Lawrie *et al.*, 2007, Sanyakamdhorn *et al.*, 2013).

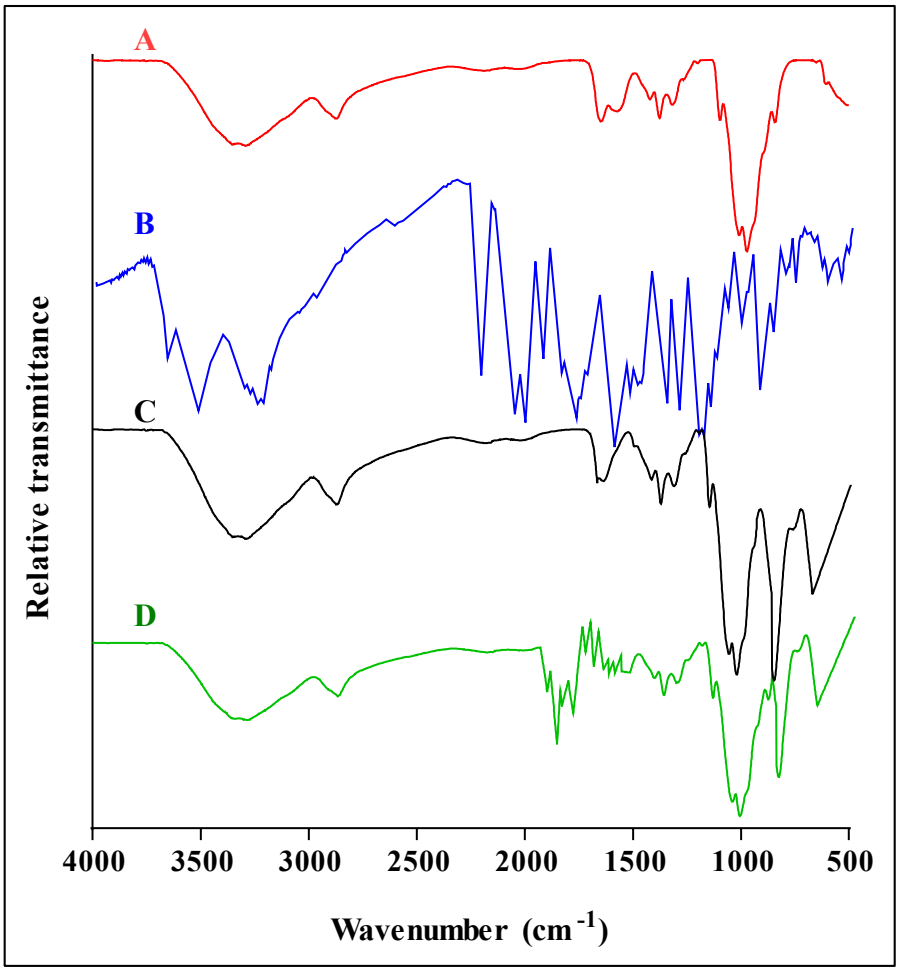

Figure 3.3: FTIR Spectra of (A) CS (B) Pure DOX (C) CTD and D) PACTD.
CTD: CS-TPP-DOX, DOX: Doxorubicin, PACTD: PtAu-CS-TPP-DOX.

Free DOX (Figure 3.3 B) presented characteristic absorption peaks near 3535 cm^{-1} ascribed to the stretching of OH bonds, a vibrational band at ~ 2950 cm^{-1} suggesting the presence of an NH_3 structure and a peak at ~ 1680 cm^{-1}, due to the stretching of the C=C of the alkenyl group. Peaks at ~ 1335 cm^{-1}, 878 cm^{-1}, 964 cm^{-1}, 696 cm^{-1} are attributed to phenyl ring O-H vibrations, N-H wagging, aromatic C-H stretching and alkyne C-H stretching respectively and correlates with the previous literature (Jayakumar *et al.*, 2012). Interestingly, the nanocomposites CTD and PACTD (Figure 3.3 C-D) displayed fingerprints of both CS and DOX, suggesting the strong presence of CS on the carriers' surface and successful encapsulation of DOX. Both

carriers displayed signature peaks of chitosan however with blue shifts at ~ 2921 cm^{-1} (C-H stretching), ~ 1647 cm^{-1} (amide I band), ~ 1573 cm^{-1} (amide II band) and reduced C-O-C stretching at ~ 1150 cm^{-1}. These peaks are possibly formed through protonated CS binding to the negatively charged surface of PtAuBNps as well as cross-linkage formation between TPP and the amine groups of CS. The peaks that indicate successful loading of DOX are at ~ 1280 cm^{-1}, due to framework vibrations of the carbonyl group in the DOX anthracycline structure, at ~ 881 cm^{-1} due to C-H stretching of the aromatic rings of DOX, and the peak at 737 cm^{-1} attributed to alkyne C-H stretching (Butt *et al.*, 2012, Das *et al.*, 2017). Overall the FTIR results confirm the presence of DOX in the nanocomposites (CTD and PACTD), while the presence of characteristic amide I bands and amide II bands suggest the presence of CS on the carrier's surface.

3.3.3. Transmission electron microscopy (TEM)

The ultrastructural morphologies of the nanoparticles and nanocomposites were examined using TEM. From the TEM images (Figure 3.4), the PtAuBNps were observed as small, circular and homogenous, showing little aggregation, similar to previous findings (Khalil *et al.*, 2014, Zhang and Toshima, 2013). There was no noticeable change in morphology for the PtAuCSBNps, however, addition of the drug and subsequent cross-linking of CS demonstrated a size increase. Drug loaded nanocomposites were spherical in shape and much larger in size. The increase in size is most likely due to the cross-linker TPP forming cross-linkages with CS resulting in the entrapment of both doxorubicin and PtAuBNps within the nanocomposite. The larger size of CTD may affect cellular uptake and cytotoxicity. Small nanoparticles (100 nm) are known to passively target tumour cells by escaping the leaky tumour vasculature and accumulating within the tumour core (Danhier *et al.*, 2010). The results obtained support the UV-Vis studies which elude to small-sized nanoparticles having less pronounced and defined peaks, and larger nanoparticles having broader peaks. Overall, all nanoparticles and nanocomposites displayed strong intensity in colour. This is due to elements with higher atomic number (Pt and Au) as well as denser, that tend to have greater light scattering capabilities, producing darker regions under TEM imaging. The colour intensity of CS nanocomposites was reported previously (Hou *et al.*, 2017, Yang and Hon, 2009). The colour contrast of CS nanocomposites are largely dependent on their molecular weight and fraction of ionic cross-linkages between TPP and the amine groups of CS.

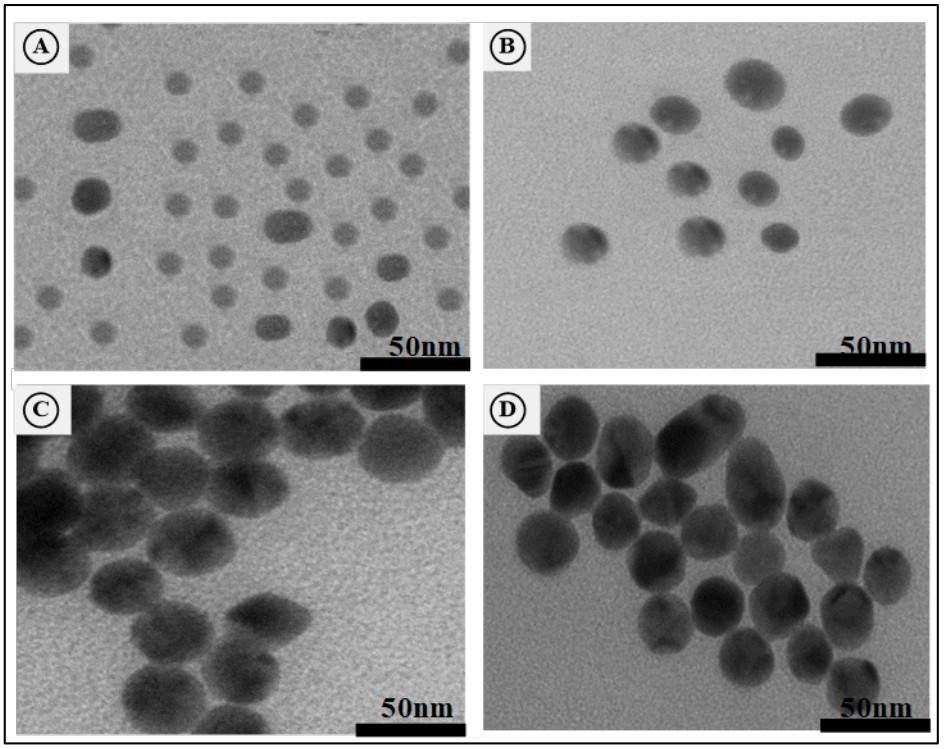

Figure 3.4: TEM images of (A) PtAuBNps, (B) PtAuCSBNps, (C) CTD, (D) PACTD. Bar = 50 nm. CTD: CS-TPP-DOX; PACTD: PtAu-CS-TPP-DOX.

3.3.4. Nanoparticle tracking analysis (NTA)

In the design and formulation of nanoscale delivery agents, the inherent size, shape and surface characteristics need to be assessed as they all affect biocompatibility. NTA was performed to accurately determine the size, dispersity and colloidal stability in real time. The size and ζ potential of each nanoparticle and nanocomposite are reported in Table 3.2 and Appendix C1-C4. Unmodified colloidal PtAuBNps were smallest in size with high negative ζ potentials (78.9 ± 8.5 nm; -19.3 ± 0.9 mV). These BNps were further stabilised upon functionalisation with chitosan as evidenced by the higher positive ζ potential and corresponding size increase (128.2 ± 3.7 nm; 58.5 ± 0.3 mV) obtained. The change to a high positive ζ potential value indicates the formation of strong covalent bonds between PtAuBNp ions and the amino groups of chitosan, resulting in BNps being well dispersed in the CS matrix (Adlim *et al.*, 2004). To ensure colloidally stable dispersions of nanoparticles a more dominant repulsive force other than an attractive force is required to cause greater dispersion. The ζ potential values greater than +30 mV or less than -30 mV are indicative of excellent colloidal stability (Gibson *et al.*, 2009). The rich density of the positively charged moieties of CS sterically stabilises PtAuBNps and prevents aggregation. While ζ potentials was consistent

with literature findings (Souto *et al.*, 2016, Xiong *et al.*, 2016), the sizes obtained from the nanoparticle analysis varied from that reported by some researchers (Khalil *et al.*, 2014, Zhang and Toshima, 2013), and could be due to different detection methods used and their sensitivity. NTA analysis is more robust, and tracks individual particles based on their Brownian motion through laser light scattering microscopy. Drug encapsulated nanocomposites had lower ζ potential values compared to PtAuCS and were also larger in size. Nevertheless, this still indicated a stable colloidal solution. A possible reason for the smaller size and higher ζ potential of PACTD compared to the CTD, could be that the addition of negatively charged PtAuBNps condensed the nanocomposite, reducing the levels of entanglement of the cross-linker TPP to CS. It has been reported that the size of the formed nanocomposite through ionic gelation, is largely attributed to the concentration and pH of TPP and CS (Masarudin *et al.*, 2015).

Table 3.2: Size distribution and zeta potential of bimetallic nanoparticles and its nanoconjugates. Data represented as mean ± SD.

Sample	Particle Size (nm)	ζ Potential (mV)
PtAuBNps	78.9 ± 8.5	-19.3 ± 0.9
PtAuCSBNps	128.2 ± 3.7	58.5 ± 0.1
PACTD	131.1 ± 2.9	28.2 ± 1.5
CTD	147.8 ± 3.6	24.2 ± 3.1

Data represented as mean ± SD. CTD: CS-TPP-DOX; PACTD: PtAu-CS-TPP-DOX.

3.3.5. Encapsulation efficiency

Sedimentation through centrifugation is an easy, reliable and accurate way to remove the unbound drug. Drug bound nanoparticles will sediment at different velocities based on viscosity, size and mass. Drug bound to the nanocomposites are generally of higher size and mass, and will consequently pellet, while the unbound drug will remain in the supernatant. The encapsulation efficiency (EE) and loading content (LC) are shown in Table 3.3. CTD had a slightly higher EE (71.85%) compared to PACTD (69.82%), which correlates to TEM and NTA results showing that CTD was larger in size compared to PACTD, hence providing a larger surface area to bind DOX. The calculated encapsulation efficiencies were used to determine the actual drug content in nanocomposites based on the theoretical drug content from which dilutions were made for cytotoxicity and apoptosis studies.

Table 3.3: Drug loading efficiency, theoretical drug content, actual drug content and drug loading content (LC) of nanocomposites.

Sample	TDC (µg)	EE (%)	ADC (µg)	LC (%)
CTD	116.00	71.85	83.34	14.62
PACTD	96.67	69.82	67.49	11.37

ADC: Actual drug content; CTD: CS-TPP-DOX; EE: Drug loading efficiency; LC: Drug loading content; PACTD: PtAu-CS-TPP-DOX; TDC: Theoretical drug content.

3.3.6. *In vitro* drug release

Tumour cells are hyper-proliferative and have high metabolic rates. As they continue to grow, the tumour vasculature becomes inadequate in providing oxygen, leading to hypoxia and an acidic microenvironment surrounding the tumour cells (Misra *et al.*, 2010). These physiological differences between normal and tumour tissue can be exploited to improve the efficacy of anticancer drugs. Carriers designed to be stable at physiological pH, but degrade at acidic pH to release the active drug will bring about selective targeting, where only hypoxic tumours cells are eradicated while normal cells are spared. The release kinetics of CTD and PACTD are shown in Figure 3.5. The release of DOX was pH dependent with more rapid dissolution kinetics at acidic conditions. At physiological pH, the release profile of both DOX carriers was subtle and sustained. There was slightly more DOX released from CTD (39.2 ± 1.3%) than PACTD (30.8 ± 1.8%) over the 24-h period, suggesting tighter encapsulation of DOX within PACTD nanocomposite. At acidic environments (pH 6.5, pH 5.0, pH 4.5) the release kinetics were much more rapid than at neutral conditions, as evidenced by higher release rate constants in all studied kinetic mathematical models. The results indicate that the nanocomposites permit pH-triggered release of DOX for selective tumour targeting. These findings were consistent with literature which report faster release kinetics at acidic pH for DOX bound to gold nanoparticles (Madhusudhan *et al.*, 2014, You *et al.*, 2010). At pH 6.5 and pH 5.0, it was evident that the polymeric CTD nanocomposites had a rapid initial burst release of DOX for the first 10 h (55.9 ± 0.9% and 66.1 ± 1.3% respectively) followed by a steady release phase during the subsequent 14 h. This appears to be a consistent feature of polymer/drug delivery systems in literature (Anitha *et al.*, 2011, Tan *et al.*, 2017). The addition of PtAuBNps dampened this effect, resulting in a gradual and steady release of DOX over 24 hours. At hypoxic conditions, DOX elution from PACTD was more restraint as there was prolonged release for 13 h (48.7 ± 0.8% at pH 6.5 and 58.4 ± 1.5% at pH 5.0).

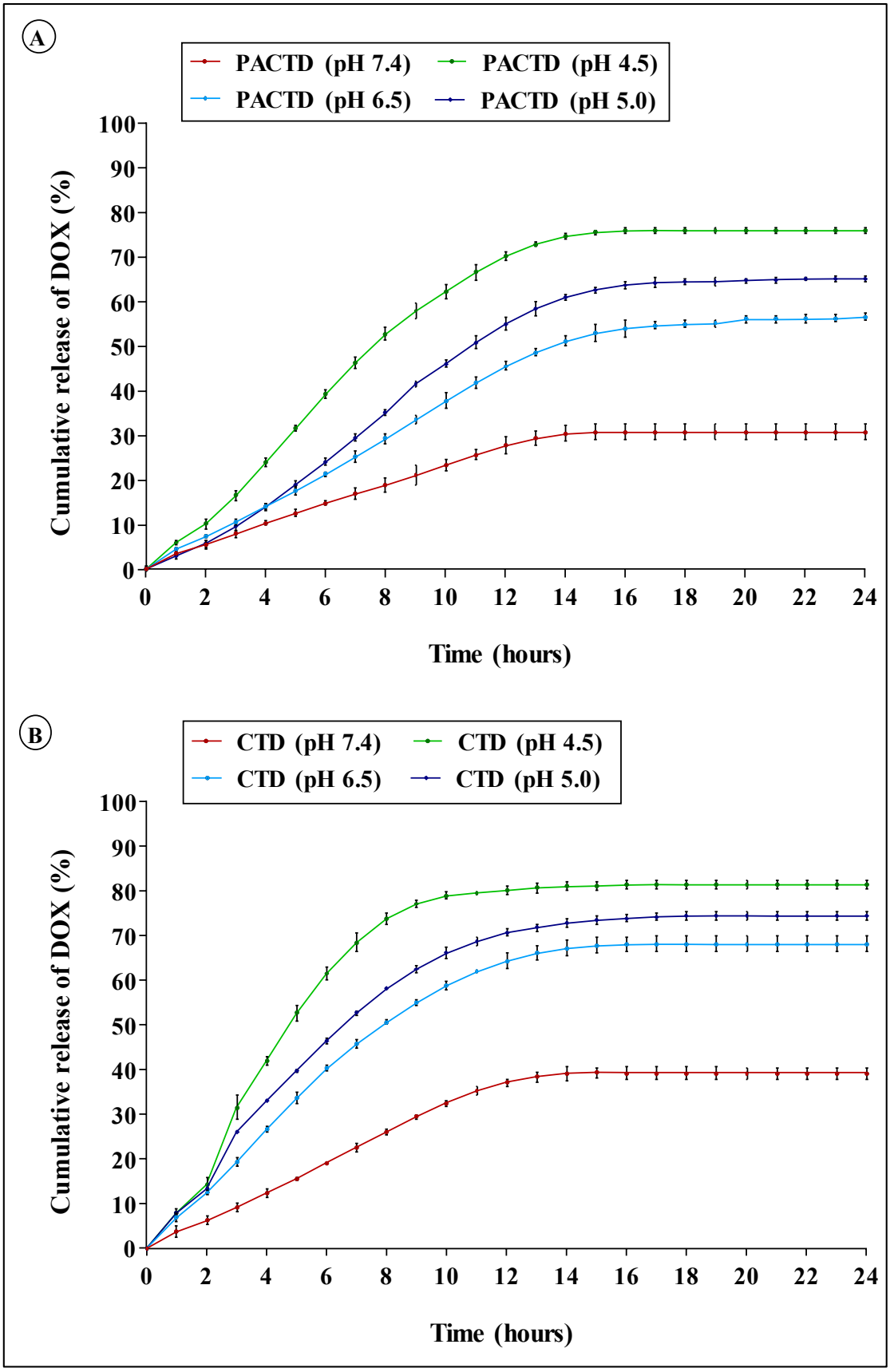

Figure 3.5: *In vitro* cumulative drug release profile of doxorubicin encapsulated nanocomposites. (A) PACTD, (B) CTD, at pH 4.5, 5.0, 6.5 and 7.4.

CTD: CS-TPP-DOX; PACTD: PtAu-CS-TPP-DOX.

The dissolution rate of a polymeric drug delivery system is affected by several variables such as drug diffusion, polymer swelling, erosion and the surrounding environment (Pourbadiei *et al.*, 2017, Siepmann and Göpferich, 2001). Different mathematical models were selected to fit the dissolution data, and elucidate the mechanism of drug release (Table 3.4 and 3.5). The exponent n of the Korsmeyer-Peppas model can characterise the release mechanism (Singhvi and Singh, 2011), as either Fickian diffusion ($0.45 \leq n$), anomalous (non-Fickian) diffusion ($0.45 < n < 0.89$), case II transport ($n = 0.89$) and super case II transport ($n > 0.89$). At physiological pH, the dissolution of DOX from both nanocomposites was through non-Fickian diffusion and kinetic profiles followed the zero-order model where minimal swelling and dissolution takes place (Nayak *et al.*, 2016). Under acidic conditions, the liberation of DOX from both nanocomposites was best explained by the zero-order model due to highest linearity ($r^2 = 0.998$). Drug delivery vehicles that have a close fit to the zero-order kinetic model do not disaggregate and release drugs slowly to achieved prolonged therapeutic action (Macheras and Iliadis, 2006). Both nanocomposites released DOX by anomalous diffusion eluding to polymer erosion, swelling and dissolution (Fu and Kao, 2010). Typically, anomalous diffusion consists of an initial burst release of drug near the surface of the nanocomposite, followed by an additional release of drug from pores within the nanocomposite formed through erosion (Huang and Brazel, 2001, Selvaraj *et al.*, 2012). This was anticipated, because at acidic pH the entanglements between chitosan and TPP that form the nanocomposite, swells due to protonation of the amine groups of chitosan, facilitating faster DOX elution (Anitha *et al.*, 2011). Erosion of nanocomposites occurs by hydrolysis of the entangled polymer matrix which generates pore formation, exposing entrapped DOX to the bathing liquid (Ismail *et al.*, 2017). It is expected that prolonged and uniform elution of DOX from the nanocomposite, with a balance between diffusion and erosion will enhance its therapeutic effects and reduce the occurrence of drug resistance.

Table 3.4: Pharmacokinetic parameters of PACTD under stimulated conditions.

Environment	Zero-order		First-order		Higuchi		Korsmeyer-Peppas		
	r^2	K_0	r^2	K_1	r^2	K_H	r^2	K_k	n
pH 7.4	0.998	1.706	0.998	0.020	0.942	7.015	0.947	3.870	0.725
pH 6.5	0.998	2.975	0.996	0.042	0.915	12.083	0.933	4.549	0.863
pH 5.0	0.998	3.483	0.974	0.054	0.846	14.134	0.902	3.561	1.016
pH 4.5	0.998	4.248	0.975	0.076	0.871	17.509	0.917	7.660	0.816

K_0, K_1, K_H, K_k: Release rate constants; r^2: Correlation coefficient; n: Release exponent (indicative of drug release mechanism)

Table 3.5: Pharmacokinetic parameters of CTD under stimulated conditions.

Environment	Zero-order		First-order		Higuchi		Korsmeyer-Peppas		
	r^2	K_0	r^2	K_1	r^2	K_H	r^2	K_k	n
pH 7.4	0.998	2.198	0.995	0.028	0.905	9.057	0.930	4.403	0.774
pH 6.5	0.995	3.725	0.987	0.060	0.900	15.224	0.922	6.281	0.833
pH 5.0	0.998	4.171	0.989	0.073	0.905	17.242	0.940	9.096	0.746
pH 4.5	0.998	4.702	0.960	0.094	0.866	19.619	0.920	10.748	0.735

K_0, K_1, K_H, K_k: Release rate constants; r^2: Correlation coefficient; n: Release exponent (indicative of drug release mechanism).

3.3.7. Mucoadhesion assay

This study was conducted to assess the binding efficiency of the chitosan containing nano-drug formulations to the model porcine mucin (PM) and estimate their mucoadhesive behaviour *in vitro*. Binding occurs through electrostatic interactions between the amino groups of chitosan to the negatively charged glycoproteins in the mucosal layers (Pilicheva *et al.*, 2013). In addition, other variables including wettability, entanglements, hydrophobic bonding and hydrogen bonding, all contribute to the mucoadhesivness (Andersen *et al.*, 2015, Serra *et al.*, 2009). The chitosan-coated PtAuBNps exhibited the highest PM binding efficacy (86.24 ± 3.82%), while free drug and plain PtAuBNps, as expected, exhibited minimal mucoadhesiveness (Table 3.6). Overall, drug loaded nanocomposites, PACTD (60.38 ± 4.17%) and CTD (54.15 ± 5.16%) had lower mucoadhesive strength compared to PtAuCSBNps. These findings were in agreement with the NTA results where PtAuCSBNps had a higher positive ζ potential value thereby favouring stability and stronger electrostatic interactions with the

mucosal layer. Chitosan cross-linking is known to reduce the mucoadhesiveness, especially the cross-linking agent glutaraldehyde producing as low as 15% adhesion (Kotadiya *et al.*, 2009). However, the cross-linking agent TPP produced nanocomposites with much better ability to adhere to the mucosal surface. The results obtained were similar to those of nanocomposites prepared through ionic gelation (Srivastava *et al.*, 2016).

Table 3.6: Binding efficiencies of nanoparticles to porcine mucin.

Compound	Mucoadhesion (%)
PtAuBNps	8.72 ± 1.67
PtAuCSBNps	86.24 ± 3.82
PACTD	60.38 ± 4.17
CTD	54.15 ± 5.16
DOX	18.79 ± 8.38

Data represented as mean ± SD. CTD: CS-TPP-DOX; DOX: Doxorubicin; PACTD: PtAu-CS-TPP-DOX.

3.3.8. *In vitro* cytotoxicity (MTT and SRB assay)

Formulation of nanocomposites that eliminate cancerous cells while sparing normal cells, is essential towards alleviating harsh toxicities associated with drug administration. To this end, the MTT and SRB colourimetric assays were carried out to estimate the level of cell death. The MTT assay is based on the premise that only viable cells with functional mitochondrial dehydrogenase enzymes can reduce MTT to an insoluble formazan product. The SRB assay is based on the principle that under mild acid conditions the anionic protein dye sulforhodamine B electrostatically binds to basic amino acid residues of TCA-fixed cells. The SRB assay provides quantification of drug-induced cytotoxicity with much greater sensitivity compared to the MTT assay (Keepers *et al.*, 1991). These two assays differ in sensitivity, therefore, comparisons between the SRB and MTT will provide a good initial assessment of the safety of the DOX loaded nanocomposites.

The cytotoxicity induced and IC_{50} values of the PtAu and its nanocomposites in four mammalian cell lines is represented in Figures 3.6-3.7 and Tables 3.7-3.8, respectively. Overall the MTT and SRB assays showed similar cytotoxicity profiles. The cytotoxicity profile of bimetallic nanocarriers without bound DOX (PtAu and PtAuCS) were relatively non-toxic to all cell lines for both assays, with PtAuCS, even displaying some growth promoting effects in

the non-cancer HEK293 cells. Hence, it can be assumed that any cytotoxic effects induced in the cancer cells will be due to the active bound drug rather than from the nanocarriers. DOX exhibited broad range cytotoxicity and reduced cell viability to less than 70% in all cell lines. The concentration range and cytotoxicity activity of free DOX were in findings with previous literature reporting (Jia *et al.*, 2017, Xiong *et al.*, 2016, Zhang *et al.*, 2017). Upon encapsulation within nanocomposites, DOX elicited dose dependent as well as cell specific cytotoxicity. There was reduced cytotoxicity towards non-cancerous HEK293 cells, indicating that the nanocomposites subdued harsh toxicities towards normal cells. Overall, PACTD was the most potent nanocomposite performing slightly better than free doxorubicin against all tested cancerous cell lines. Despite free DOX having an IC_{50} value at a lower concentration, the induced toxicity levels at highest dose concentrations 15 µg/mL and 20 µg/mL plateaued out. Interestingly, this was not the case for the nanocomposites which were more lethal at higher doses. This result highlights problems associated with free DOX administration including, poor biodistribution, low level of drug accumulation and degradation of the drug (Anselmo and Mitragotri, 2014, Mousa and Bharali, 2011, Robert *et al.*, 1985, Singh and Lillard, 2009), all leading to the development of drug resistance. The HepG2 cell line was the least tolerant cell line with approximately 80% cell death induced by PACTD and IC_{50} values of 11.22 µg/mL and 11.12 µg/mL in both the MTT and SRB assays respectively. The Caco-2 cell line was slightly more resistant to formulations of PACTD with IC_{50} values of 15.28 µg/mL and 15.24 µg/mL for the MTT and SRB assay respectively. The MCF-7 cell line was the most resilient toward PACTD with IC_{50} values of 19.31 µg/mL and 18.11 µg/mL for the MTT and SRB assay respectively. A similar trend was observed for CTD in the MTT and SRB assays, however with lower anticancer activity probably due to reduced ability to deliver active DOX successfully to cancerous cells. The results obtained correlate with the drug release studies, where PACTD had prolonged and steady drug release, thereby enhancing the therapeutic effect by delivering DOX gradually to the acidic tumour microenvironment. The result also correlates with the results of NTA analyses, where the smaller sized nanoparticles with a net positive surface charge would preferential have a greater affinity for the negatively charged cell membrane, and are therefore more readily internalised.

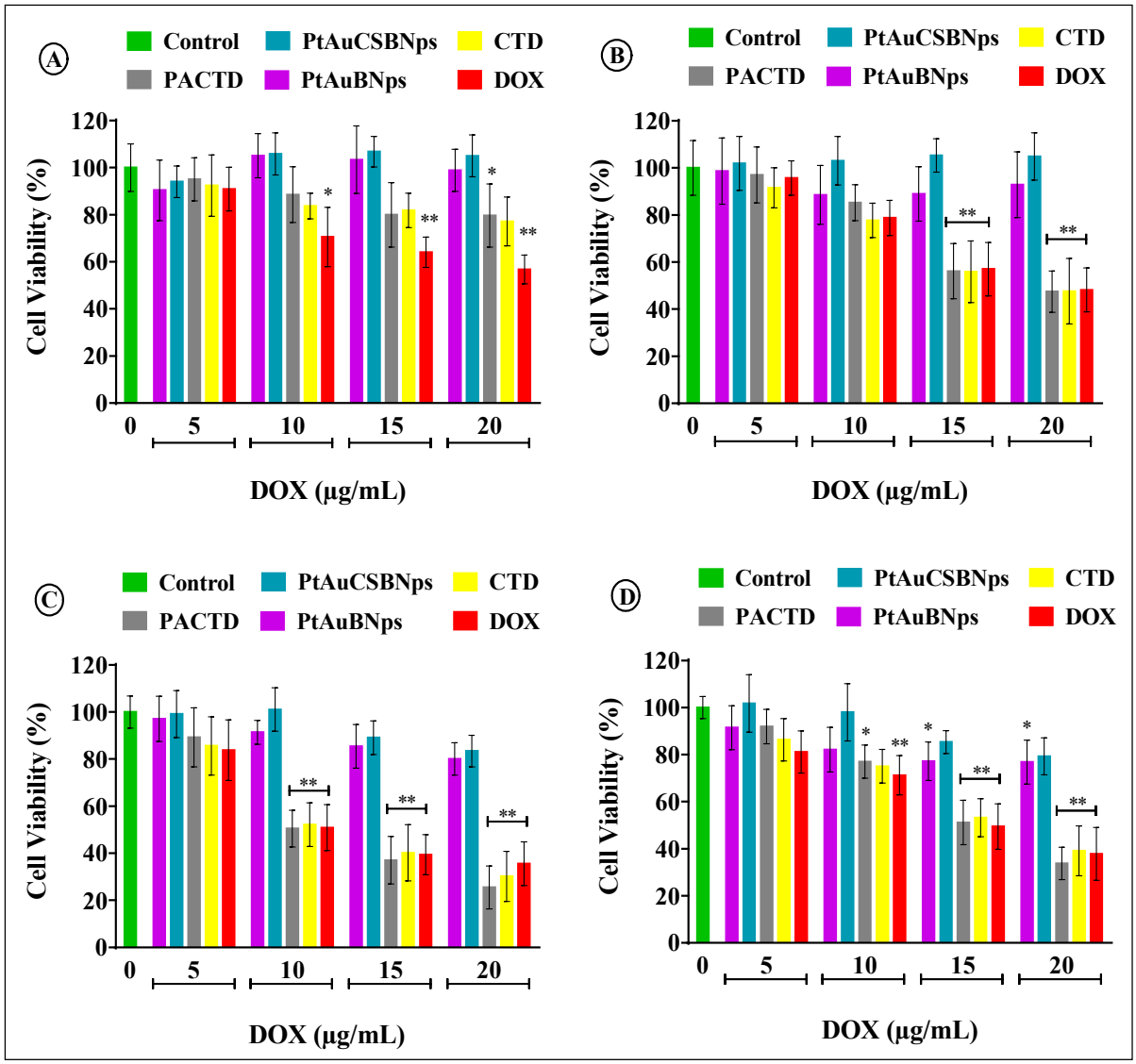

Figure 3.6: MTT cytotoxicity assay of bimetallic nanoparticles and drug loaded nanocomposites in (A) HEK293, (B) MCF-7, (C) HepG2 and (D) Caco-2 cell lines. Data represented as mean ± SD (n=3). * $p<0.05$, **$p<0.01$ were considered statistically significant.

Table 3.7: IC_{50} values of free DOX and DOX loaded nanocomposites on HEK293, HepG2, Caco-2 and MCF-7 cell lines for the MTT assays.

	IC_{50} calculation (µg/mL)		
Cell Lines	**PACTD**	**CTD**	**DOX**
HEK293	-	-	28.80
MCF-7	19.31	19.63	19.50
HepG2	11.22	11.64	11.83
Caco-2	15.28	16.41	15.14

- Where IC_{50} could not be estimated accurately. CTD: CS-TPP-DOX; DOX: Doxorubicin; PACTD: PtAu-CS-TPP-DOX.

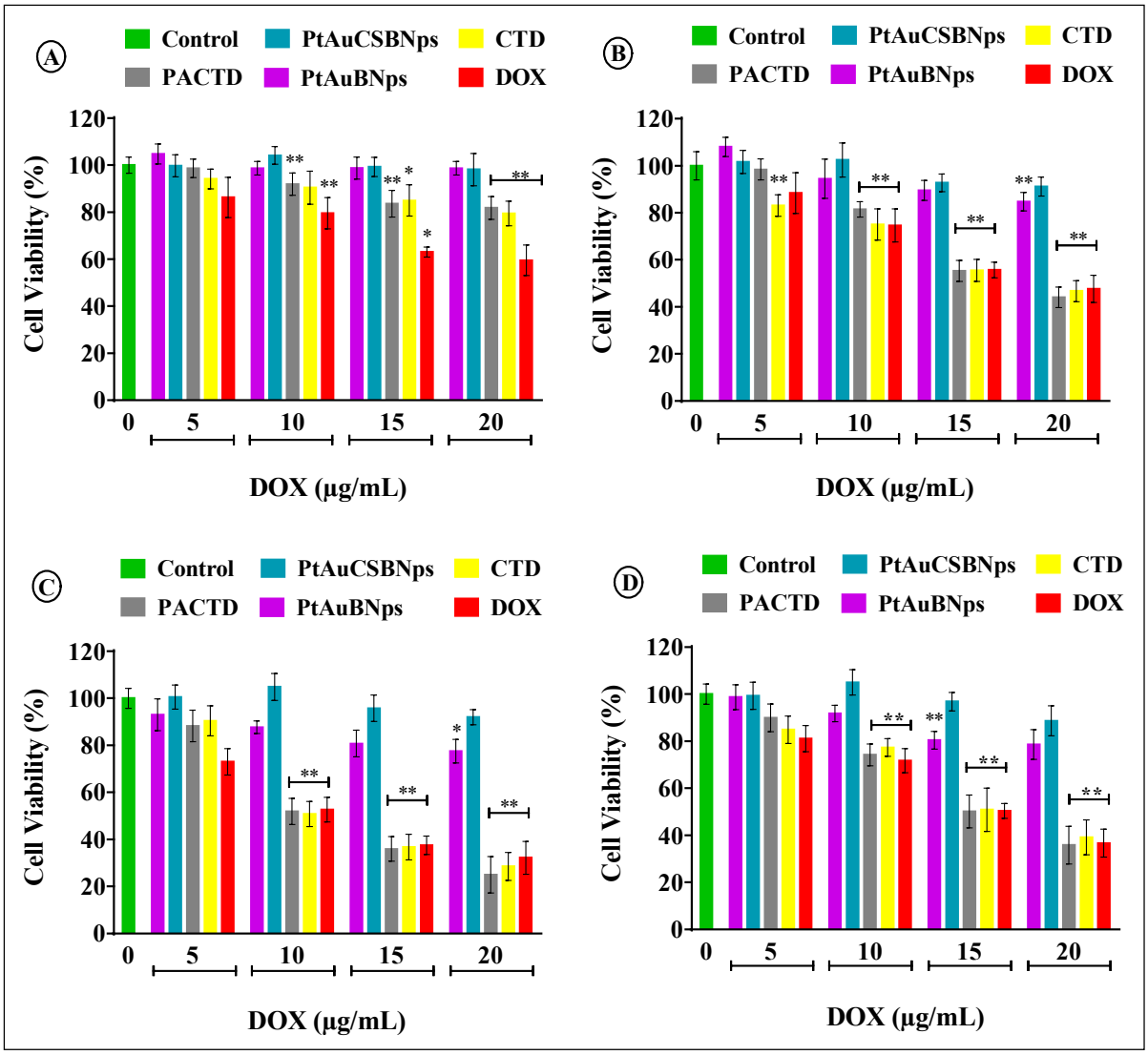

Figure 3.7: SRB cytotoxicity assay of bimetallic nanoparticles and drug loaded nanocomposites in (A) HEK293, (B) MCF-7, (C) HepG2 and (D) Caco-2 cell lines. Data represented as mean ± SD (n=3). * $p<0.05$, ** $p<0.01$ were considered statistically significant.

Table 3.8: IC_{50} values of free DOX and DOX loaded nanocomposites on HEK293, HepG2, Caco-2 and MCF-7 cell lines for the SRB assays.

	IC_{50} calculation (µg/mL)		
Cell Lines	**PACTD**	**CTD**	**DOX**
HEK293	-	-	32.51
MCF-7	18.11	19.41	19.19
HepG2	11.12	11.48	10.64
Caco-2	15.24	16.29	15.10

- Where IC_{50} could not be estimated accurately.

CTD: CS-TPP-DOX; DOX: Doxorubicin; PACTD: PtAu-CS-TPP-DOX.

3.3.9. Apoptosis study

Apoptosis studies were conducted to determine the mechanism of cell death and correlate this to any observed cytotoxicity seen in the MTT and SRB assays for free doxorubicin, PACTD and CTD. The dual fluorescent acridine orange/ethidium bromide (AO/EB) assay was used to detect morphological changes induced when cytotoxic agents were administered at IC_{50} concentrations (Tables 3.7 and 3.8). This staining technique is based on the premise that acridine orange permeates all cells resulting in the emittance of green fluorescence. Conversely, ethidium is bromide is only taken up by non-viable cells leading to the emittance of yellow to red fluorescence. Hence under a fluorescent microscope, viable cells fluoresce green, early apoptotic cells bright green, late apoptotic with condensed chromatin yellow/orange, and necrotic cells with no condensed chromatin orange/red in colour (Bezabeh *et al.*, 2001). Accordingly, administration of free DOX and DOX loaded nanocomposites induced apoptotic body formation in all cancer cell lines (Figure 3.8), with no specificity as shown by high apoptotic index values (Table 3.9). The lower apoptotic index values for the non-cancerous HEK293 cell lines, indicate that the DOX loaded nanocomposites have selective apoptosis induction. Higher levels of cell shrinkage, chromatin condensation, fragmentation of the nucleus and cell membrane blebbing were observed in the HepG2 and Caco-2, compared to MCF-7 and HEK293 cell lines. These were in keeping with findings from the MTT and SRB assays, and further confirms cell specificity for DOX loaded nanocomposites.

Table 3.9: Apoptotic index of free DOX and DOX loaded nanocomposites.

	Apoptosis Index		
Cell Lines	**PACTD**	**CTD**	**DOX**
HEK293	0.201	0.205	0.401
MCF-7	0.280	0.241	0.292
HepG2	0.762	0.667	0.533
Caco-2	0.360	0.324	0.375

CTD: CS-TPP-DOX; DOX: Doxorubicin; PACTD: PtAu-CS-TPP-DOX.

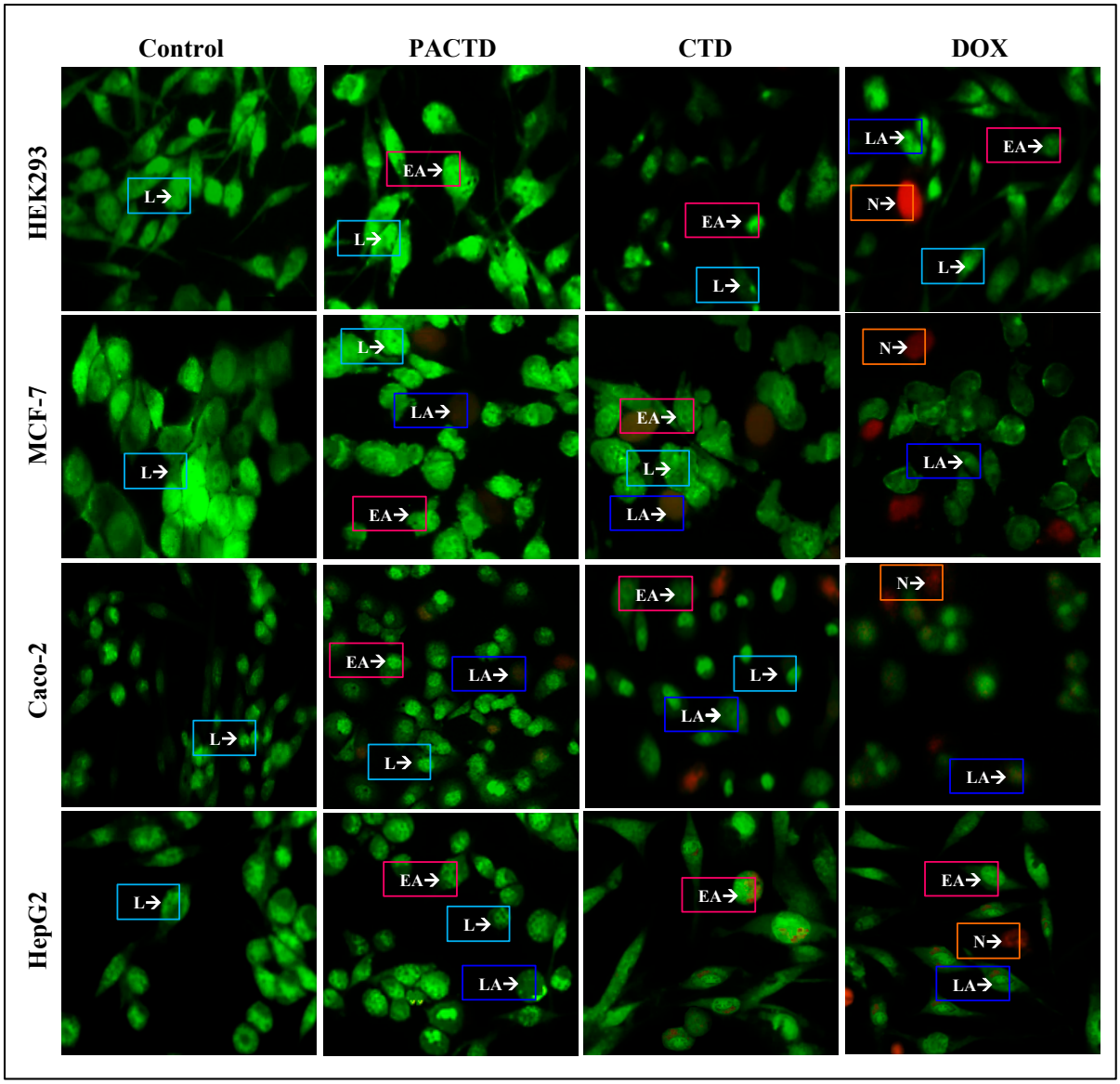

Figure 3.8: Fluorescence micrographs of duel acridine orange/ethidium bromide stained cells showing induced morphological changes in HEK293, MCF-7, Caco-2 and HepG2 cell lines at 20x magnification. L= live cells; EA= Early apoptotic cells; LA= late apoptotic cells N=necrotic cells.

3.4. Conclusion

The PtAu/chitosan nanocomposites synthesised were able to encapsulate high amounts of DOX, and further induce a pH-triggered release at intracellular acidic conditions to bring about selective cancer targeting. The kinetic modelling of dissolution data revealed that elution of DOX from both nanocomposites followed zero-order kinetics with PACTD having a reduced burst release compared to CTD. Hence, PACTD shows immense potential for enhancing therapeutic effects due to prolonged release. The cytotoxicity assays performed validated the above findings. The nanocomposite PACTD and CTD induced dose dependent cancer specific

cell death possibly through the induction of apoptosis. In addition, the chitosan containing nanocomposites exhibited strong binding to mucin, advancing to the possibility of drug administration through the mucosal tissue. From the aforementioned results, chitosan polymerised nanoparticles appear to be safe excipients for controlled drug delivery strategies.

References

Adlim, M., Bakar, M. A., Liew, K. Y., and Ismail, J. 2004. Synthesis of chitosan-stabilized platinum and palladium nanoparticles and their hydrogenation activity. *Journal of Molecular Catalysis A: Chemical,* 212, 141-149.

Andersen, T., Bleher, S., Eide Flaten, G., Tho, I., Mattsson, S., and Škalko-Basnet, N. 2015. Chitosan in mucoadhesive drug delivery: focus on local vaginal therapy. *Marine Drugs,* 13, 222-236.

Anitha, A., Deepagan, V., Rani, V. D., Menon, D., Nair, S., and Jayakumar, R. 2011. Preparation, characterization, *in vitro* drug release and biological studies of curcumin loaded dextran sulphate-chitosan nanoparticles. *Carbohydrate Polymers,* 84, 1158-1164.

Anselmo, A. C., and Mitragotri, S. 2014. An overview of clinical and commercial impact of drug delivery systems. *Journal of Controlled Release,* 190, 15-28.

Bezabeh, T., Mowat, M., Jarolim, L., Greenberg, A., and Smith, I. 2001. Detection of drug-induced apoptosis and necrosis in human cervical carcinoma cells using 1H NMR spectroscopy. *Cell Death and Differentiation,* 8, 219.

Butt, A. M., Amin, M. C. I. M., Katas, H., Sarisuta, N., Witoonsaridsilp, W., and Benjakul, R. 2012. *In vitro* characterization of pluronic F127 and D-α-tocopheryl polyethylene glycol 1000 succinate mixed micelles as nanocarriers for targeted anticancer-drug delivery. *Journal of Nanomaterials,* 2012, 112.

Chavda, H., and Patel, C. 2011. Preparation and *in vitro* evaluation of a stomach specific drug delivery system based on superporous hydrogel composite. *Indian Journal of Pharmaceutical Sciences,* 73, 30-37.

Danhier, F., Feron, O., and Préat, V. 2010. To exploit the tumor microenvironment: passive and active tumor targeting of nanocarriers for anti-cancer drug delivery. *Journal of Controlled Release,* 148, 135-146.

Daraee, H., Eatemadi, A., Abbasi, E., Fekri Aval, S., Kouhi, M., and Akbarzadeh, A. 2016. Application of gold nanoparticles in biomedical and drug delivery. *Artificial Cells, Nanomedicine, and Biotechnology,* 44, 410-422.

Das, J., Choi, Y. J., Han, J. W., Reza, A. M. M. T., and Kim, J. H. 2017. Nanoceria-mediated delivery of doxorubicin enhances the anti-tumour efficiency in ovarian cancer cells via apoptosis. *Scientific Reports,* 7, 9513.

Dhamecha, D., Jalalpure, S., and Jadhav, K. 2015. Doxorubicin functionalized gold nanoparticles: Characterization and activity against human cancer cell lines. *Process Biochemistry,* 50, 2298-2306.

Dutta, D., Sahoo, A. K., Chattopadhyay, A., and Ghosh, S. S. 2016. Bimetallic silver nanoparticle-gold nanocluster embedded composite nanoparticles for cancer theranostics. *Journal of Materials Chemistry B,* 4, 793-800.

Feng, J. J., Chen, L. X., Song, P., Wu, X.-L., Wang, A. J., and Yuan, J. 2016. Bimetallic AuPd nanoclusters supported on graphitic carbon nitride: one-pot synthesis and enhanced electrocatalysis for oxygen reduction and hydrogen evolution. *International Journal of Hydrogen Energy,* 41, 8839-8846.

Fu, Y., and Kao, W. J. 2010. Drug release kinetics and transport mechanisms of non-degradable and degradable polymeric delivery systems. *Expert Opinion on Drug Delivery,* 7, 429-444.

Gibson, N., Shenderova, O., Luo, T., Moseenkov, S., Bondar, V., Puzyr, A., Purtov, K., Fitzgerald, Z., and Brenner, D. 2009. Colloidal stability of modified nanodiamond particles. *Diamond and Related Materials,* 18, 620-626.

González-Fernández, Y., Imbuluzqueta, E., Zalacain, M., Mollinedo, F., Patiño-García, A., and Blanco-Prieto, M. J. 2017. Doxorubicin and edelfosine lipid nanoparticles are effective acting synergistically against drug-resistant osteosarcoma cancer cells. *Cancer letters,* 388, 262-268.

Green, P. S., and Leeuwenburgh, C. 2002. Mitochondrial dysfunction is an early indicator of doxorubicin-induced apoptosis. *Biochimica et Biophysica Acta (BBA)-Molecular Basis of Disease,* 1588, 94-101.

Hou, J., Yu, X., Shen, Y., Shi, Y., Su, C., and Zhao, L. 2017. Triphenyl Phosphine-Functionalized Chitosan Nanoparticles Enhanced Antitumor Efficiency Through

Targeted Delivery of Doxorubicin to Mitochondria. *Nanoscale Research Letters,* 12, 158.

Huang, X., and Brazel, C. S. 2001. On the importance and mechanisms of burst release in matrix-controlled drug delivery systems. *Journal of Controlled Release,* 73, 121-136.

Ismail, S. T., Al-Kotaji, M. M., and Khayrallah, A. A. 2017. Formulation and Evaluation of Nystatin Microparticles as a Sustained Release System. *Iraqi Journal of Pharmaceutical Sciences,* 24, 1-10.

Jayakumar, R., Nair, A., Rejinold, N. S., Maya, S., and Nair, S. 2012. Doxorubicin-loaded pH-responsive chitin nanogels for drug delivery to cancer cells. *Carbohydrate Polymers,* 87, 2352-2356.

Jia, N., Ye, Y., Wang, Q., Zhao, X., Hu, H., Chen, D., and Qiao, M. 2017. Preparation and evaluation of poly (L-histidine) based pH-sensitive micelles for intracellular delivery of doxorubicin against MCF-7/ADR cells. *Asian Journal of Pharmaceutical Sciences,* 12, 433-441.

Kamba, S. A., Ismail, M., Hussein-Al-Ali, S. H., Ibrahim, T. a. T., and Zakaria, Z. a. B. 2013. *In vitro* delivery and controlled release of doxorubicin for targeting osteosarcoma bone cancer. *Molecules,* 18, 10580-10598.

Keepers, Y. P., Pizao, P. E., Peters, G. J., Van Ark-Otte, J., Winograd, B., and Pinedo, H. M. 1991. Comparison of the sulforhodamine B protein and tetrazolium (MTT) assays for *in vitro* chemosensitivity testing. *European Journal of Cancer and Clinical Oncology,* 27, 897-900.

Khalil, M. M., Mostafa, Y. M., and Torad, E. 2014. Biosynthesis and characterization of Pt and Au-Pt nanoparticles and their photo catalytic degradation of methylene blue. *International Journal,* 2, 694-703.

Kotadiya, R., Patel, V., Patel, H., and Koradiya, H. 2009. Effect of cross-linking on physicochemical properties of chitosan mucoadhesive microspheres: A factorial approach. *International Journal of Green Pharmacy,* 3, 58.

Lawrie, G., Keen, I., Drew, B., Chandler-Temple, A., Rintoul, L., Fredericks, P., and Grøndahl, L. 2007. Interactions between alginate and chitosan biopolymers characterized using FTIR and XPS. *Biomacromolecules,* 8, 2533-2541.

Macheras, P., and Iliadis, A. 2006. Modeling in biopharmaceutics, pharmacokinetics, and pharmacodynamics. *Interdisciplinary Applied Mathematics,* 30, 15-36.

Madhusudhan, A., Reddy, G. B., Venkatesham, M., Veerabhadram, G., Kumar, D. A., Natarajan, S., Yang, M.-Y., Hu, A., and Singh, S. S. 2014. Efficient pH dependent drug delivery to target cancer cells by gold nanoparticles capped with carboxymethyl chitosan. *International Journal of Molecular Sciences,* 15, 8216-8234.

Masarudin, M. J., Cutts, S. M., Evison, B. J., Phillips, D. R., and Pigram, P. J. 2015. Factors determining the stability, size distribution, and cellular accumulation of small, monodisperse chitosan nanoparticles as candidate vectors for anticancer drug delivery: application to the passive encapsulation of [14C]-doxorubicin. *Nanotechnology, Science and Applications,* 8, 67-80.

Misra, R., Acharya, S., and Sahoo, S. K. 2010. Cancer nanotechnology: application of nanotechnology in cancer therapy. *Drug Discovery Today,* 15, 842-850.

Mousa, S. A., and Bharali, D. J. 2011. Nanotechnology-based detection and targeted therapy in cancer: nano-bio paradigms and applications. *Cancers,* 3, 2888-2903.

Nayak, A. K., Pal, D., and Santra, K. 2016. Swelling and drug release behavior of metformin HCl-loaded tamarind seed polysaccharide-alginate beads. *International Journal of Biological Macromolecules,* 82, 1023-1027.

Nivethaa, E., Dhanavel, S., Narayanan, V., Vasu, C. A., and Stephen, A. 2015. An *in vitro* cytotoxicity study of 5-fluorouracil encapsulated chitosan/gold nanocomposites towards MCF-7 cells. *RSC Advances,* 5, 1024-1032.

Pilicheva, B., Zagorchev, P., Uzunova, Y., and Kassarova, M. 2013. Development and *in vitro* evaluation of mucoadhesive microsphere carriers for intranasal delivery of betahistine dihydrochloride. *International Journal of Drug Delivery,* 5, 389.

Pourbadiei, B., Pyadar, R., and Mansouri, F. 2017. pH-Sensitive Nanoscale Polymers: Highly Efficient Systems for DOX Delivery in Cancer Treatment. *Journal Nanomedicine Research,* 5, 1-6.

Robert, J., Vrignaud, P., Nguyen-Ngoc, T., Iliadis, A., Mauriac, L., and Hurteloup, P. 1985. Comparative pharmacokinetics and metabolism of doxorubicin and epirubicin in patients with metastatic breast cancer. *Cancer Treatment Reports,* 69, 633-640.

Sanyakamdhorn, S., Agudelo, D., and Tajmir-Riahi, H. A. 2013. Encapsulation of antitumor drug doxorubicin and its analogue by chitosan nanoparticles. *Biomacromolecules,* 14, 557-563.

Selvaraj, S., Karthikeyan, J., and Saravanakumar, N. 2012. Chitosan loaded microspheres as an ocular delivery system for acyclovir. *International Journal of Pharmacy and Pharmaceutical Sciences,* 4, 125-32.

Serra, L., Doménech, J., and Peppas, N. A. 2009. Engineering design and molecular dynamics of mucoadhesive drug delivery systems as targeting agents. *European Journal of Pharmaceutics and Biopharmaceutics,* 71, 519-528.

Siepmann, J., and Göpferich, A. 2001. Mathematical modeling of bioerodible, polymeric drug delivery systems. *Advanced Drug Delivery Reviews,* 48, 229-247.

Singh, R., and Lillard, J. W. 2009. Nanoparticle-based targeted drug delivery. *Experimental and Molecular Pathology,* 86, 215-223.

Singhvi, G., and Singh, M. 2011. Review: *in-vitro* drug release characterization models. *International Journal of Pharmaceutical Sciences and Research,* 2, 77-84.

Singla, A., and Chawla, M. 2001. Chitosan: Some pharmaceutical and biological aspects-an update. *Journal of Pharmacy and Pharmacology,* 53, 1047-1067.

Souto, G. D., Farhane, Z., Casey, A., Efeoglu, E., Mcintyre, J., and Byrne, H. J. 2016. Evaluation of cytotoxicity profile and intracellular localisation of doxorubicin-loaded chitosan nanoparticles. *Analytical and Bioanalytical Chemistry,* 408, 5443-5455.

Srivastava, G., Walke, S., Dhavale, D., Gade, W., Doshi, J., Kumar, R., Ravetkar, S., and Doshi, P. 2016. Tartrate/tripolyphosphate as co-crosslinker for water soluble chitosan

used in protein antigens encapsulation. *International Journal of Biological Macromolecules,* 91, 381-393.

Suarato, G., Li, W., and Meng, Y. 2016. Role of pH-responsiveness in the design of chitosan-based cancer nanotherapeutics: A review. *Biointerphases,* 11, 04B201.

Szymańska, E., and Winnicka, K. 2015. Stability of chitosan-a challenge for pharmaceutical and biomedical applications. *Marine drugs,* 13, 1819-1846.

Tan, Q., Chu, Y., Bie, M., Wang, Z., and Xu, X. 2017. Preparation and Investigation of Amphiphilic Block Copolymers/Fullerene Nanocomposites as Nanocarriers for Hydrophobic Drug. *Materials,* 10, 192.

Thanh, N. T., and Green, L. A. 2010. Functionalisation of nanoparticles for biomedical applications. *Nano Today,* 5, 213-230.

Vigderman, L., and Zubarev, E. R. 2013. Therapeutic platforms based on gold nanoparticles and their covalent conjugates with drug molecules. *Advanced Drug Delivery Reviews,* 65, 663-676.

Von Roemeling, C., Jiang, W., Chan, C. K., Weissman, I. L., and Kim, B. Y. 2017. Breaking down the barriers to precision cancer nanomedicine. *Trends in Biotechnology,* 35, 159-171.

Xiong, W., Li, L., Wang, Y., Yu, Y., Wang, S., Gao, Y., Liang, Y., Zhang, G., Pan, W., and Yang, X. 2016. Design and evaluation of a novel potential carrier for a hydrophilic antitumor drug: Auricularia auricular polysaccharide-chitosan nanoparticles as a delivery system for doxorubicin hydrochloride. *International Journal of Pharmaceutics,* 511, 267-275.

Yamada, M., Foote, M., and Prow, T. W. 2015. Therapeutic gold, silver, and platinum nanoparticles. *Wiley Interdisciplinary Reviews: Nanomedicine and Nanobiotechnology,* 7, 428-445.

Yang, C. L., Chen, J. P., Wei, K. C., Chen, J. Y., Huang, C. W., and Liao, Z. X. 2017. Release of Doxorubicin by a Folate-Grafted, Chitosan-Coated Magnetic Nanoparticle. *Nanomaterials,* 7, 85.

Yang, F., Teves, S. S., Kemp, C. J., and Henikoff, S. 2014. Doxorubicin, DNA torsion, and chromatin dynamics. *Biochimica et Biophysica Acta (BBA)-Reviews on Cancer,* 1845, 84-89.

Yang, H. C., and Hon, M. H. 2009. The effect of the molecular weight of chitosan nanoparticles and its application on drug delivery. *Microchemical Journal,* 92, 87-91.

Yin, Y., Chen, D., Qiao, M., Lu, Z., and Hu, H. 2006. Preparation and evaluation of lectin-conjugated PLGA nanoparticles for oral delivery of thymopentin. *Journal of Controlled Release,* 116, 337-345.

You, J., Zhang, G., and Li, C. 2010. Exceptionally high payload of doxorubicin in hollow gold nanospheres for near-infrared light-triggered drug release. *ACS Nano,* 4, 1033-1041.

Zhang, H., and Toshima, N. 2013. Synthesis of Au/Pt bimetallic nanoparticles with a Pt-rich shell and their high catalytic activities for aerobic glucose oxidation. *Journal of Colloid and Interface Science,* 394, 166-176.

Zhang, M., Yuan, P., Zhou, N., Su, Y., Shao, M., and Chi, C. 2017. pH-Sensitive N-doped carbon dots-heparin and doxorubicin drug delivery system: preparation and anticancer research. *RSC Advances,* 7, 9347-9356.

CHAPTER FOUR

IN VITRO TARGET ACTIVATED DELIVERY OF 5-FLOUROURACIL USING CHITOSAN POLYMERISED PtAu BIMETALLIC NANOCOMPOSITES

Vareessh Maney[1] and Moganavelli Singh[1]

[1]Non-Viral Gene Delivery Laboratory, Discipline of Biochemistry, School of Life Sciences, University of KwaZulu Natal, Private Bag X54001, Durban, South Africa

[*]Corresponding author: Moganavelli Singh, email: Singhm1@ukzn.ac.za

Abstract

The application of nanoparticles in the area of nanomedicine has had a significant impact and is currently revolutionising cancer therapy. The burgeoning necessity to develop novel drugs with higher therapeutic potential has stimulated the development of innovative delivery strategies to mitigate the potent side effects associated with cytotoxic chemotherapeutic drugs. This study describes the synthesis of PtAu bimetallic nanoparticles (PtAuBNps), their functionalisation with chitosan, and entrapment of the anticancer drug 5-Fluorouracil (5-FU). All PtAuBNps and their drug nanocomposites were structurally and chemically characterised using ATR-FTIR, NTA, TEM and UV-Vis spectroscopy. All PtAuBNps and their nanocomposites displayed desirable physiochemical properties with regards to shape, size (<120 nm) and colloidal stability. Drug binding efficiencies and loading capacity studies were found to be 90.17% and 22.56% respectively. *In vitro* cytotoxicity profiles were determined using the MTT and SRB assays, with up to 65% cell death recorded in MCF-7, HepG2 and Caco-2 cell lines. Overall the nanocomposites exhibited excellent physiochemical attributes, high specificity towards cancerous cells and displayed pH-sensitive drug release in a simulated acidic tumour microenvironment through zero-order release kinetics. In addition, the nanocomposites showed good bioadhesiveness and the potential to pass through the mucous lining to facilitate oral administration of the drug nanocomposites. Overall, the encapsulation of 5-FU assured improved bioavailability of the drug in cancer cell lines for a prolonged duration, with the promise of enhancing its therapeutic effect, biocompatibility and safety. These positive results highlight PtAuBNps as a promising *in vitro* delivery system and merit future research for *in vivo* application.

Keywords: 5-Fluorouracil, bimetallic nanoparticles, cancer, gold, pH-responsive, platinum

4.1. Introduction

Cancer, the unrestrained proliferation of dysfunctional cells, is a dreadful scourge and a leading cause of mortality worldwide. Several efforts have been made to advance treatment regimens. However, the astounding complexity at cellular, genetic and epigenetic levels allow this menacing disease to show great diversity, to resist treatment, re-emerge and invade surrounding tissue. Some of the well-established treatments options include surgery, radiation, hormonal therapy, immunotherapy and hyperthermia (El-Hammadi *et al.*, 2017). Among these approaches, chemotherapy utilises therapeutic compounds either alone or in combination, to thwart cellular proliferation in both solid tumours and haematological cancers.

5-FU is a hydrophilic, water soluble, antimetabolite drug that is used extensively in clinical chemotherapy for the treatment of breast, brain, liver, pancreatic and lung cancers (Kevadiya *et al.*, 2012). It is often a stand-alone drug for treatment of colorectal cancers, and together with modulators such as leucovorin and oxaliplatin, is the most effective treatment for metastatically advanced colorectal cancers (Rejinold *et al.*, 2016). However, its clinical application has limitations including dose dependent side effects, rapid metabolism *in vivo*, short half-life, non-uniform oral absorption, compromised tissue penetration and non-selective biodistribution (Reddy *et al.*, 2016). To overcome these underlying predicaments the multipronged approach incorporating potent biological agents together with nanotechnology is rapidly gaining ground. The desirable inherent properties of nanomaterials hold great promise in the treatment of cancer. Their favourable size, shape and surface morphology are bringing the “magic bullet” concept envisioned by Paul Ehrlich into realisation. Nanotechnology provides a dynamic strategy to exploit pathophysiological tumour abnormalities, bypass tedious biological barriers, infiltrate deep into subcellular compartments, and deliver therapeutic agents to their pathological target site, thus improving their therapeutic efficiency (Couvreur, 2013, Lammers *et al.*, 2010).

Of the multitude of framework materials envisioned to deliver drugs safely, AuNps and PtNps have emerged most promising owing to their inert core, high atomic number and enhanced optical and structural properties. Moreover, they can be easily fabricated within a favourable biomedical size range to possess high colloidal stability giving them the advantage over other nanoparticulate systems (Arvizo *et al.*, 2012). Interestingly, noble metals possess the ability to absorb light or radiowaves, which has generated a new wave of non-invasive cancer therapy options including, photodynamic therapy (PDT) and radiotherapy, which can

be utilised with chemotherapy for better eradication of tumour cells (Misra *et al.*, 2010). While AuNps are bio-inert, stable and relatively non-toxic in biological systems, PtNps possess chemotherapeutic and chemo-preventative properties (Buchtelova *et al.*, 2017, Yamada *et al.*, 2015). These remarkable features have inspired research into the synthesis of hybrid PtAuBNps, imbued with properties of both metals as well as novel properties through quantum confinement and synergism. In fact, many of these hybrid materials have replaced their monometallic counterparts in chemical processing as catalysts to drive the Hendry reaction, Suzuki-Miyaura reaction and oxidation reactions (Toshima and Yonezawa, 1998, Toshima *et al.*, 1990). Recently, the synergistic combination of noble metals has presented its potential in nanomedicine, particularly in cancer therapy as drug delivery vehicles and theranostic agents (Liu *et al.*, 2016). Modern metallurgy on the nanoscale presents unique features including an enhanced band gap, surface chemistry, photoluminescence, electrical and magnetic properties that excel rivalling monometallic systems (Cheng *et al.*, 2010). Furthermore, through embracing surface functionalisation paradigms, these modern platforms can be tailored to release their payloads through either passive and sustained drug release or active targeting for site-specific drug delivery.

Chitosan (CS), a polycationic biopolymer is an exceptionally popular stabilising agent in drug delivery owing to its biodegradability, non-toxicity, mucoadhesiveness, feasibility and permeation enhancing effects (Kumar *et al.*, 2016). In recent years, CSNps have emerged as promising carriers for sustained release preparations, to improve storage stability, solubility and prolong the half-life of anticancer drugs (Singla and Chawla, 2001). The ionic gelation reaction based on the electrostatic interaction between the amine group of chitosan with TPP is a facile and inexpensive way to form chitosan nanospheres endowed with its inherent characteristics (Elgadir *et al.*, 2015). The entangled polymeric framework provides a large surface area to volume ratio for the encapsulation of PtAuBNps and 5-FU. In addition, the flexible nature of the cross-linked framework allows the tailored release of drugs through pH-induced gel-sol transitioning (Chandran and Sandhyarani, 2014). The addition of the PEG bearing emulsifier Tween 80 has stabilising effects and confers the CS nanocomposites with fusogenic properties similar to dioleoylphosphatidylethanolamine (DOPE) (Huang *et al.*, 2011). This is essential for successful endolysosomal escape and maximising the transport of 5-FU into the nucleus to exert its cytotoxic effects. It is anticipated that precisely engineered target activated delivery systems, instilled with good physiochemical characteristics will bring about site-specific cancer targeting through apoptosis induction.

In this study, PtAuBNps and 5-FU were ensconced into an entangled CS framework to support (1) favourable physiochemistry, (2) high mucoadhesive propensity, (3) pH-responsive release and (6) site-specific induced toxicity *in vitro* (Figure 4.1). Currently, there is a dearth of scientific knowledge regarding the cytotoxicity, delivery and therapeutic capabilities of PtAuBNps. To the best of our knowledge, this is the first reported delivery of 5-FU with PtAuBNps.

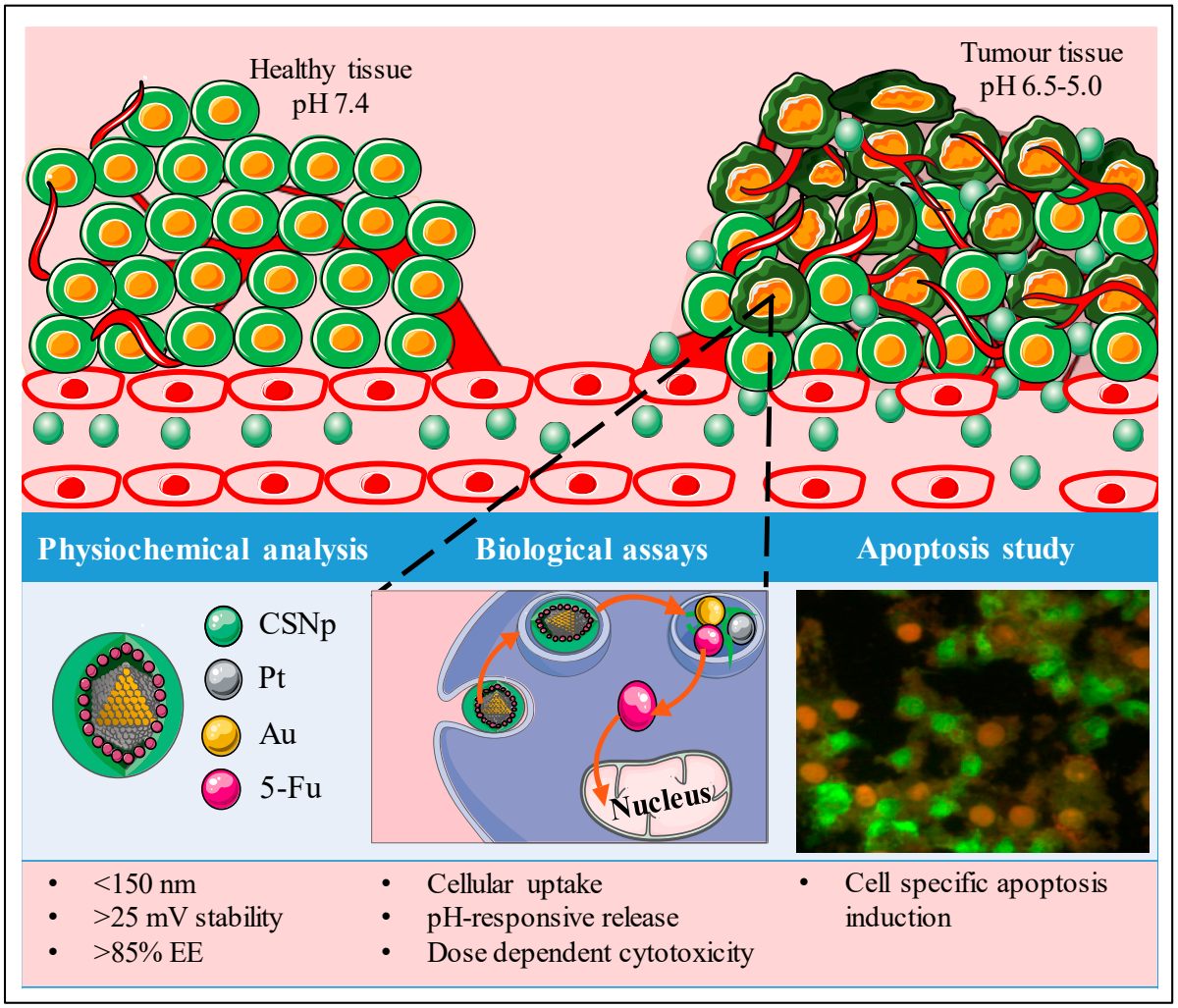

Figure 4.1: Schematic illustration of 5-fluorouracil encapsulated platinum-gold/chitosan bimetallic nanoparticles for systemic delivery and release to mildly acidic cancer cells leading to cytotoxic responses and apoptosis induction.

4.2. Materials and methods

Hydrogen hexachloroplatinate(IV) hexahydrate ($H_2PtCl_6.6H_2O$, Mw:517.90 g mol^{-1}), gold (III) chloride trihydrate ($HAuCL_4.3H_2O$, Mw: 393.83 g mol^{-1}), polyvinylpyrrolidone (PVP, Mw 40,000), sodium borohydride ($NaBH_4$, Mw 37.83 g mol^{-1}), sodium triphosphate ($Na_5P_3O_{10}$, Mw: 367.86 g mol^{-1}), sulforhodamine B (SRB Dye, $C_{27}H_{30}N_2O_7S_2$, Mw: 558.67 g mol^{-1}), 5-fluorouracil (5-FU, $C_4H_3FN_2O_2$, Mw: 130.1 g mol^{-1}), polysorbate 80 (Tween 80, Mw: 1,310 g mol^{-1}, $C_{64}H_{124}O_{26}$), acridine orange hemi (zinc chloride) salt [3,6-Bis(dimethylamino) acridine hydrochloride zinc chloride double salt] ($C_{17}H_{19}N_3$, Mw: 265.36, g mol^{-1}), chitosan (75% deacetylation) and dialysis tubing (MWCO ~ 12000 Daltons) was purchased from Sigma-Aldrich (St. Louis, USA). Ethidium bromide, glacial acetic acid, dimethyl sulfoxide [DMSO], 3-[(4,5-dimethylthiazol-2-yl)-2,5-diphenyl-2H-tetrazolium bromide] (MTT) and phosphate buffered saline tablets [PBS, (140 mM NaCl, 10 mM phosphate buffer, 3 mM KCl)] were sourced from Merck (Darmstadt, Germany). Eagle's Minimum Essential Medium (EMEM) with L-glutamine (4.5gL^{-1}), trypsin-versene-EDTA mixture and antibiotic mixture [(penicillin (10000 U/mL), streptomycin (10000 μg/mL), and amphotericin B (25 μg/mL)] were purchased from Lonza BioWhittaker (Verviers, Belgium). Sterile foetal bovine serum (FBS) was purchased from Hyclone GE Healthcare (Utah, USA). Human embryonic kidney cells (HEK293), breast adenocarcinoma (MCF-7), human epithelial colorectal adenocarcinoma cells (Caco-2), and human hepatocellular carcinoma cells (HepG2) was obtained from the ATCC (Pty) Ltd, Manassas, Virginia, USA. All sterile tissue culture plasticware were obtained from Corning Inc., (New York, USA). All chemical reagents were of analytical quality and were used without further purification. Ultrapure (18 MOhm) water (Milli-Q50, Millipore, France) was used throughout.

4.2.1. Preparation of bimetallic $Pt_{50}Au_{50}$ nanoparticles (PtAuBNps)

The PtAuBNps where prepared by concomitant chemical reduction of $HAuCL_4.3H_2O$ and $H_2PtCl_6.6H_2O$ with $NaBH_4$ in the presence of a PVP stabiliser. Briefly, an aqueous solution of PVP (0.44 mM, 50 mL) was added to the $HAuCl_4.4H_2O$ (25 mL, 0.44 mM) solution under gentle, constant stirring at 0°C for 15 min. Thereafter, 25 mL of $H_2PtCl_6.6H_2O$ (0.4 mM) was added and stirred for 30 min at 0°C. This was followed by a rapid injection of $NaBH_4$ (6.67 mL, 16.5 mM, 0°C) under vigorous stirring, until a dark brown colloidal suspension of PtAuBNps were formed. The final concentration of synthesised BNps was 0.18 mg/mL.

4.2.2. Preparation of nanocomposites

The anticancer drug 5-FU was encased within a Tween 80 stabilised CS based nanocomposite. Briefly, a 0.75 mg/mL CS solution (in 2% glacial acetic acid) was added to 3.8 mM of 5-FU solution (in 18 Mohm water) in a 1:1 ratio ($^{v}/_{v}$) with constant mixing. Thereafter, Tween 80 (0.5% $^{v}/_{v}$) was added as a surfactant, and the pH adjusted to 4.8 with 0.1 M NaOH. The prepared drug-polymer solution was mixed with 1.4 mM TPP solution to obtain a CS: TPP ratio of (2:1 $^{v}/_{v}$). The nanoparticle suspension was gently stirred for 30 min to allow adsorption of 5-FU onto the CSNps (CTF). Finally, 0.18 mg/mL of colloidal PtAuBNps was added dropwise to the CTF nanoparticles at a ratio of (1:1 $^{v}/_{v}$) under gentle, constant stirring for 180 min, forming the nanocomposite PtAu-CS-TPP-5-FU/Tween 80 (PACTF). Finally, all drug loaded nanocomposites were purified by centrifugation at 15 000 rpm at 4°C for 15 min (Beckman Ultracentrifuge), and the pellet re-dispersed in 18 Mohm water. The theoretical drug concentrations are outlined in Table 4.3.

4.2.3. Imaging, nanoparticle sizing and zeta potential analysis

The surface morphology, uniformity and size distribution of PtAuBNps, PtAuCSBNps, PACTF and CTF were investigated using TEM (JEOL JEM 1010, Tokyo, Japan, functioning at 100 kV). Aqueous solutions of Nps/nanocomposites were deposited onto separate formvar/carbon coated 40- mesh copper grids (Ted Pella Inc. Redding, USA), and air dried. Images were recorded using the iTEM Soft Imaging Systems (SIS) Megaview III fitted with a side-mounted 3-megapixel digital camera.

The particle size distribution, particle concentration and colloidal stability were measured by NTA (Nanosight NS500; Malvern Instruments, Worcestershire, UK). Briefly, the system was primed, flushed with 18 mohm water and the camera set to the zero position. All PtAuBNps formulations were diluted 1:1000 in 18 mohm water and run in triplicates. Individual particles undergoing Brownian motion are captured and visualised through the light they scatter upon laser illumination. The NTA software measures the theoretical hydrodynamic diameter of particles by application of the Stokes-Einstein equation and the ζ potential by Laser-Doppler microelectrophoresis through Smoluchowski modelling. All measurements were performed at 25°C and 24 V.

4.2.4. UV-Vis spectrophotometry analysis

The confirmation of the PtAu core-shell formation, successful chitosan polymerisation and 5-FU entrapment was based on the optical changes of specific samples and verified against that in known literature. Briefly, solutions of approximately 10 µL were analysed over a wavelength range of 200-800 nm using a UV-vis spectrophotometer (JASCO V-730, Japan).

4.2.5. Chemical composition analysis

To identify surface-bound functional groups, and the chemical interactions between the carrier and that drug, ATR-FTIR analysis were conducted in a Perkin Elmer spectrum 100 FTIR spectrometer equipped with a diamond universal ATR sampling accessory. The spectra were acquired at a programmed range of 400-4000 cm^{-1} at a 1 cm^{-1} resolution. The spectra requisition was carried out using the Spectrum 10 analysis software (Perkin Elmer).

4.2.6. Binding studies

The entrapment efficiency (EE) and loading content (LC) was estimated by the amount of drug liberated after centrifugation. Briefly, drug laden nanocomposites were centrifuged at 21 000 rpm for 15 min at 10°C (Beckman Ultracentrifuge), to separate the bound and unbound drug. The analysis of 5-FU content present in nanocomposites was determined by UV-Vis spectroscopy at a wavelength 481 nm. All the samples were measured in triplicates. The theoretical drug content (TDC), entrapment efficiency (EE), actual drug content and loading capacity (LC) were calculated using Equations (4.1-4.4).

$$\text{TDC } (\mu g) = \frac{\text{Weight of 5-FU}}{\text{Weight of nanocomposite}} \tag{4.1}$$

$$\text{EE } (\%) = \frac{\text{Total 5-FU added - Free 5-FU}}{\text{Total 5-FU added}} \times 100 \tag{4.2}$$

$$\text{ADC } (\mu g) = \text{TDC} \times \text{EE } (\%) \tag{4.3}$$

$$\text{LC } (\%) = \frac{\text{Total 5-FU added - Free 5-FU}}{\text{weight of nanocomposite}} \times 100 \tag{4.4}$$

4.2.7. *In vitro* interactions with porcine mucin

The bioadhesive propensity of the nanocomposites was studied *in vitro* as a means of the rheological synergism that occurs at the functional group level between nanoparticles/nanocomposites and the porcine mucin model. Approximately, 1 mL of porcine mucin (PM, 400 µg/mL) suspension in simulated intestinal fluid (25% $^{v}/_{v}$, pH 6.8) was mixed with 1 mL of the respective nanocomposite suspensions (20 µg/mL), and gently shaken (50 rpm) at 37°C for 6 h. Thereafter, free PM was separated by centrifugation at 21 000 rpm for 30 min at 10°C (Eppendorf 5424R). The degree of interaction between the nanocomposites and mucin was determined by measuring the absorbance of the remaining free PM in the supernatant in a spectrophotometer set at wavelength of 251 nm, with intestinal fluid as the blank. The percentage mucoadhesion was calculated using Equation 4.5.

$$\text{Mucoadhesion (\%)} = \frac{\text{Total Mucin before - Free Mucin after}}{\text{Total Mucin before}} \times 100 \qquad (4.5)$$

4.2.8. Pharmacokinetic studies

The ability of prepared nanocomposites to release the loaded drug in response to specific biological environments was investigated. Approximately, 5 mL of drug loaded nanocomposites (50 µg/mL) was placed in a dialysis bags (MWCO 2000 Da), hermetically sealed and immersed in 10 mL of PBS (7.4, 6.5, 5.0 and pH 4.5), with gentle stirring at 37°C. Periodically, 10 µL of aliquots were withdrawn and analysed. The amount of 5-FU released was determined using UV-Vis spectroscopy at 266 nm. The cumulative drug release percent was calculated relative to the total absorbance of 5-FU loaded onto nanocomposites using Equation (4.6).

$$\text{Cumulative (\%)} = \frac{\text{Abs of free 5-FU}}{\text{Abs of total 5-FU loaded}} \times 100 \qquad (4.6)$$

Finally, the drug release data were modelled using the zero-order, first-order, Higuchi's square root of time equation and the Korsmeyer-Peppas power law kinetic equation's (Patel *et al.*, 2008, Ramteke *et al.*, 2014, Singhvi and Singh, 2011), as shown in Table 4.1.

Table 4.1: Time-dependent pharmacokinetic modelling of dissolution data to ascertain drug release mechanisms at acidic and physiological pH conditions.

Kinetic model	Equation
Zero-order	$R_t=R_0 + K_0t$
First-order	$Ln\ R_t = lnR_0+ K_1t$
Higuchi	$R_t=K_Ht^{1/2}$
Korsmeyer-Peppas	$R_t/R_\infty = K_kt^n$

K_0, K_1, K_H, K_k: Release rate constants; n: Release exponent (indicative of drug release mechanism); R_0: initial amount of 5-FU in the nanocomposite; R_∞: Total amount of drug dissolved when the dosage form is exhausted; R_t: Amount of 5-FU released at time t.

4.2.9. Cell culture

All cells were cultured in complete EMEM supplemented with 10% FBS and 1% antibiotics. The cells were maintained in 25 cm^2 culture flasks under standard culture conditions (37°C, 5% CO_2 and 95% relative humidity) and were sub-cultured every two-three routinely with trypsin-EDTA (Appendix B). All biological assays were conducted under aseptic conditions in an Airvolution Class II biosafety laminar flow hood.

4.2.10. *In vitro* cytotoxicity assessment

The antitumour activities of PtAuBNps and their nanocomposites were evaluated *in vitro* by using the MTT and SRB assay on three cancer cell lines (Caco-2, HepG2 and MCF-7) and a non-cancerous cell line (HEK293). Exponentially growing cells were trypsinised, seeded in a 96-well plate at a cell density of 2.5×10^2 cells/well and incubated overnight at 37°C. Thereafter, spent medium was replenished with 100 µL fresh growth medium, to which the respective compounds were added at various concentrations (5, 15, 35 and 50 µg/mL), and incubated for 48 h at 37°C. Wells containing cells only served as the positive control. All assays were done in triplicate. The MTT and SRB assay were carried out in different procedures described below, after the 48-hour incubation period. The cell viability (%) in each of the assays was calculated using Equation (4.7).

$$\text{Cell viability (\%)} = \frac{\text{Abs of treated cells}}{\text{Abs of untreated cells}} \times 100 \qquad (4.7)$$

4.2.10.1. MTT assay

The culture medium was aspirated and replenished with 100 µL of EMEM and MTT reagent (5 mg/mL in PBS) and incubated for 4 h at 37°C. Thereafter, the MTT-medium solution was carefully removed, and 100 µL of DMSO added to each well to ensure cell permeation and solubilisation of the formazan sediment. Absorbance was read using a Mindray MR-96A microplate reader (Vacutec, Hamburg, Germany) at 570 nm with DMSO as a blank.

4.2.10.2. SRB assay

The cell monolayers were fixed by gently layering 25 µL of cold TCA (50% $^{w}/_{v}$) onto the spent growth medium. The cells were incubated for 1 h at 4°C, washed (3x) with distilled water and air dried. The TCA-fixed cells were then stained with 50 µL of SRB (0.4% $^{w}/_{v}$ in 1% glacial acetic acid) dye for 30 min at 37°C, washed (3x) with 1% acetic acid to remove the non-ligated dye, and the plates air dried. Finally, the protein-bound dye was extracted with 100 µL of Tris buffer (10 mM, pH 10.5), and plates read on a Mindray MR-96A microplate reader at 565 nm using Tris base as the blank.

4.2.11. Apoptosis assay

The acridine orange/ethidium bromide (AO/EB) dual staining method is a convenient, rapid and economical method for the quantitative and qualitative analysis of possible apoptosis induction by the drug laden PtAuBNps. Cells were seeded at a cell density of 1.5 x 10^5 in a 24 well plate and incubated at 37°C in 5% CO_2 for 24 h, to allow cell attachment. Thereafter, the culture medium was aspirated, replenished with 0.5 mL of complete medium, and cells were treated with nanocomposites at predetermined IC_{50} values (average of the two assays). A nanoparticle/nanocomposite free positive control was included. After, a 24 h incubation at 37°C, spent medium was removed, and cells washed (2x) with 100 µL of cold PBS. Cells were stained with 12 µL of the dye solution (1:1 $^{v}/_{v}$ AO: EB, 100 mg/mL in PBS) for 5 min. Cells were viewed under an Olympus fluorescent microscope (200x magnification), fitted with a CC12 fluorescent camera (Olympus Co., Tokyo, Japan). The number of viable cells and apoptotic bodies were tallied using the Soft Imaging System (SIS) software (Olympus Co., Tokyo, Japan). The apoptotic indices were calculated according to Equation (4.8).

$$\text{Apoptotic Index} = \frac{\text{Number of Apoptotic cells}}{\text{Total number of cells counted}} \quad (4.8)$$

4.2.12. Statistical analysis

The results in triplicate are reported as mean ± SD (standard deviation). All statistical analyses were performed using GraphPad Prism version 5.01 (GraphPad Software Inc., La Jolla, CA, USA). The significance of results and differences between the control and test were determined using a one-way analysis of variance (ANOVA). The Dunnett's post hoc test was used for the growth inhibition assays. Statistical significance between groups was considered significant at **$p<0.01$ and * $p<0.05$. Dissolution kinetics parameters were evaluated using Microsoft Excel 2016 ™ and DD Solver software. The parameters are indicated in Table 4.1. The best-fit dissolution profile was identified at r^2 values ≥ 0.99.

4.3. Results and discussion

4.3.1. Nanoparticle morphology, sizing and zeta potential

The ultrastructural morphology, distribution and uniformity of all nano-formulations were examined using TEM. The TEM images of PtAuBNps, PtAuCS Nps, PACTF and CTF nanocomposites are presented in Figure 4.2 A-D. The PtAuBNps (Figure 2 A) displayed a near spherical morphology and were well dispersed due to passivation with PVP, as observed in the literature (Ekrami-Kakhki *et al.*, 2011, Khalil *et al.*, 2014, Zhang and Toshima, 2013). All CS based nano-formulations (Figure 2 B-D) presented predominantly monodispersed, uniform spherical nanostructures with smooth surfaces. There was an evident increase in size for the drug bearing nanocomposites CTF (Figure 4.2 C), and PACTF (Figure 4.2 D), with the latter appearing denser and more compact. The morphological features and colouration of the CSNps, were similar to previously reported findings (Hou *et al.*, 2017, Mohammadpour Dounighi *et al.*, 2012). Characteristically, metallic nanoparticles with high atomic numbers possess excellent light scattering power and appear dark in colouration. Nanocomposite PACTF appeared to have areas of dark pigmentation, suggesting the presence of small-sized PtAuBNps within dense chitosan cross-linked nanospheres.

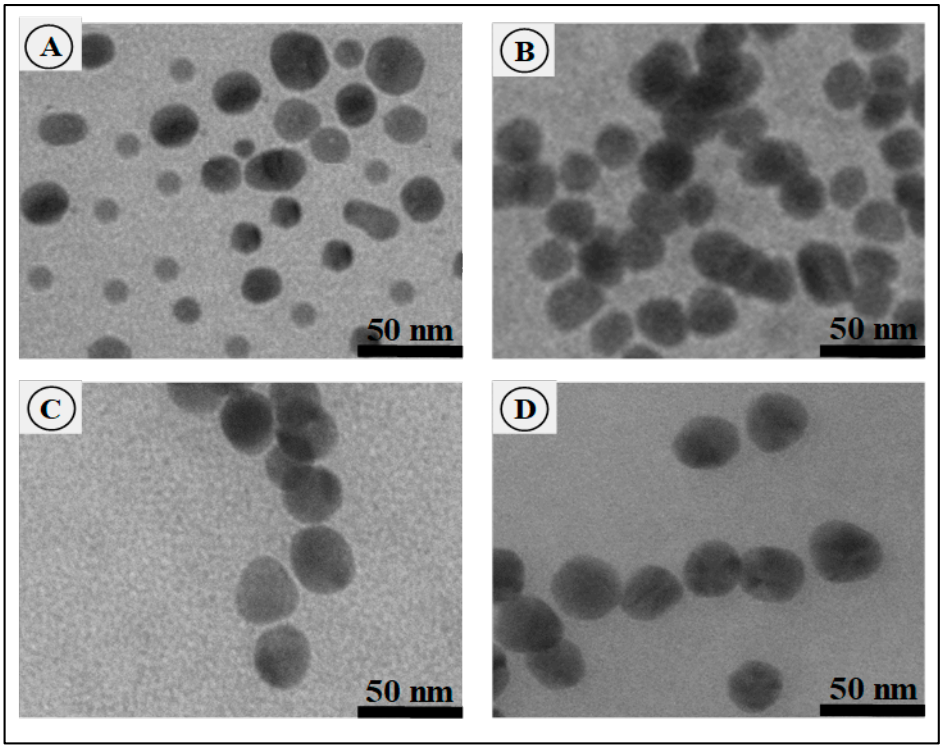

Figure 4.2: TEM micrographs of (A) PtAuBNps, (B) PtAuCSBNps, (C) CTF, (D) PACTF. Bar = 50 nm.
CTF: CS-TPP-5-FU/Tween 80; PACTF: PtAu-CS-TPP-5-FU/Tween 80.

Zeta (ζ) potential is the magnitude of the electrostatic potential generated on the edge of the slipping plane between the particle and the dispersant medium. In general, particles displaying a ζ potential value higher than 30 mV or -30 mV, will have a strong degree of electrostatic repulsion between adjacent similarly charged particles, leading to better colloidal dispersion (Doostmohammadi *et al.*, 2012). On the other hand, a ζ potential less than 15 mV or -15 mV, will have attractive forces that exceed repulsive forces, causing particles to aggregate. The NTA results (Table 4.2 and Appendix C5-C8) strongly correlated with the TEM results. NTA analysis revealed PtAuBNps to have a hydrodynamic size of 69.9 ± 3.2 nm and ζ potential of -21.5 mV. Conjugation of CS to PtAuBNps increased the average hydrodynamic size to 88.4 ± 10.8 nm, with a shift from a negative to a highly positive ζ potential value (58.2 ± 1.1 mV). This finding was in keeping with similar analysis conducted on CS functionalised AuNps (Boyles *et al.*, 2015, Chen *et al.*, 2015). The change in surface potential for PtAuCSBNps suggest strong electrostatic interactions between the protonated CS and the negatively charged surface of the PtAuBNps. Such high surface potential imparts a high degree of colloidal stability, to facilitate efficient cellular uptake by the negatively charged cell membrane. The loading of 5-FU brought about an increase in size to 118.8 ± 8.6 nm for CTF

and 108.6 ± 8.2 nm for PACTF. Furthermore, CTF (28.3 ± 2.6 mV) and PACTF (30.5 ± 0.6 mV) had lower ζ potentials than PtAuCSBNps, which can be ascribed to the consumption of free amine groups through TPP cross-linking and drug encapsulation, which corroborates the FTIR findings. The smaller hydrodynamic size of PACTF is possibly due to the addition of PtAuBNps which condensed the CS framework. Overall, all the drug bearing nanostructures displayed the physiochemical properties deemed to be critical for better tissue penetration, long-term storage and enhanced therapeutic effects.

Table 4.2: Size distribution and zeta potential of BNps and its nanocomposites. Data represented as mean ± SD (n=3).

Sample	Particle Size (nm)	ζ Potential (mV)
PtAuBNps	69.9 ± 3.2	-21.5 ± 1.4
PtAuCSBNps	88.4 ± 10.8	58.2 ± 1.1
PACTF	108.6 ± 8.2	30.5 ± 0.6
CTF	118.8 ± 8.6	28.3 ± 2.6

Data represented as mean ± SD.
CTF: CS-TPP-5-FU/Tween 80; PACTF: PtAu-CS-TPP-5-FU/Tween 80

4.3.2. UV-Vis and FTIR spectroscopy

Spherical AuNps dispersed in water display a strong SPR absorbance band in the visible region (520 nm), and PtNps in the near-infrared region (220 nm), which is attributed to in-plane dipole resonance (Hung *et al.*, 2016). Figure 4.3 shows the UV-Vis spectroscopy analysis of PtAuCSBNp's, PACTF, CTF and 5-FU. The SPR of PtAuBNPs (Figure 4.3 A) presented as a single narrow peak centred at 224 nm, correlating with literature and confirming the successful synthesis of core-shell nanostructures (Testa *et al.*, 2016). The formation of Au core-Pt shell nanostructures is accompanied by a blue shift and quenching of AuNps' SPR as Pt shell atoms epitaxially nucleate and grow on the surface of the Au core, until there is complete disappearance of the AuNps SPR (Fan *et al.*, 2008). Chitosan functionalised PtAuBNps (Figure 4.3 B) exhibited a single broad red shift with an SPR resonant extinction peak at 235 nm, indicating a change in the local refractive index due to successful polymer conjugation and an increase in particle size. The red shift following polymer conjugation was anticipated as previously reported (Guan *et al.*, 2013, Sugunan *et al.*, 2005). Successful encapsulation and loading of 5-FU were confirmed in the nanocomposites PACTF and CTF (Figure 4.3 C-D).

The characteristic absorbance peak of 5-FU at 266 nm (figure 4 E) displayed a blue shift to 261 nm and 263 nm for PACTF and CTF respectively. This phenomenon has previously been reported and confirms the successful encapsulation of 5-FU (Chandran and Sandhyarani, 2014).

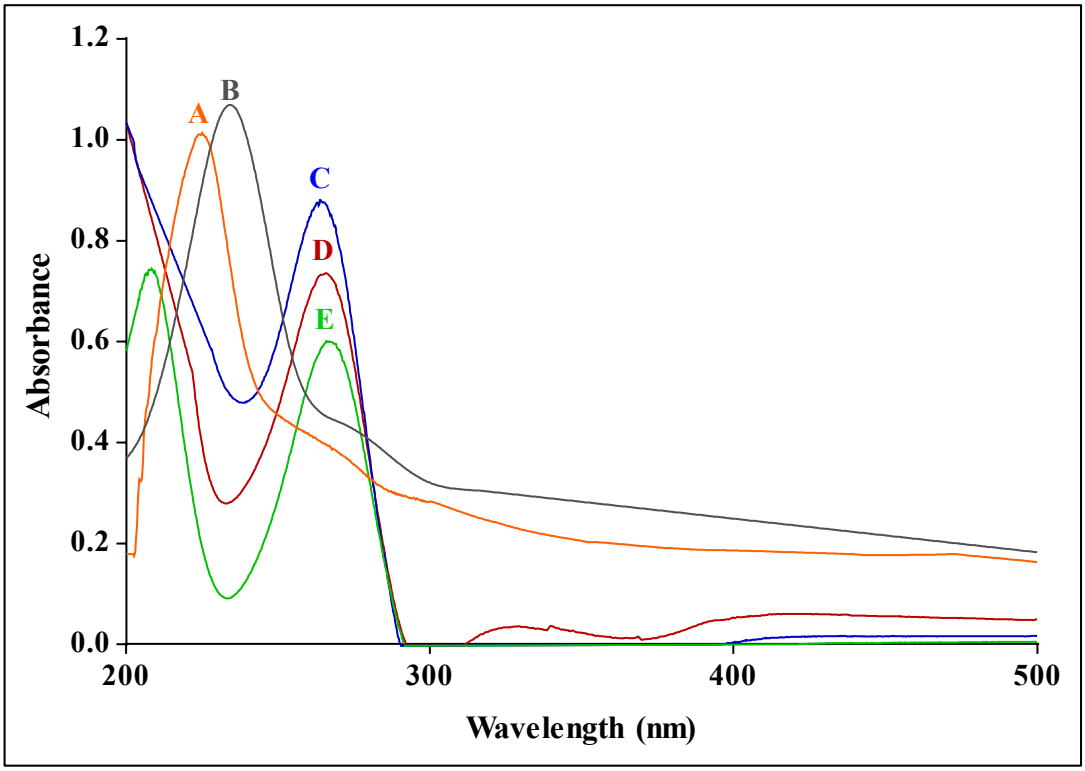

Figure 4.3: UV-Vis spectra of (A) PtAuBNps, (B) PtAuCSBNps, (C) PACTF, (D) CTF and (E) 5-FU in ultrapure water.
5-FU: 5-Fluorouracil; CTF: CS-TPP-5-FU/Tween 80; PACTF: PtAu-CS-TPP-5-FU/Tween 80.

FTIR is a well-established technique to identify and confirm the functional groups present by the magnitude, relative intensity and shape of the absorption bands that arise through stretching and deformation vibration. FTIR spectroscopy confirmed the chemical structure and functional groups present in CS, PtAuCSBNp, PACTF, CTF and 5-FU (Figure 4.4). The FTIR spectrum of pure 5-FU (Figure 4.4 A) displayed aliphatic and aromatic vibrational bands between 3070-2825 cm^{-1}. Peaks at ~ 1726 cm^{-1} are ascribed to imide C=O stretching of the heterocyclic ring, at ~ 1669 cm^{-1} due to N-H vibrations and at ~ 1504 cm^{-1} due to alkenyl C=C stretching. Finally, a band at ~ 1428 cm^{-1} is ascribed to C-H in-plane bending of the CF=CH group, at ~ 1242 cm^{-1} due to C-N wagging and peaks between 810-750 cm^{-1} are attributed to CH out of plane vibrations of the CF=CH group (Kevadiya *et al.*, 2012, Nivethaa *et al.*, 2015).

The spectra of CS (Figure 4.4 B) exhibits OH stretching and N-H stretching of the amide A band at ~ 3352 cm^{-1}, stretching vibrations of C-H bond at ~ 2935 cm^{-1}, C=O stretching of the amide I band at ~ 1647 cm^{-1}, bending vibrations of the N-H group of the amide II band at ~ 1573cm^{-1}, anti-symmetric stretching of the (C-O-C) bridge at ~ 1150 cm^{-1}, and NH_2 twisting peak at ~ 895 cm^{-1}, are observed, and correspond to the peaks of CS observed in the literature (Lawrie *et al.*, 2007, Sanyakamdhorn *et al.*, 2013).

Interestingly, drug loaded nanocomposites (Figure 4.3 C-D) displayed the signature stretching and deformation vibrations similar to CS and 5-FU, suggesting successful loading of the drug. Both carriers exhibited characteristic absorption peaks at ~ 2919 cm^{-1}, attributed to C-H stretching, and at ~ 1645 cm^{-1} ascribed to C=O amide I band stretch vibrations. Further signals at ~ 1570 cm^{-1} due to N-H bending vibrations, at ~ 1150 cm^{-1} due to C-O-C stretching, and at ~ 755 cm^{-1} due to C-H plane vibrations of the CF=CH functional group, were observed. These results corroborated well with that of the UV-Vis spectroscopy, confirming the successful loading and encapsulation of 5-FU within the CS based nanocomposites.

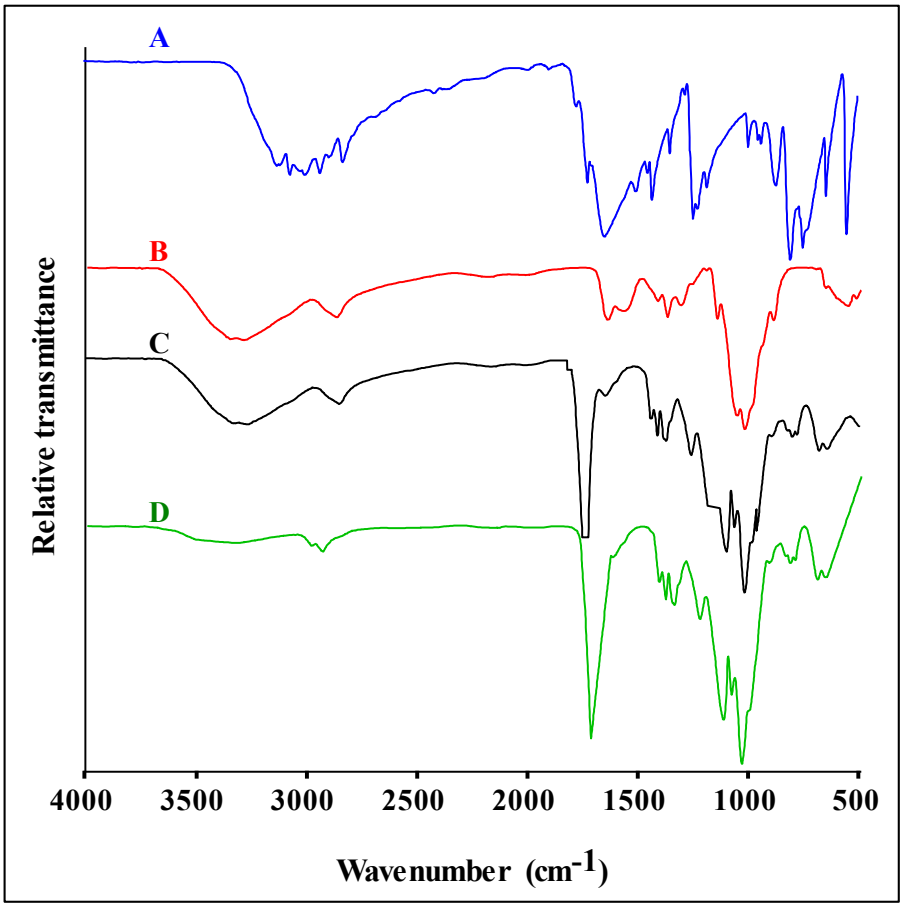

Figure 4.4: FTIR Spectra of (A) PACTF, (B) CTF, (C) CS and (D) 5-FU
5-FU: 5-Fluorouracil; CTF: CS-TPP-5-FU/Tween 80; PACTF: PtAu-CS-TPP-5-FU/Tween 80

4.3.3. Drug binding studies

The efficacy of the drug delivery system to encapsulate 5-FU was determined through UV-Vis spectroscopy. Through exerting a centrifugal force, drug bound nanocomposites in solution can be separated from the unbound drug in the supernatant. As anticancer drugs are expensive, obtaining a high entrapment efficiency is an important prerequisite to deliver therapeutic agents in small dosage. The encapsulation efficiency (EE) and loading content (LC) are shown in Table 4.3. The EE and LC of 5-FU was found to be 90.17% and 22.56% in PACTF, while CTF had a lower EE of 87.24% and a higher LC of 23.24%. These results suggest that there is a strong correlation between ζ potential analysis and EE, with a higher ζ potential in PACTF relating to a higher EE, while the compactness possibly resulted in the lower LC. These findings were consistent with similar 5-FU binding studies conducted with CS/Au nanocomposites (Nivethaa *et al.*, 2015).

Table 4.3: Drug loading efficiency, theoretical drug content, actual drug content and drug loading content of nanocomposites.

Sample	TDC (µg)	EE (%)	ADC (µg)	LC (%)
CTF	139.21	87.24	121.45	23.24
PACTF	96.34	90.17	88.80	22.56

ADC: Actual drug content; CTF: CS-TPP-5-FU/Tween 80; EE: Drug loading efficiency; LC: Drug loading content; PACTF: PtAu-CS-TPP-5-FU/ Tween 80; TDC: Theoretical drug content.

4.3.4. Mucin binding study

The development of a bioadhesive drug delivery systems has the potential to increase the residence time at the application site, increase drug permeation and bioavailability. The *in vitro* mucoadhesion results reflecting the degree of binding between prepared nano-formations and porcine mucin (PM) are outlined in Table 4.4. A general observation was that nanoparticles/nanocomposites with a higher positive ζ potential achieved higher PM binding efficiencies. These findings support the notion that the positively charged amine groups of CS are mainly responsible for the carrier's bioadhesive propensity (Wang *et al.*, 2000). This phenomenon occurs specifically at the molecular level, through electrostatic interactions between the positively charged amino groups of CS and the negatively charged sulfonic acid resides in PM, bringing about rheological synergism (Pilicheva *et al.*, 2013). The CS functionalised PtAuBNps exhibited the highest PM binding efficiency (86.24 ± 3.82%), while

free drug and PtAuBNps, as anticipated, had a lower mucoadhesive ability, possibly due to charge repulsions. The drug laden nanocomposites, PACTF (68.74 ± 2.87%) and CTF (67.05 ± 4.21%), demonstrated a slightly lower degree of mucoadhesion than PtAuCSBNps, possibly due to the utilisation of the free surface amino groups through TPP cross-linking, resulting in weaker binding interactions. These results were in keeping with findings for similar studies conducted with CSNps (Nagarwal *et al.*, 2012, Srivastava *et al.*, 2016).

Table 4.4: Binding efficiencies of nanoparticles to porcine mucin.

Compound	Mucoadhesion (%)
PtAuBNps	8.72 ± 1.67
PtAuCSBNps	86.24 ± 3.82
PACTF	68.74 ± 2.87
CTF	60.05 ± 4.21
5-FU	21.51 ± 3.28

Data represented as mean ± SD (n=3).
5-FU: 5-Fluorouracil, CTF: CS-TPP-5-FU/Tween 80; PACTF: PtAu-CS-TPP-5-FU/Tween 80.

4.3.5. *In vitro* pharmacokinetics studies

Tumour tissue presents a unique microenvironment that is mildly acidic (pH 6.5-5.0) due to vascular irregularities, hypoxia and high glycolytic metabolism, that lead to the exacerbated production and accumulation of acidic metabolites. Acidity is further reduced in the intracellular organelles, such as endosomes and lysosomes (pH 5.5- 4.0), within the cancer cell (Du *et al.*, 2014, Yu *et al.*, 2014). Recently, pH-responsive release systems have emerged as an attractive means to selectively target tumour acidity, enhance the therapeutic index and reduce side effects by providing spatiotemporal control over drug release in the body (Kamaly *et al.*, 2016, Kong *et al.*, 2017). The pH-responsiveness of PACTF and CTF, and their pharmacokinetic profiles are shown in Figure 4.5 and Tables 4.5-4.6.

The release of 5-FU was exceptionally slow at neutral conditions for CTF (35.11% ± 1.17 in 24 h) and PACTF (30.80 ± 1.75 in 24 h), but accelerated at lower pH values. Both nanocomposites released rapidly at pH 4.5 with up to 70% of 5-FU eluted over the 24-h period. It was evident that CTF displayed a characteristic biphasic release pattern at acidic environments, comprised of an initial release surge over the first 10 h, followed by a slow

gradual release of 5-FU in a plateau phase for the subsequent 14 h. This release behaviour has previously been reported for polymeric nanoparticles (Dubey and Parikh, 2004, Shi *et al.*, 2012). The 24-h release percentage of CTF was approximately 68.2 ± 1.0, 74.4 ± 0.9 and 79.2 ± 0.97 at pH 6.5, 5.0 and 4.5 respectively. The initial burst displayed in the dissolution profile of CTF can be attributed to release of the surface-associated drug, while the long plateau phase is probably due to release of the encapsulated drug within the dense polymeric matrix (Rafiei and Haddadi, 2017).

Interestingly, PACTF displayed limited burst release at acidic conditions (pH 6.5, pH 5.0 and pH 4.5), providing a gradual release for 18 h and a 6-h slow release phase. This finding clearly demonstrates better encapsulation of 5-FU within the core of the PACTF nanostructure. Approximately, 54.0 ± 1.8%, 65.2 ± 0.66% and 74.1 ± 0.88% was eluted from PACTF at pH 6.5, 5.0 and 4.5 respectively. The pH-sensitive behaviour of PACTF and CTF can be attributed to conformational changes that take place in response to variations in physiological pH. At neutral conditions, CS remains stable/deprotonated, while at acidic conditions the protonation of the pendant amine groups causes the carriers to undergo gel-sol transitions, swell and releases the encapsulated drug into the bathing liquid (Islam and Yasin, 2012).

Kinetic modelling of the release data was conducted to further characterise the dissolution of 5-FU from the nanocomposites (CTF and PACTF) by analysing their goodness of fit. The dissolution of encapsulated drugs through the dialysis method is affected mainly by water imbibition, drug diffusion and polymer dissociation (Streubel *et al.*, 2000). The importance of the exponent n of the Korsmeyer-Peppas model, is that it can provide valuable insights into the release mechanism as either, Fickian diffusion ($0.45 \leq n$), non-Fickian (anomalous) diffusion ($0.45 < n < 0.89$), case II transport ($n = 0.89$) and super case II transport ($n > 0.89$) (Singhvi and Singh, 2011). At neutral milieu, the release from both nanocomposites closely followed the zero-order kinetic model with limited dissolution of 5-FU by non-Fickian diffusion. Similarly, release under acidic conditions followed the zero-order model ($r^2 = 0.977$), however, the liberation of 5-FU from CTF and PACTF occurred through anomalous diffusion. These findings suggest that 5-FU encapsulated within the CS based nano-formulations was retained, and released slowly over a prolonged period through a combination of diffusion and polymer erosion. Overall, both nanocomposites displayed pH-liable release, with PACTF displaying the best pharmacokinetics profile as it had limited burst release and a more linear zero-order release profile for enhanced therapeutic effects.

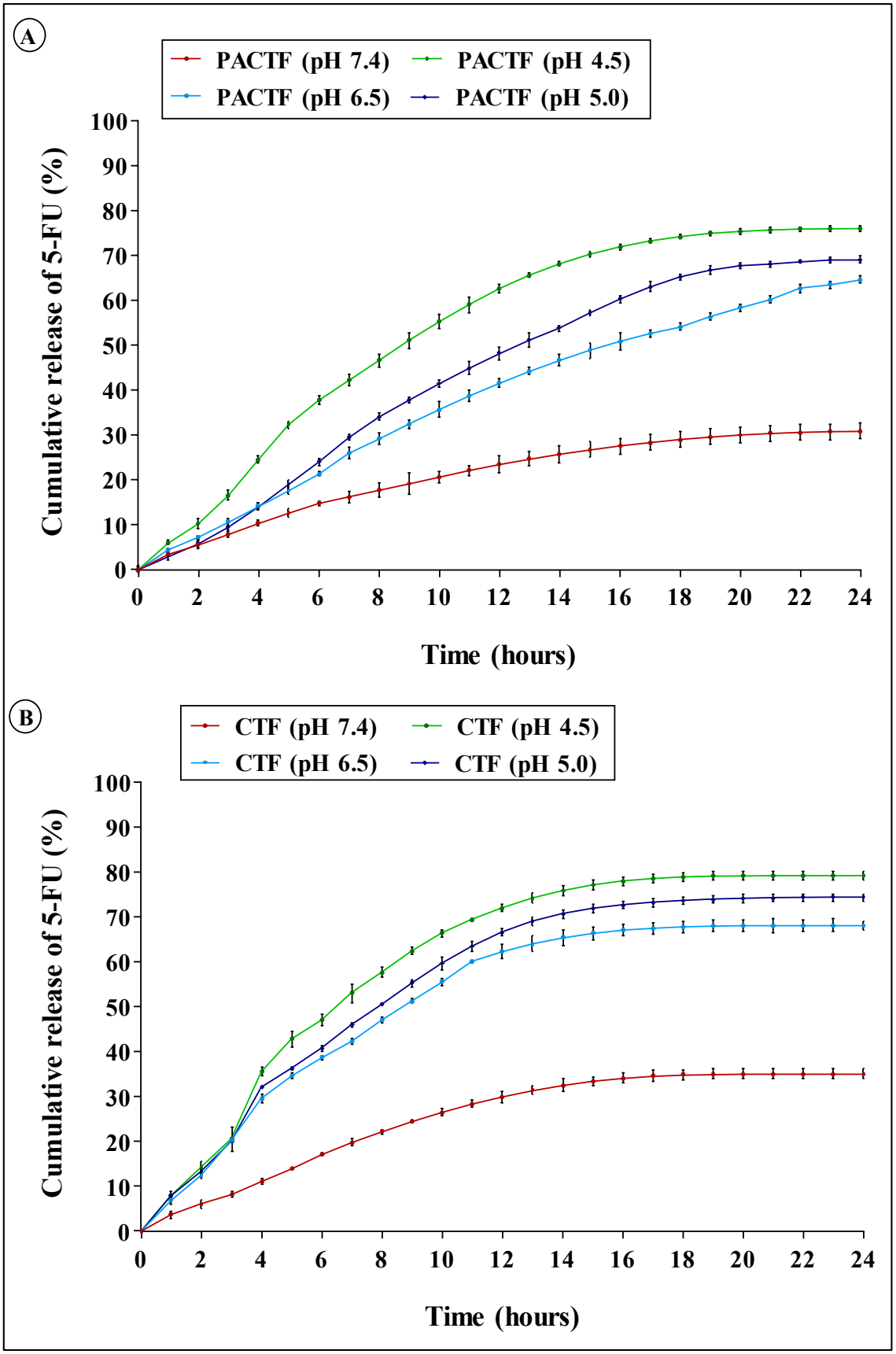

Figure 4.5: *In vitro* cumulative drug release profile of 5-fluorouracil encapsulated nanocomposites. (A) PACTF, (B) CTF, at pH 4.5, 5.0, 6.5 and 7.4.

CTF: CS-TPP-5-FU/Tween 80; PACTF: PtAu-CS-TPP-5-FU/Tween 80.

Table 4.5: Pharmacokinetic parameters of PACTF under stimulated conditions.

Environment	Zero-order		First-order		Higuchi		Korsmeyer-Peppas		
	r^2	K_0	r^2	K_1	r^2	K_H	r^2	K_k	n
pH 7.4	0.998	1.598	0.956	0.019	0.986	6.539	0.964	3.847	0.701
pH 6.5	0.998	3.028	0.997	0.044	0.993	12.183	0.924	4.388	0.877
pH 5.0	0.997	3.455	0.990	0.054	0.985	13.908	0.934	6.545	0.789
pH 4.5	0.997	4.077	0.966	0.071	0.959	16.709	0.966	7.486	0.806

K_0, K_1, K_H, K_k: release rate constants; r^2: correlation coefficient; n: release exponent (indicative of drug release mechanism).

Table 4.6: Pharmacokinetic parameters of CTF under stimulated conditions.

Environment	Zero-order		First-order		Higuchi		Korsmeyer-Peppas		
	r^2	K_0	r^2	K_1	r^2	K_H	r^2	K_k	n
pH 7.4	0.998	1.917	0.908	0.023	0.945	7.871	0.953	4.175	0.741
pH 6.5	0.998	3.818	0.899	0.062	0.916	15.823	0.965	9.637	0.693
pH 5.0	0.996	4.133	0.923	0.072	0.925	17.101	0.966	10.298	0.697
pH 4.5	0.996	4.457	0.913	0.0838	0.901	18.507	0.963	11.193	0.697

K_0, K_1, K_H, K_k: release rate constants; r^2: correlation coefficient; n: release exponent (indicative of drug release mechanism).

4.3.6. *In vitro* cytotoxicity

Bimetallic nanostructures are at a nascent stage of development and require preliminary toxicological screening *in vitro* to investigate their potentially harmful effects to cells in culture. The degree of toxicity exerted by PtAuBNp nano-formulations (PtAuCSBNps, PACTF and CTF) on a panel of human cell lines (HEK293, Caco-2, HepG2 and MCF-7 cell lines) was evaluated through the MTT and SRB assay. The MTT assay provides an estimation of cell viability centred on the principle that only metabolically active cells can convert MTT into a purple insoluble formazan product. The SRB assay estimates cell number by staining trichloroacetic acid fixed cellular protein with the pink aminoxanthine SRB dye (Keepers *et al.*, 1991). Principally, both approaches were conducted to provide a reliable assessment of cytotoxicity, since each method differs in their working principle and sensitivity.

The cytotoxicity profiles and IC_{50} values of PtAuBNPs, PtAuCSBNPs, CTF and PACTF are represented in Figures 4.6-4.7 and Tables 4.7-4.8 respectively. Overall, similar trends in

cytotoxicity in both assays suggest a strong correlation between the two colourimetric assays. It was found that the PtAuBNps exerted low cytotoxicity at the highest tested concentration with up to 75% maximum cell viability in all tested human cell lines in both assays. The cytotoxicity induced could have occurred through free radical-mediated DNA damage (Butterworth *et al.*, 2012). Interestingly, PtAuCSBNps displayed no relevant *in vitro* cytotoxicity and even stimulated the growth of the HEK293 cells, suggesting good biocompatibility and possibly CS moieties serving as a nutrient source. Exposure to pure 5-FU elicited a dose dependent decrement of cell survival to less than 45% in all cell lines. The free drug-induced cytotoxicity in the tested concentration range was similar to findings that were reported previously in the literature (Babaei *et al.*, 2017, Nivethaa *et al.*, 2015, Sahu *et al.*, 2017). Impressively, drug laden nanocomposites (PACTF and CTF) were well tolerated in the HEK293 cell line with more than 75% maximum cell viability, but inflicted significantly greater damage to all cancer cell lines compared to the 5-FU at equivalent concentrations. Drug loaded nano-formulations exerted the most profound antiproliferative effects in the Caco-2 cells with up to 30% cell viability at the highest tested dosage. The IC_{50} values of PACTF and CTF for the Caco-2 cells are approximately 18.98 µg/mL and 21.99 µg/mL in MTT assay, and 19.25 µg/mL and 22.58 µg/mL in the SRB assay. In the HEPG2 cell line, PACTF and CTF displayed slightly higher IC_{50} values, of approximately 22.85 µg/mL, and 25.21 µg/mL in the MTT assay and 23.10 µg/mL and 26.24 µg/mL in the SRB assay. The nanocomposites PACTF and CTF were least effective towards the MCF-7 cell line with high IC_{50} values of 29.73 µg/mL and 33.57 µg/mL in the MTT assay, and 30.12 µg/mL and 34.99 µg/mL in the SRB assay. The toxicity profiles obtained clearly support enhanced cytotoxicity after 5-FU loading. Notably, from the two nanocomposites, PACTF executed the most lethal anticancer activity *in vitro* in all cancer cell models, and demonstrated excellent tolerance by the non-cancerous HEK293 cell line. The results suggest that the addition of PtAuBNps acted synergistically with 5-FU to enhance cytotoxicity. These findings were in consonance with the physiochemical characterisations and drug release profiles. Basically, the combination of small size, cationic surface, high stability and excellent buffering capacity improved tissue penetration, uptake via the cell membrane by endocytosis, and release within the tumour vicinity. These underlying attributes promote better biotransformation of 5-FU into putative cytotoxic nucleotides that can affect the intracellular deoxynucleotides pools more proficiently.

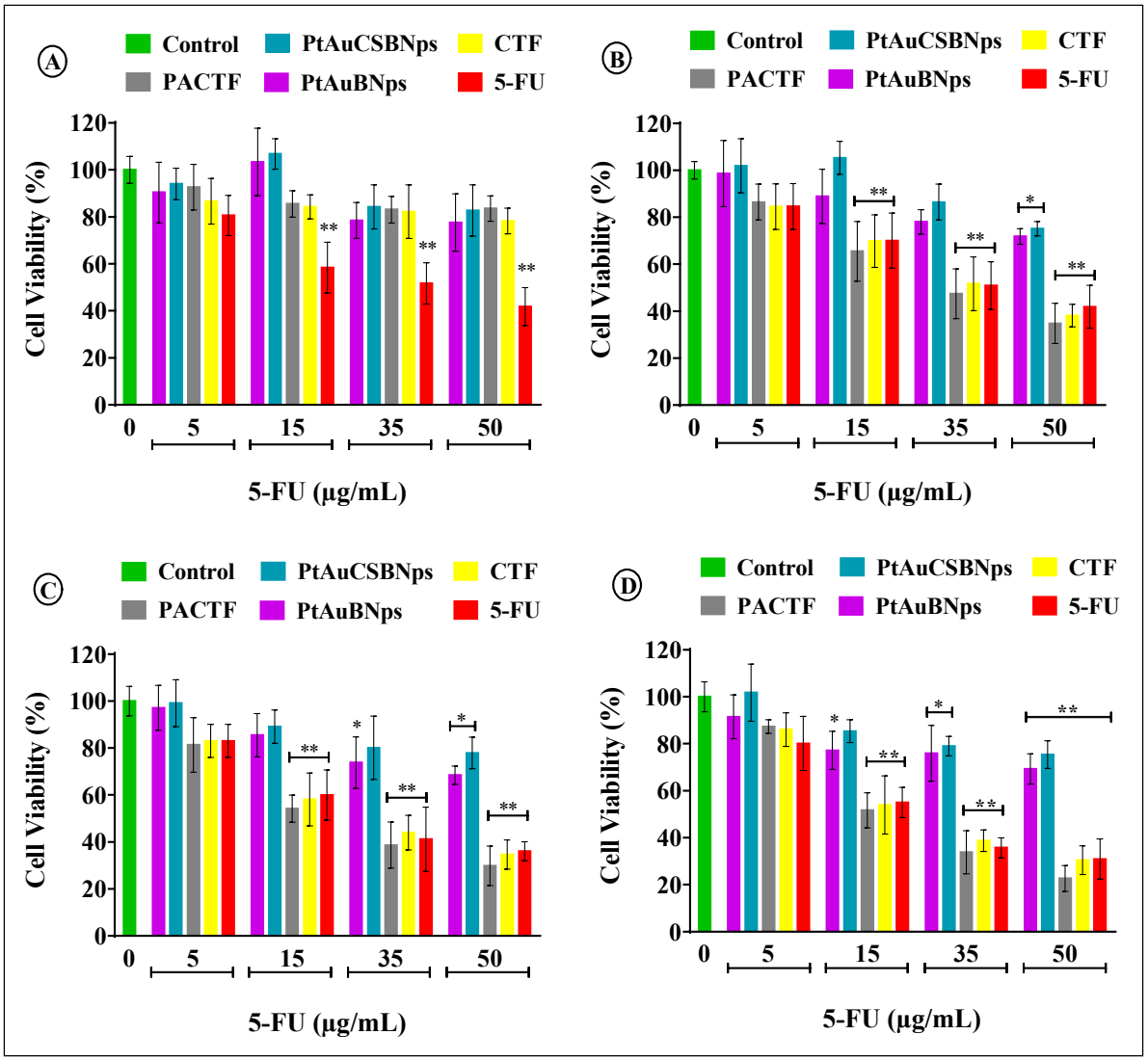

Figure 4.6: MTT cytotoxicity assay of bimetallic nanoparticles and drug bearing nanocomposites in (A) HEK293, (B) MCF-7, (C) HepG2 and (D) Caco-2 cell lines. Data represented as mean ± SD (n=3). * $p<0.05$, **$p<0.01$ were considered statistically significant.

Table 4.7: IC_{50} values of free 5U and 5-FU loaded nanocomposites on HEK293, HepG2, Caco-2 and MCF-7 cell lines for the MTT assays.

Cell Lines	IC_{50} calculation (µg/mL)		
	PACTF	CTF	5-FU
HEK293	-	-	31.79
MCF-7	29.73	33.57	36.06
HepG2	22.85	25.21	25.27
Caco-2	18.98	21.99	20.41

- Where IC_{50} could not be estimated accurately.

5-FU: 5-Fluorouracil; CTF: CS-TPP-5-FU/Tween 80; PACTF: PtAu-CS-TPP-5-FU/Tween 80.

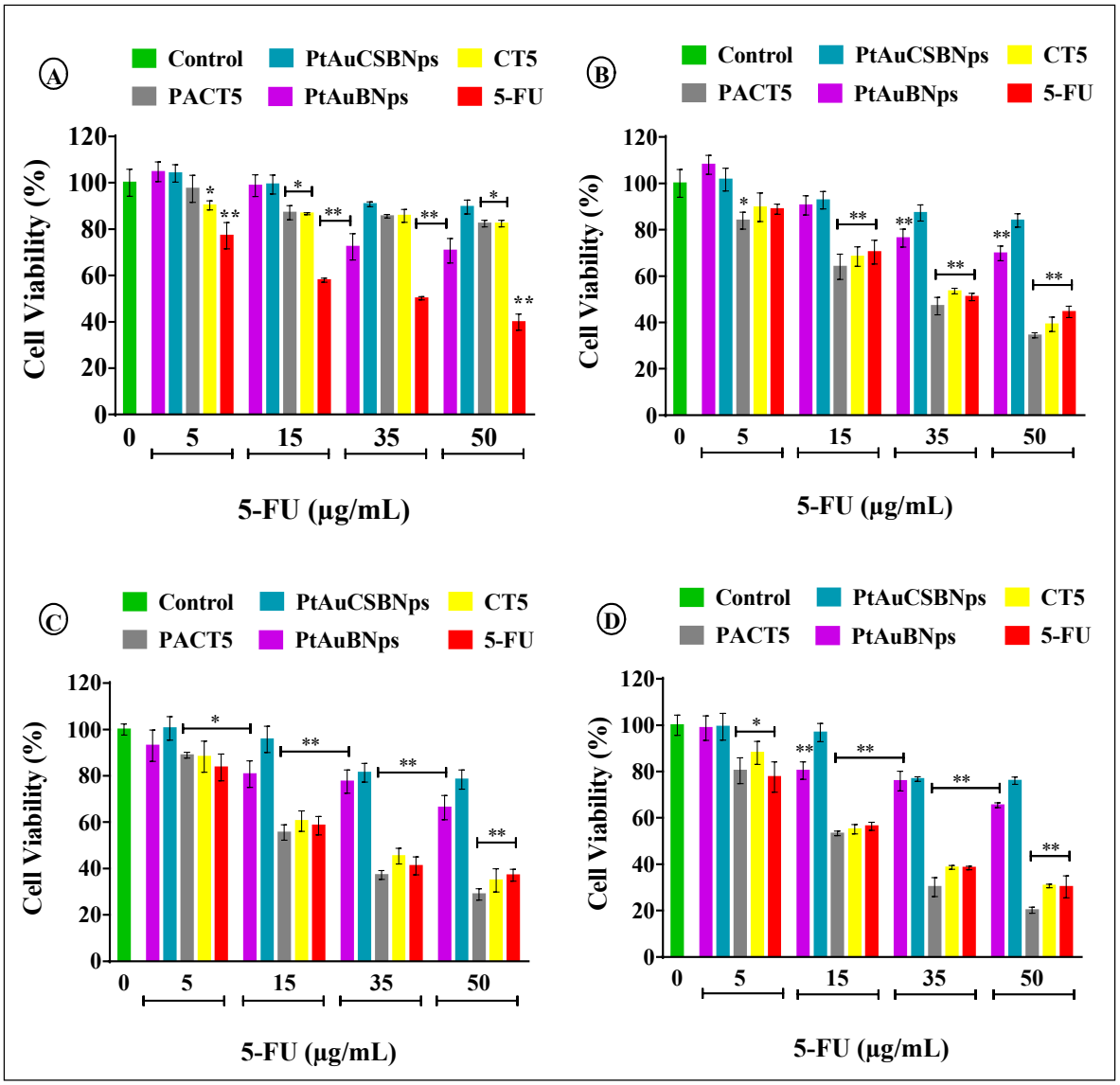

Figure 4.7: SRB cytotoxicity assay of bimetallic nanoparticles and drug bearing nanocomposites in (A) HEK293, (B) MCF-7, (C) HepG2 and (D) Caco-2 cell lines. Data represented as mean ± SD (n=3). * $p<0.05$, ** $p<0.01$ were considered statistically significant.

Table 4.8: IC_{50} values of free 5-FU and 5-FU loaded nanocomposites on HEK293, HepG2, Caco-2 and MCF-7 cell lines for the SRB assays.

	IC_{50} calculation (µg/mL)		
Cell Lines	**PACTF**	**CTF**	**5-FU**
HEK293	-	-	30.84
MCF-7	30.12	34.99	38.67
HepG2	23.10	26.24	25.38
Caco-2	19.25	22.58	21.19

- Where IC_{50} could not be estimated accurately.

5-FU: 5-Fluorouracil; CTF: CS-TPP-5-FU/Tween 80; PACTF: PtAu-CS-TPP-5-FU/Tween 80.

4.3.7. Apoptosis induction studies

The process of programmed cell death or apoptosis is a regulatory mechanism for the removal of physiologically defective, unwanted, damaged or dysfunctional cells (Liu *et al.*, 2015). Cancer therapy strategy can trigger apoptosis induction in cancer cells through an intrinsic apoptotic stimulus, such as DNA damage that causes changes in the mitochondrial function leading to activation of caspase 9, or extrinsic activation such as the binding of death ligands to death receptors (Koff *et al.*, 2015). Cells undergoing apoptosis have distinct morphological features that include cytoplasmic shrinkage, chromatin condensation, loss of membrane phospholipid asymmetry, DNA fragmentation and membrane blebbing, before the cell is lysed to form apoptotic bodies that undergo phagocytosis without eliciting an immune response (Ćurčić *et al.*, 2012, Fadok *et al.*, 2001). Apoptosis is distinguished from necrosis in which cells lose their plasma membrane integrity and burst, affecting neighbouring cells, and triggering an inflammatory response (Fadok *et al.*, 2001).

The ability of drug laden nanocomposites to stimulate cancer cell death by apoptosis rather than necrosis was investigated through fluorescent microscopy, and the AO/EB dual staining method. Acridine orange permeates all cells resulting in the emittance of green fluorescence, whereas ethidium bromide is only taken up by non-viable cells that have lost their cytoplasmic membrane integrity causing the nucleus to fluoresce red. Thus, the nucleus of viable cells emits a homogenous green fluorescence, early apoptotic cells with condensed or fragmented chromatin bright green, late apoptotic with condensed and fragmented chromatin yellow/orange and necrotic cells with no condensed chromatin orange/red (Bezabeh *et al.*, 2001).

The fluorescent images of the control and treated cells are depicted in Figure 4.8, and the apoptotic index (AI) represented in Table 4.9. All control cells emitted green fluorescence indicative of healthy cells with an intact cell membrane. Conversely, all cells treated with 5-FU, PACTF and CTF at their IC_{50} values, formed apoptotic body of varying degrees in all four mammalian cell lines. Noticeably, 5-FU induced high degrees of cell death in all cell lines through both apoptotic and necrotic pathways. The encapsulation of 5-FU brought about biocompatibility and controlled cell death as nanocomposites displayed very low apoptosis indices in the HEK293 (<0.052) cells, and considerably higher in the three cancerous cell lines (>0.360). The MCF-7 cell was the most resistant cell line with cells mainly in early apoptosis, while the Caco-2 and HEPG2 cell line demonstrated a greater degree of sensitivity with higher

apoptotic indices and characteristic apoptotic features (membrane blebs, chromatin condensation and fragmentation). Overall, the apoptosis studies corroborated well with growth inhibition (MTT and SRB assay), and drug release studies, and further confirmed the notion that pH-sensitive drug release brought about cell specific apoptosis induction.

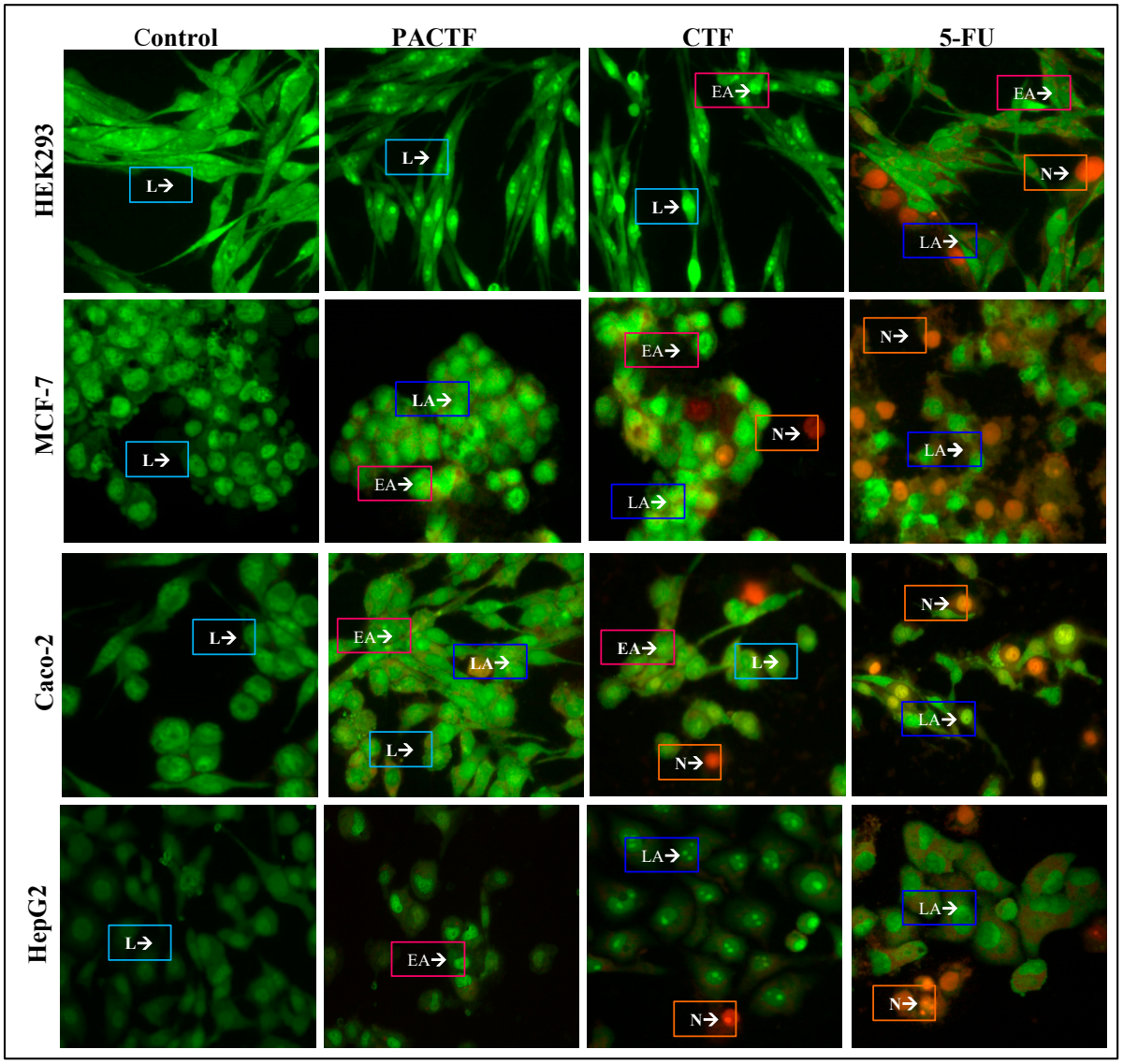

Figure 4.8: Fluorescence micrographs of duel acridine orange/ethidium bromide stained cells showing induced morphological changes in HEK293, MCF-7, Caco-2 and HepG2 cell lines at 20x magnification. L= Live cells; EA= Early apoptotic cells; LA= Late apoptotic cells N=Necrotic cells.

Table 4.9: Apoptotic indices of free 5-FU and 5-FU loaded nanocomposites.

Cell Lines	Apoptosis Index		
	PACTF	**CTF**	**5-FU**
HEK293	0.034	0.052	0.389
MCF-7	0.345	0.321	0.361
HepG2	0.542	0.512	0.549
Caco-2	0.621	0.549	0.624

5-FU: 5-Fluorouracil; CTF: CS-TPP-5-FU/Tween 80; PACTF: PtAu-CS-TPP-5-FU/Tween 80.

4.4. Conclusion

A novel, multifunctional, practical, customizable, stable, nanosized and pH-responsive PtAuCS bimetallic delivery system, exhibiting significantly higher anticancer potency than free 5-FU alone was established in this preclinical study. The embedding of PtAuBNps with CSNps acted synergistically with 5-FU to enhance the *in vitro* cytotoxicity, offering the prospects of reducing drug concentration and the frequency of dosage. Furthermore, the study strongly supports the notion that pH-triggered drug release brings about site-specific toxicity and enhances intracellular bioaccumulation of drugs, such as 5-FU that require metabolic activation to exert its cytotoxic effects. Overall, the PtAuCS bimetallic platform was shown to display superior optical properties, physiochemical features, pharmacokinetics, drug encapsulation, mucoadhesion and biocompatibility to the polymeric CSNps and the free 5-FU. These favourable physiochemical and biological attributes augur well for future *in vivo* and theranostic applications, especially in the area of cancer therapy.

References

Arvizo, R. R., Bhattacharyya, S., Kudgus, R. A., Giri, K., Bhattacharya, R., and Mukherjee, P. 2012. Intrinsic therapeutic applications of noble metal nanoparticles: past, present and future. *Chemical Society Reviews,* 41, 2943-2970.

Babaei, M., Abnous, K., Taghdisi, S. M., Amel Farzad, S., Peivandi, M. T., Ramezani, M., and Alibolandi, M. 2017. Synthesis of theranostic epithelial cell adhesion molecule targeted mesoporous silica nanoparticle with gold gatekeeper for hepatocellular carcinoma. *Nanomedicine* 12, 1261-1279.

Bezabeh, T., Mowat, M., Jarolim, L., Greenberg, A., and Smith, I. 2001. Detection of drug-induced apoptosis and necrosis in human cervical carcinoma cells using 1H NMR spectroscopy. *Cell Death and Differentiation,* 8, 219.

Boyles, M. S., Kristl, T., Andosch, A., Zimmermann, M., Tran, N., Casals, E., Himly, M., Puntes, V., Huber, C. G., and Lütz-Meindl, U. 2015. Chitosan functionalisation of gold nanoparticles encourages particle uptake and induces cytotoxicity and pro-inflammatory conditions in phagocytic cells, as well as enhancing particle interactions with serum components. *Journal of Nanobiotechnology,* 13, 84.

Buchtelova, H., Dostalova, S., Michalek, P., Krizkova, S., Strmiska, V., Kopel, P., Hynek, D., Richtera, L., Ridoskova, A., and Adam, P. 2017. Size-related cytotoxicological aspects of polyvinylpyrrolidone-capped platinum nanoparticles. *Food and Chemical Toxicology,* 105, 337-346.

Butterworth, K. T., Mcmahon, S. J., Currell, F. J., and Prise, K. M. 2012. Physical basis and biological mechanisms of gold nanoparticle radiosensitization. *Nanoscale,* 4, 4830-4838.

Chandran, P. R., and Sandhyarani, N. 2014. An electric field responsive drug delivery system based on chitosan-gold nanocomposites for site specific and controlled delivery of 5-fluorouracil. *RSC Advances,* 4, 44922-44929.

Chen, Z., Zhang, C., Tan, Y., Zhou, T., Ma, H., Wan, C., Lin, Y., and Li, K. 2015. Chitosan-functionalized gold nanoparticles for colorimetric detection of mercury ions based on chelation-induced aggregation. *Microchimica Acta,* 182, 611-616.

Cheng, C., Sie, E., Liu, B., Huan, C., Sum, T., Sun, H., and Fan, H. 2010. Surface plasmon enhanced band edge luminescence of ZnO nanorods by capping Au nanoparticles. *Applied Physics Letters,* 96, 071107.

Couvreur, P. 2013. Nanoparticles in drug delivery: past, present and future. *Advanced drug delivery reviews,* 65, 21-23.

Ćurčić, M. G., Stanković, M. S., Mrkalić, E. M., Matović, Z. D., Banković, D. D., Cvetković, D. M., Đačić, D. S., and Marković, S. D. 2012. Antiproliferative and proapoptotic activities of methanolic extracts from *Ligustrum vulgare L.* as an individual treatment and in combination with palladium complex. *International Journal of Molecular Sciences,* 13, 2521-2534.

Doostmohammadi, A., Monshi, A., Salehi, R., Fathi, M., Karbasi, S., Pieles, U., and Daniels, A. 2012. Preparation, chemistry and physical properties of bone-derived hydroxyapatite particles having a negative zeta potential. *Materials Chemistry and Physics,* 132, 446-452.

Du, J. Z., Mao, C. Q., Yuan, Y. Y., Yang, X. Z., and Wang, J. 2014. Tumor extracellular acidity-activated nanoparticles as drug delivery systems for enhanced cancer therapy. *Biotechnology Advances,* 32, 789-803.

Dubey, R. R., and Parikh, R. H. 2004. Two-stage optimization process for formulation of chitosan microspheres. *AAPS PharmSciTech,* 5, 20-28.

Ekrami-Kakhki, M. S., Khorasani-Motlagh, M., and Noroozifar, M. 2011. Platinum nanoparticles self-assembled onto chitosan membrane as anode for direct methanol fuel cell. *Journal of Applied Electrochemistry,* 41, 527-534.

El-Hammadi, M. M., Delgado, Á. V., Melguizo, C., Prados, J. C., and Arias, J. L. 2017. Folic acid-decorated and PEGylated PLGA nanoparticles for improving the antitumour activity of 5-fluorouracil. *International Journal of Pharmaceutics,* 516, 61-70.

Elgadir, M. A., Uddin, M. S., Ferdosh, S., Adam, A., Chowdhury, A. J. K., and Sarker, M. Z. I. 2015. Impact of chitosan composites and chitosan nanoparticle composites on various drug delivery systems: A review. *Journal of Food and Drug Analysis,* 23, 619-629.

Fadok, V. A., De Cathelineau, A., Daleke, D. L., Henson, P. M., and Bratton, D. L. 2001. Loss of phospholipid asymmetry and surface exposure of phosphatidylserine is required for phagocytosis of apoptotic cells by macrophages and fibroblasts. *Journal of Biological Chemistry,* 276, 1071-1077.

Fan, F. R., Liu, D. Y., Wu, Y. F., Duan, S., Xie, Z. X., Jiang, Z. Y., and Tian, Z. Q. 2008. Epitaxial growth of heterogeneous metal nanocrystals: from gold nano-octahedra to palladium and silver nanocubes. *Journal of the American Chemical Society,* 130, 6949-6951.

Guan, H., Yu, J., and Chi, D. 2013. Label-free colorimetric sensing of melamine based on chitosan-stabilized gold nanoparticles probes. *Food Control,* 32, 35-41.

Hou, J., Yu, X., Shen, Y., Shi, Y., Su, C., and Zhao, L. 2017. Triphenyl Phosphine-Functionalized Chitosan Nanoparticles Enhanced Antitumor Efficiency Through Targeted Delivery of Doxorubicin to Mitochondria. *Nanoscale Research Letters,* 12, 158.

Huang, Y., Rao, Y., Chen, J., Yang, V. C., and Liang, W. 2011. Polysorbate cationic synthetic vesicle for gene delivery. *Journal of Biomedical Materials Research Part A,* 96, 513-519.

Hung, S. F., Yu, Y. C., Suen, N. T., Tzeng, G. Q., Tung, C. W., Hsu, Y. Y., Hsu, C. S., Chang, C. K., Chan, T. S., and Sheu, H. S. 2016. The synergistic effect of a well-defined Au@ Pt core-shell nanostructure toward photocatalytic hydrogen generation: interface engineering to improve the Schottky barrier and hydrogen-evolved kinetics. *Chemical Communications,* 52, 1567-1570.

Islam, A., and Yasin, T. 2012. Controlled delivery of drug from pH sensitive chitosan/poly (vinyl alcohol) blend. *Carbohydrate Polymers,* 88, 1055-1060.

Kamaly, N., Yameen, B., Wu, J., and Farokhzad, O. C. 2016. Degradable controlled-release polymers and polymeric nanoparticles: mechanisms of controlling drug release. *Chemical Reviews,* 116, 2602-2663.

Keepers, Y. P., Pizao, P. E., Peters, G. J., Van Ark-Otte, J., Winograd, B., and Pinedo, H. M. 1991. Comparison of the sulforhodamine B protein and tetrazolium (MTT) assays for

in vitro chemosensitivity testing. *European Journal of Cancer and Clinical Oncology,* 27, 897-900.

Kevadiya, B. D., Patel, T. A., Jhala, D. D., Thumbar, R. P., Brahmbhatt, H., Pandya, M. P., Rajkumar, S., Jena, P. K., Joshi, G. V., and Gadhia, P. K. 2012. Layered inorganic nanocomposites: a promising carrier for 5-fluorouracil (5-FU). *European Journal of Pharmaceutics and Biopharmaceutics,* 81, 91-101.

Khalil, M. M., Mostafa, Y. M., and Torad, E. 2014. Biosynthesis and characterization of Pt and Au-Pt nanoparticles and their photo catalytic degradation of methylene blue. *International Journal,* 2, 694-703.

Koff, J. L., Ramachandiran, S., and Bernal-Mizrachi, L. 2015. A time to kill: targeting apoptosis in cancer. *International Journal of Molecular Sciences,* 16, 2942-2955.

Kong, M., Zuo, Y., Wang, M., Bai, X., Feng, C., and Chen, X. 2017. Simply constructed chitosan nanocarriers with precise spatiotemporal control for efficient intracellular drug delivery. *Carbohydrate Polymers,* 169, 341-350.

Kumar, A., Vimal, A., and Kumar, A. 2016. Why chitosan? From properties to perspective of mucosal drug delivery. *International Journal of Biological Macromolecules,* 91, 615-622.

Lammers, T., Kiessling, F., Hennink, W. E., and Storm, G. 2010. Nanotheranostics and image-guided drug delivery: current concepts and future directions. *Molecular Pharmaceutics,* 7, 1899-1912.

Lawrie, G., Keen, I., Drew, B., Chandler-Temple, A., Rintoul, L., Fredericks, P., and Grøndahl, L. 2007. Interactions between alginate and chitosan biopolymers characterized using FTIR and XPS. *Biomacromolecules,* 8, 2533-2541.

Liu, K., Liu, P. C., Liu, R., and Wu, X. 2015. Dual AO/EB staining to detect apoptosis in osteosarcoma cells compared with flow cytometry. *Medical Science Monitor Basic Research,* 21, 15.

Liu, X., Zhang, X., Zhu, M., Lin, G., Liu, J., Zhou, Z., Tian, X., and Pan, Y. 2016. PEGylated Au@ Pt nanodendrites as novel theranostic agents for computed tomography imaging

and photothermal/radiation synergistic therapy. *ACS Applied Materials & Interfaces,* 9, 279-285.

Misra, R., Acharya, S., and Sahoo, S. K. 2010. Cancer nanotechnology: application of nanotechnology in cancer therapy. *Drug Discovery Today,* 15, 842-850.

Mohammadpour Dounighi, N., Eskandari, R., Avadi, M., Zolfagharian, H., Mir Mohammad Sadeghi, A., and Rezayat, M. 2012. Preparation and *in vitro* characterization of chitosan nanoparticles containing *Mesobuthus eupeus* scorpion venom as an antigen delivery system. *Journal of Venomous Animals and Toxins Including Tropical Diseases,* 18, 44-52.

Nagarwal, R. C., Kumar, R., and Pandit, J. 2012. Chitosan coated sodium alginate-chitosan nanoparticles loaded with 5-FU for ocular delivery: *In vitro* characterization and *in vivo* study in rabbit eye. *European Journal of Pharmaceutical Sciences,* 47, 678-685.

Nivethaa, E., Dhanavel, S., Narayanan, V., Vasu, C. A., and Stephen, A. 2015. An *in vitro* cytotoxicity study of 5-fluorouracil encapsulated chitosan/gold nanocomposites towards MCF-7 cells. *RSC Advances,* 5, 1024-1032.

Patel, N., Chotai, N., Patel, J., Soni, T., Desai, J., and Patel, R. 2008. Comparison of *in vitro* dissolution profiles of oxcarbazepine-HP b-CD tablet formulations with marketed oxcarbazepine tablets. *Dissolution Technologies,* 15, 28-34.

Pilicheva, B., Zagorchev, P., Uzunova, Y., and Kassarova, M. 2013. Development and *in vitro* evaluation of mucoadhesive microsphere carriers for intranasal delivery of betahistine dihydrochloride. *International Journal of Drug Delivery,* 5, 389.

Rafiei, P., and Haddadi, A. 2017. Pharmacokinetic Consequences of PLGA Nanoparticles in Docetaxel Drug Delivery. *Pharmaceutical Nanotechnology,* 5, 3-23.

Ramteke, K., Dighe, P., Kharat, A., and Patil, S. 2014. Mathematical models of drug dissolution: a review. *Scholars Academic Journal of Pharmacy,* 3, 388-396.

Reddy, A. B., Manjula, B., Jayaramudu, T., Sadiku, E., Babu, P. A., and Selvam, S. P. 2016. 5-Fluorouracil Loaded Chitosan-PVA/Na+. *Nano-Micro Letters,* 8, 260-269.

Rejinold, N. S., Thomas, R. G., Muthiah, M., Lee, H. J., Jeong, Y. Y., Park, I.-K., and Jayakumar, R. 2016. Breast tumor targetable Fe_3O_4 embedded thermo-responsive nanoparticles for radiofrequency assisted drug delivery. *Journal of Biomedical Nanotechnology,* 12, 43-55.

Sahu, P., Kashaw, S. K., Jain, S., Sau, S., and Iyer, A. K. 2017. Assessment of penetration potential of pH responsive double walled biodegradable nanogels coated with eucalyptus oil for the controlled delivery of 5-fluorouracil: *In vitro* and *ex vivo* studies. *Journal of Controlled Release,* 253, 122-136.

Sanyakamdhorn, S., Agudelo, D., and Tajmir-Riahi, H. A. 2013. Encapsulation of antitumor drug doxorubicin and its analogue by chitosan nanoparticles. *Biomacromolecules,* 14, 557-563.

Shi, L., Tang, C., and Yin, C. 2012. Glycyrrhizin-modified O-carboxymethyl chitosan nanoparticles as drug vehicles targeting hepatocellular carcinoma. *Biomaterials,* 33, 7594-7604.

Singhvi, G., and Singh, M. 2011. Review: *in-vitro* drug release characterization models. *International Journal of Pharmaceutical Sciences and Research,* 2, 77-84.

Singla, A., and Chawla, M. 2001. Chitosan: Some pharmaceutical and biological aspects-an update. *Journal of Pharmacy and Pharmacology,* 53, 1047-1067.

Srivastava, G., Walke, S., Dhavale, D., Gade, W., Doshi, J., Kumar, R., Ravetkar, S., and Doshi, P. 2016. Tartrate/tripolyphosphate as co-crosslinker for water soluble chitosan used in protein antigens encapsulation. *International Journal of Biological Macromolecules,* 91, 381-393.

Streubel, A., Siepmann, J., Peppas, N., and Bodmeier, R. 2000. Bimodal drug release achieved with multi-layer matrix tablets: transport mechanisms and device design. *Journal of Controlled Release,* 69, 455-468.

Sugunan, A., Thanachayanont, C., Dutta, J., and Hilborn, J. 2005. Heavy-metal ion sensors using chitosan-capped gold nanoparticles. *Science and Technology of Advanced Materials,* 6, 335-340.

Testa, G., Fontana, L., Venditti, I., and Fratoddi, I. 2016. Functionalized platinum nanoparticles with surface charge trigged by pH: synthesis, characterization and stability studies. *Beilstein Journal of Nanotechnology,* 7, 1822.

Toshima, N., and Yonezawa, T. 1998. Bimetallic nanoparticles-novel materials for chemical and physical applications. *New Journal of Chemistry,* 22, 1179-1201.

Toshima, N., Yonezawa, T., Harada, M., Asakura, K., and Iwasawa, Y. 1990. The polymer-protected Pd-Pt bimetallic clusters having catalytic activity for selective hydrogenation of diene. Preparation and EXAFS investigation on the structure. *Chemistry Letters,* 19, 815-818.

Wang, J., Tauchi, Y., Deguchi, Y., Morimoto, K., Tabata, Y., and Ikada, Y. 2000. Positively charged gelatin microspheres as gastric mucoadhesive drug delivery system for eradication of H. pylori. *Drug Delivery,* 7, 237-243.

Yamada, M., Foote, M., and Prow, T. W. 2015. Therapeutic gold, silver, and platinum nanoparticles. *Wiley Interdisciplinary Reviews: Nanomedicine and Nanobiotechnology,* 7, 428-445.

Yu, X., Yang, X., Horte, S., Kizhakkedathu, J. N., and Brooks, D. E. 2014. A pH and thermosensitive choline phosphate-based delivery platform targeted to the acidic tumor microenvironment. *Biomaterials,* 35, 278-286.

Zhang, H., and Toshima, N. 2013. Synthesis of Au/Pt bimetallic nanoparticles with a Pt-rich shell and their high catalytic activities for aerobic glucose oxidation. *Journal of Colloid and Interface Science,* 394, 166-176.

CHAPTER FIVE
CONCLUSIONS AND RECOMMENDATIONS

5.1. General conclusion

Nanotechnology is heralded as a boon for drug delivery, promising to improve treatment efficiency, administration and patient compliance. As this field of science is becoming more advanced and multidisciplinary, it increasingly challenges classical approaches in medicine. Hence, over the past decade, the research paradigm has been to develop hybrid drug delivery systems with duel therapeutic and diagnostic capabilities. PtAuBNps are dynamic multifunctional scaffolds suitable for future theranostic applications owing to their highly modular nature, enhanced structural, physiochemical and optical properties. However, this delivery system is at a nascent stage of development and requires rigorous screening *in vitro* to merit progression to clinical trials. This study aimed to develop a pH-responsive platform with proficient binding capabilities, low toxicity, facile synthesis and amenability to surface functionalisation, in aspiration for potentially cutting-edge applications within the field of oncology. In this *in vitro* study, PtAuBNps, as well as the anticancer drugs DOX and 5-FU, were successfully ensconced within CS/PtAu-based nanocomposites. The data established in this study show the promising potential for the utilisation of these nanoparticles in future *in vitro* and *in vivo* drug delivery applications.

Overall, the synthesised PtAuBNps were uniform, spherically shaped, ultra-small in size and displayed a negatively charged surface conducive to surface functionalisation with cationic polymers. Passivation with CS improved the surface characteristics of the PtAuBNps and endowed the carriers with biocompatibility, target activated release and mucoadhesive capabilities. Drug laden nanocomposites were less than 150 nm in size, displayed a cationic nature and were colloidally stable (> 25 mV). These physiochemical attributes are deemed critical for enhanced cellular uptake, increased intracellular drug concentrations and long term storage stability. In addition, drug loaded nanocomposites displayed excellent binding capabilities with up to 69.82% EE of DOX and 90.17% EE of 5-FU. This is important as poor encapsulation would mean higher concentrations of Nps being administered. Furthermore, carriers demonstrated excellent mucin binding capabilities and may improve drug absorption through the intestinal mucosal surface.

All drug bearing nano-delivery systems (PACTD, CTD, PACTF and CTF) provided efficient pH-triggered drug release *in vitro* with faster release kinetics in mildly acidic tumour conditions, than neutral pH, imparting differential drug accumulation between cancerous and normal tissue. The *in vitro* cytotoxicity studies support the concept that pH-liable release would bring about cell specific cytotoxicity and enhanced therapeutic effects. Nanocomposites, PACTD, CTD, PACTF and CTF generated a dose dependent and cell specific cytotoxicity profile. It was evident that these nanocomposites performed comparably well compared to their free drug counterparts (DOX and 5-FU), suggesting no loss of anticancer activity following drug loading. Impressively, the nanocomposites induced relatively low cytotoxic effects in the HEK293 cell line, confirming their targeting specificity. From the two studied nanoscaffolds, the PtAuCSBNps formulations (PACTD and PACTF) performed considerably better the CSNp drug formulations (CTD and CTF), and even increased anticancer activity of DOX and 5-FU respectively. This is a particularly important finding, and suggests that this carrier system may reduce the need for high drug concentrations and limit the frequency of drug administration. Finally, apoptosis studies revealed the induction of cell specific apoptosis, and a relatively lower necrotic index compared to the free drug for these carrier systems.

Overall, the PtAuBNps was found to be practical and robust scaffolds, capable of providing safe and controlled drug release for enhanced therapeutic effect. The data established in this study are encouraging and show great potential for future applications in reformulating ineffective drugs, live cell tracking, clinical oncology and improving delivery across the blood brain barrier, placental barrier and stomach epithelium. In addition, the research provides crucial techniques and concepts that allow elegant tailoring of the carrier systems physiochemical attributes to fit many other pharmaceutical research endeavours. However further studies in this revolutionary field of science will require a laborious multidisciplinary approach to achieve the best possible outcomes for cancer patients.

5.2. Recommendations for future studies

The advanced tailoring capabilities of novel PtAuBNps offer a research scope far beyond monometallic systems. Further research will require an interdisciplinary approach entailing projects covering the following suggestions:

- To fully investigate the synergistic effects between Pt and Au. This can be achieved by conducting an extensive investigation on the effect that different stoichiometric ratios of Pt and Au have on stability, morphology and cell viability *in vitro*. Alternatively, it is suggested that the reciprocal drug delivery system, i.e. Au (shell)-Pt (core) be tested and compared to the current system, i.e. Pt (shell)-Au (core).
- To fully characterise the thickness of the core and shell through elemental mapping studies.
- To test the targeting ability of the nanocomposites in a co-culture system composed of normal and cancer cells to better mimic the cancer microenvironment.
- Design a targeted delivery system capable of conjugating and safely releasing multiple therapeutic agents within cancers.
- Designing and testing the activity of "cocktail" nano-formulations of PACTF and PACTD.
- To improve the mucoadhesive capabilities, pharmacokinetics and physicochemistry by conjugation of other suitable polymers or ligands. The grafting of the steric stabiliser polyethylene glycol, in particular is most appealing especially if the carrier is to progress to clinical trials.
- Perform detailed studies on the fate of the nanoparticle, mechanism of cellular uptake and biodistribution.

APPENDIX A

PUBLICATION

Research Article

For reprint orders, please contact: reprints@futuremedicine.com

Nanomedicine

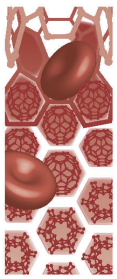

An *in vitro* assessment of novel chitosan/bimetallic PtAu nanocomposites as delivery vehicles for doxorubicin

Vareessh Maney[1] & Moganavelli Singh*,[1]

[1]Non-Viral Gene Delivery Laboratory, Discipline of Biochemistry, School of Life Sciences, University of Kwa-Zulu Natal, Private Bag X54001, Durban, Kwa-Zulu Natal, South Africa

* Author for correspondence: Singhm1@ukzn.ac.za

Aim: To synthesize and functionalize platinum (core)-gold (shell) bimetallic nanoparticles (PtAuBNps) with chitosan and doxorubicin to display favorable pharmacokinetics, biodegradability, biological activity and safety *in vitro*. **Materials & methods:** PtAuBNps and their drug nanocomposites were morphologically and physico-chemically characterized. Binding studies determined the efficiency and stability of the platform. *In vitro* release kinetics were evaluated under simulated environments, cytotoxicity profiles through MTT and Sulforodhamine B assays and apoptosis induction using the dual EtBr/AO staining. **Results & discussion:** The results obtained indicate that functionalized PtAuBNps displayed favorable physio-chemical attributes, high binding capabilities, pH-triggered drug release through zero-order release kinetics, cell-specific cytotoxicity and good colloidal stability. **Conclusion:** The positive attributes of this novel delivery system bodes well for future *in vivo* studies.

First draft submitted: 4 July 2017; Accepted for publication: 29 August 2017; Published online: 2 October 2017

Keywords: bimetallic nanoparticles • cancer • cytotoxicity • doxorubicin • gold • platinum

The use of nanosized materials has become increasingly popular in diverse nanomedical fields as biosensors, drug delivery systems, imaging and tracking agents [1,2]. The arsenal of nanoparticles used in cancer therapeutics includes liposomes, metal and polymeric nanoparticles, polymeric micelles, dendrimers, nanocantilevers, carbon nanotubes and quantum dots [3]. Nanoscale materials are expected to revolutionize cancer therapy through advances in early detection, diagnosis and treatment. Drug-loaded nanoparticles (10–200 nm in diameter) offer the prospects of site-specific delivery, improved potency of bound therapeutic agents, improved delivery of infective drugs, prevention of early degradation, and the ability to overcome multidrug resistance [4–7]. Moreover, nanoparticle drug delivery vehicles can penetrate various biological barriers including the tumor vasculature and the mucosal membrane, and may further facilitate transport across the blood–brain barrier [8,9].

To date, doxorubicin (DOX) is one of the most potent anticancer drugs available and exhibits a broad spectrum of activity toward nearly all human cancers [10]. The antineoplastic activity of DOX is mainly believed to be attributed to DOX acting as a topoisomerase II poison, DNA cross-linking, mitochondrial dysfunction, generation of free radicals and induction of apoptosis [11,12]. DOX administration has been known to induce life-threatening side effects including cardiotoxicity, myelosuppression and mucositis [13]. The unendurable toxicity caused due to the accumulation of DOX within healthy organs can lead to patient fatality rather than from the disease itself.

With the hope to ameliorate these potent side effects, nano-platforms synthesized of nobel metals (Au and Pt) were preferred owing to their physiochemical, biological and photonic properties. The use of gold nanoparticles as drug delivery agents is the most prominent in literature, since they are inert, nontoxic, easily synthesized and amenable to surface functionalization with targeting molecules [14]. Platinum nanoparticles share similar chemical, physical and optical properties, however unlike gold nanoparticles, the emergence of platinum nanoparticles for therapeutic purposes is recent. Topical platinum-based chemotherapeutic drugs (cisplatin and derivatives) are known to kill cancer cells through inducing DNA damage resulting in apoptosis [15,16]. It is believed that the use of platinum nanoparticles will serve as a reservoir for generating platinum ions, and will have the same mode of

Future Medicine

APPENDIX B
ROUTINE CELL CULTURE AND MAINTENANCE

Resuscitation of frozen cells

Stored ampoules of cryopreserved cells were thawed in a 37°C water bath, pelleted through centrifugation (3000rpm for 2 min) in an Eppendorf centrifuge (model 5451D, New York, USA), and reconstituted into 1mL of complete medium pre-warmed at 37°C. The 1 mL cell suspension was then transferred into a 25 cm^2 tissue culture flask containing 5 mL complete medium, and incubated for 24 h in a HEPA class 100 Steri-Cult CO_2 incubator (Thermo-Fisher Corporation, Waltham, Massachusetts, USA). Following the 24-h incubation period residual DMSO was removed by washing flask with 2mL sterile PBS and 5mL of fresh complete medium. The cells were allowed to attach to the culture flask and were checked daily under a Nikon TMS inverted light microscope (Nikon Co., Tokyo, Japan).

Trypsinisation

Briefly, spent medium was removed and cells washed with 5 mL PBS, followed by the addition of 1mL trypsin-versene to cells. Cells were monitored under an inverted microscope until the cells "rounding off "and the process was terminated by the addition of 1 mL complete medium containing serum, followed by gently tapping the culture flask against the palm of the hand.

Cryopreservation

Following trypsinisation cell suspensions were pelleted by centrifugation at 3000 rpm for 5 min, followed by resuspension in 0.9 mL complete medium and 0.1 mL of dimethylsulphoxide (DMSO) cryoprotective medium Cells suspensions were then gently vortexed and thereafter, aliquoted into 2 mL cryogenic vials which were placed into a Nalgene™ "Mr. Frosty" Cryo 1°C freezing container (Thermo-Fischer Scientific Inc., Waltham, Massachusetts, USA) filled with isopropanol to slowly freeze the cells at a rate of 1°C per minute to a temperature of -70°C. Thereafter, cryogenic vials were placed into a cryocontainer and stored a -80°C biofreezer (Nuaire, Lasec Laboratory and Scientific Equipment) for short term, or in liquid nitrogen for long term recovery of cells.

APPENDIX C

NTA RESULTS

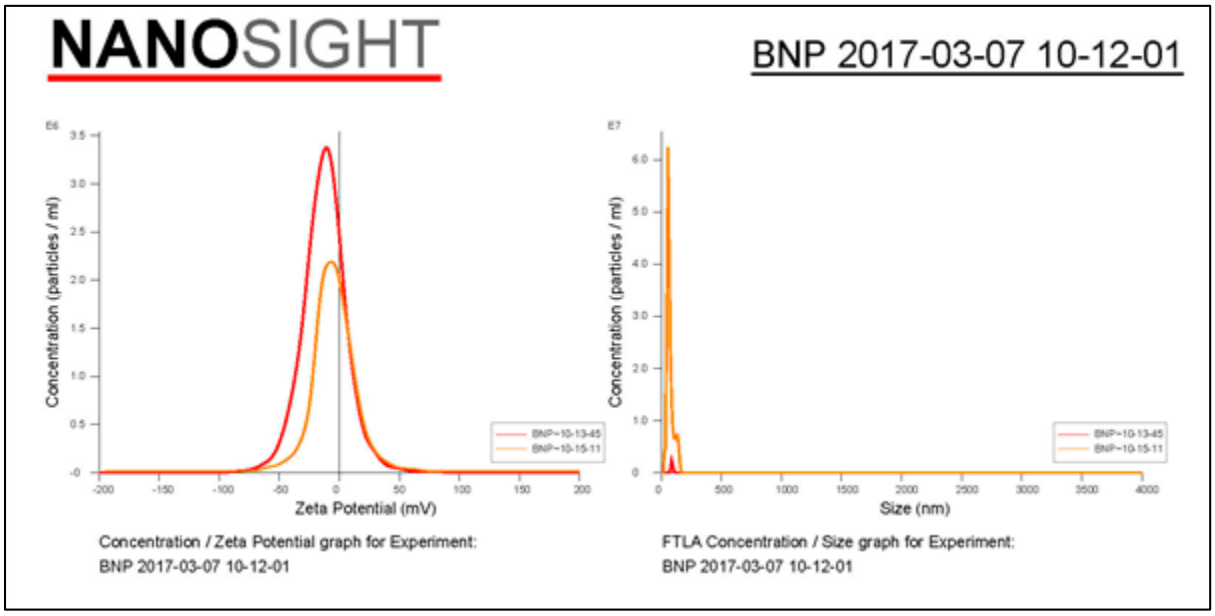

C1: NTA zeta potential and sizing analysis of PtAuBNps.

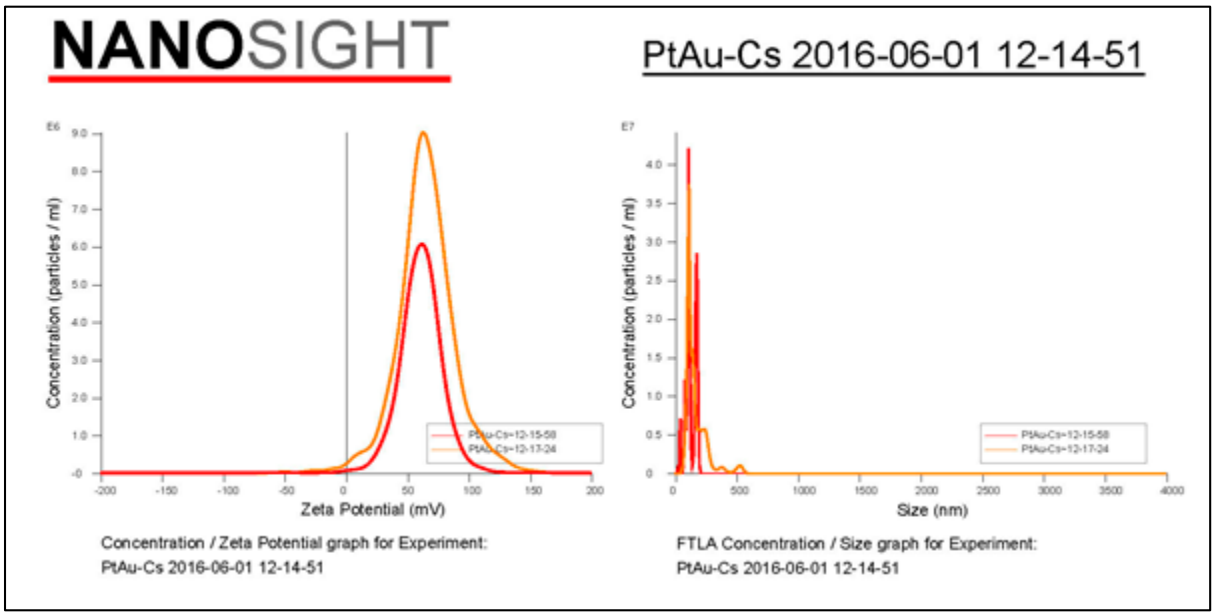

C2: NTA zeta potential and sizing analysis of PtAuCSBNps.

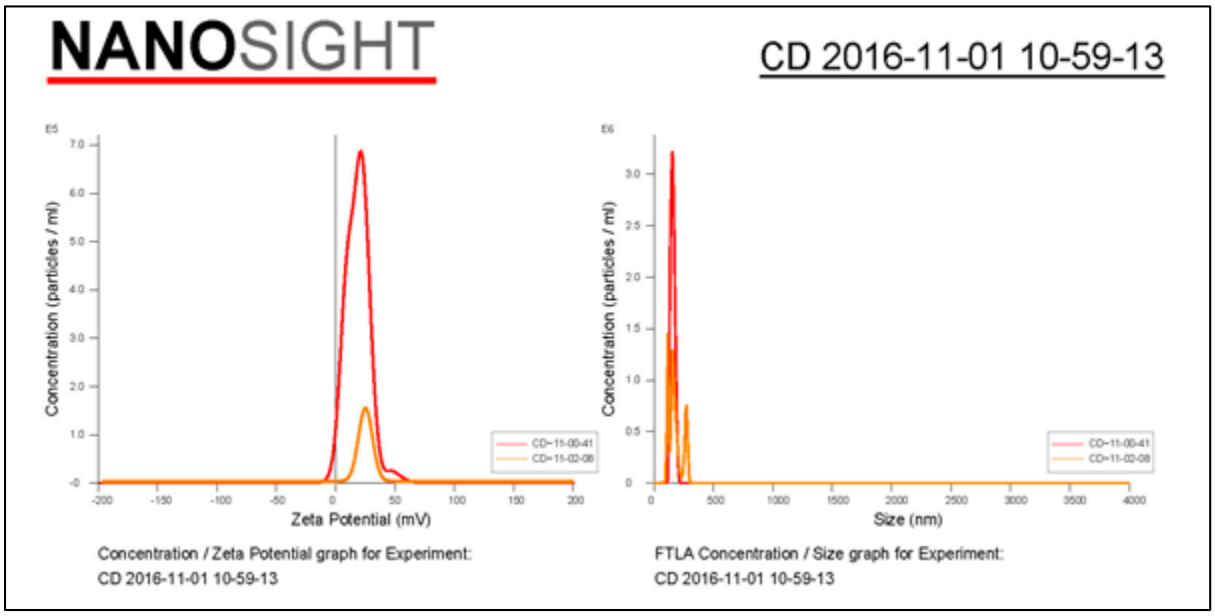

C3: NTA zeta potential and sizing analysis of the nanocomposite CTD.

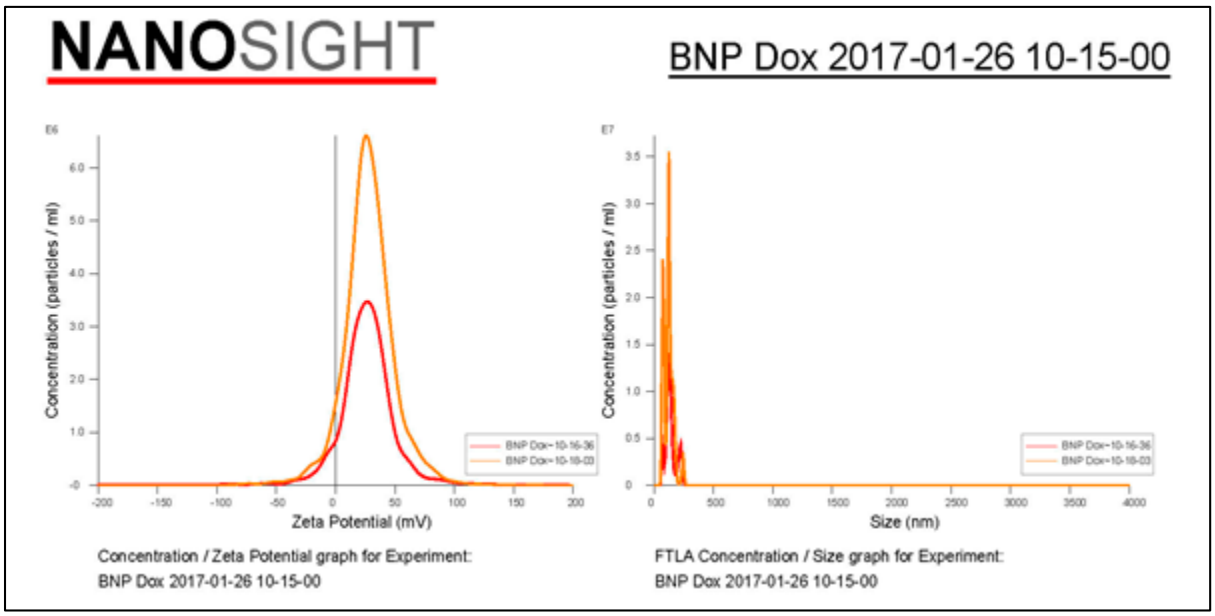

C4: NTA zeta potential and sizing analysis of the nanocomposite PACTD.

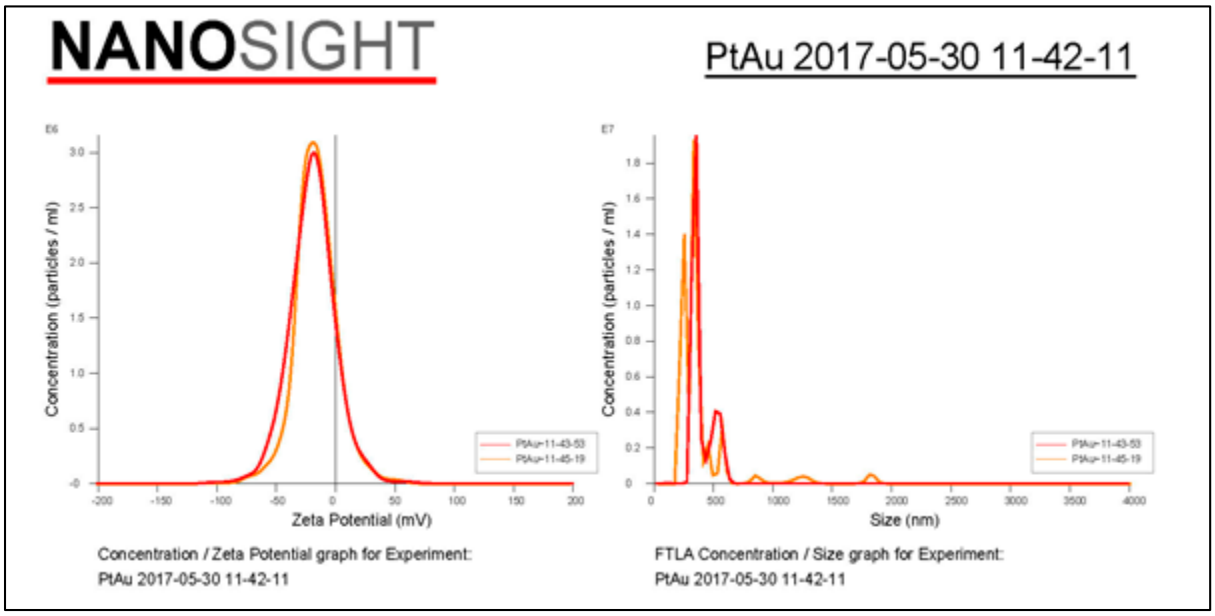

C5: NTA zeta potential and sizing analysis of PtAuBNps. Most recent analysis.

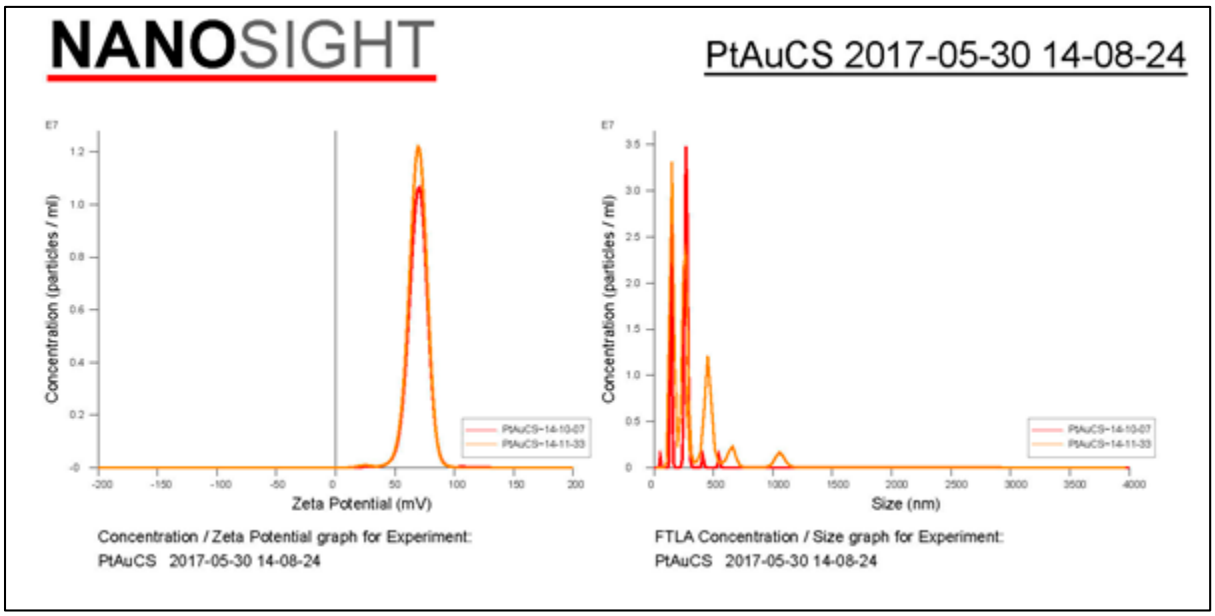

C6: NTA zeta potential and sizing analysis of PtAuCSBNps. Most recent analysis.

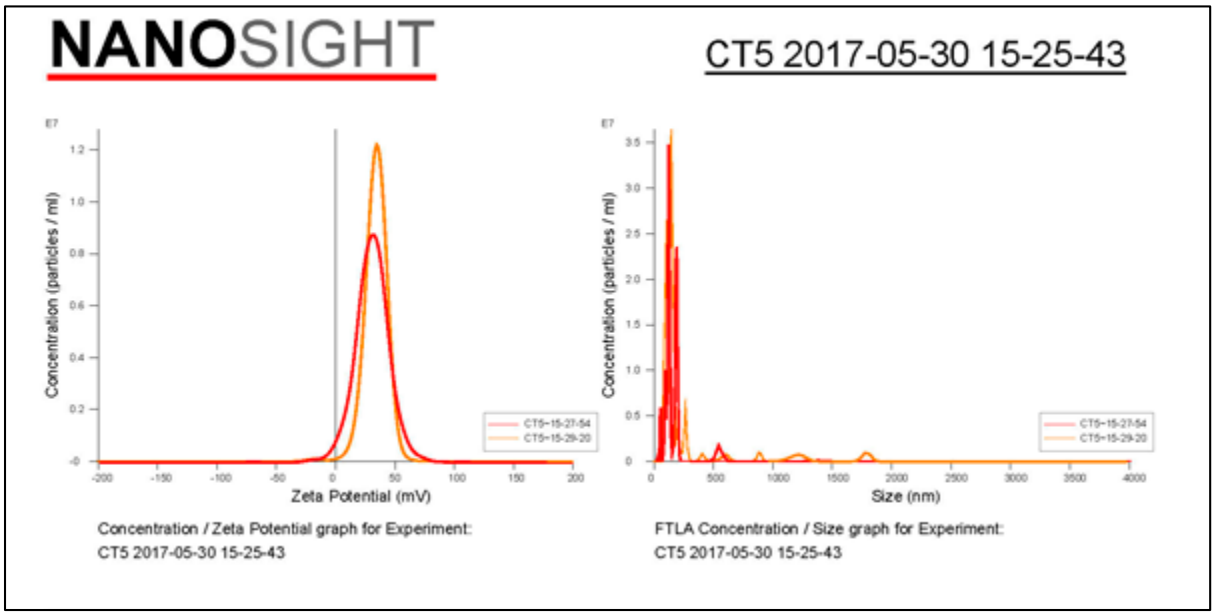

C7: NTA zeta potential and sizing analysis of the nanocomposite CTF.

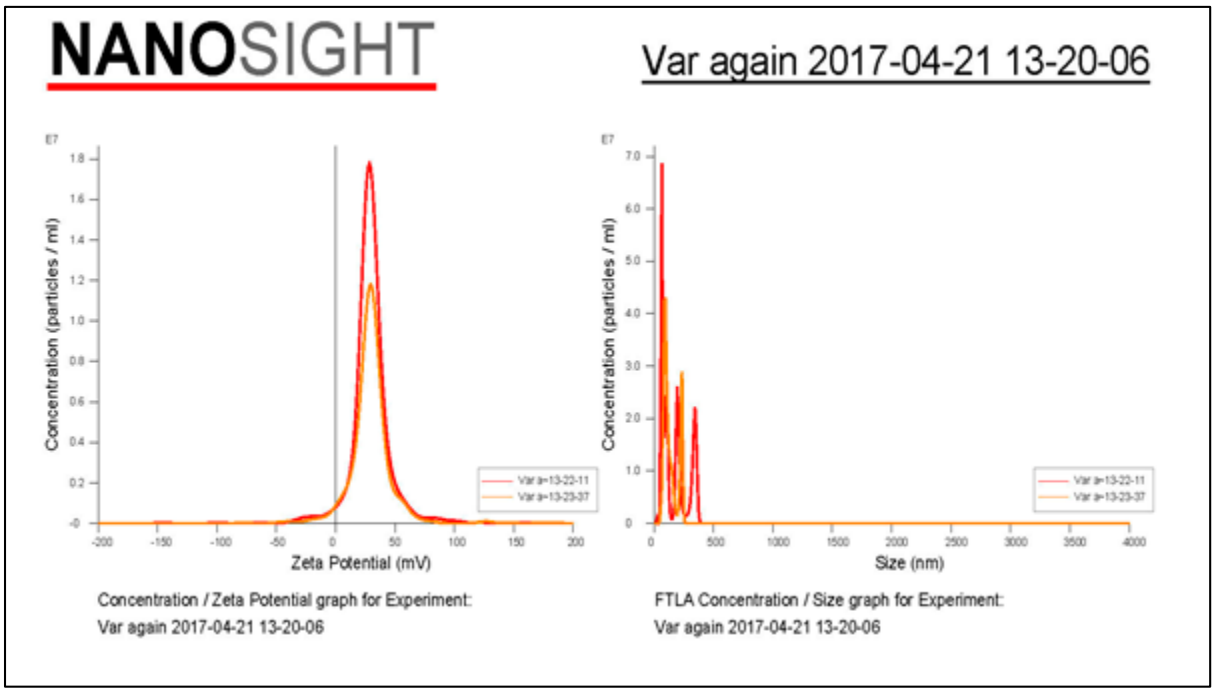

C8: NTA zeta potential and sizing analysis of the nanocomposite PACTF.

APPENDIX D

TURNITIN REPORT

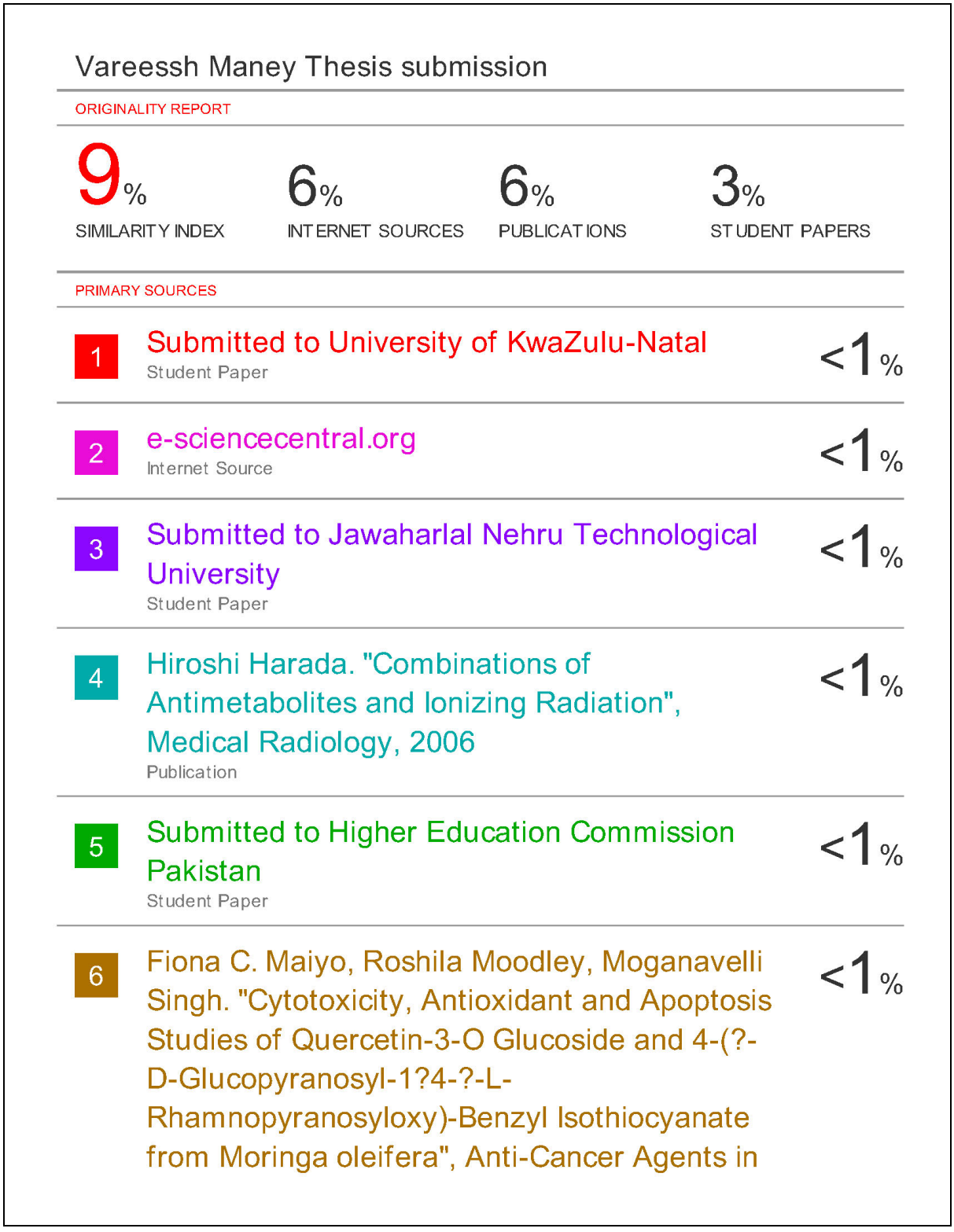

Vareessh Maney Thesis submission

ORIGINALITY REPORT

9%	6%	6%	3%
SIMILARITY INDEX	INTERNET SOURCES	PUBLICATIONS	STUDENT PAPERS

PRIMARY SOURCES

1	Submitted to University of KwaZulu-Natal Student Paper	<1%
2	e-sciencecentral.org Internet Source	<1%
3	Submitted to Jawaharlal Nehru Technological University Student Paper	<1%
4	Hiroshi Harada. "Combinations of Antimetabolites and Ionizing Radiation", Medical Radiology, 2006 Publication	<1%
5	Submitted to Higher Education Commission Pakistan Student Paper	<1%
6	Fiona C. Maiyo, Roshila Moodley, Moganavelli Singh. "Cytotoxicity, Antioxidant and Apoptosis Studies of Quercetin-3-O Glucoside and 4-(?-D-Glucopyranosyl-1?4-?-L-Rhamnopyranosyloxy)-Benzyl Isothiocyanate from Moringa oleifera", Anti-Cancer Agents in	<1%

D1: Turnitin similarity index, excluding chapter 3 and the references.

APPENDIX E

CONFERENCE PRESENTATION

Awarded 1st prize

An *in vitro* assessment of Chitosan/ bimetallic PtAu nanocomposites as delivery vehicles for Doxorubicin

Vareessh Maney and Moganavelli Singh

Non-Viral Gene Delivery Laboratory, Discipline of Biochemistry,
University of KwaZulu Natal, Durban, South Africa

INTRODUCTION

The booming interest in designing innovative drug delivery vectors at the nanoscale in light of the global cancer crisis is set to advance cancer therapy. This approach delivers versatile chemotherapeutics with favourable pharmacokinetics, biodegradability, biodistribution and safety. Classical chemotherapeutic drugs such as doxorubicin (DOX) have potent biological activity, however, lack targeting specificity, are rapidly extruded by drug efflux pumps and metabolised *in vivo*. With aim to mitigate these underlying bottlenecks, novel Platinum (shell)-Gold (core) Bimetallic Nanoparticles (PtAuBNps) were synthesised and functionalised with Chitosan to encapsulate Doxorubicin (DOX) as well as support biocompatibility and bioadhesiveness. The physico-chemical features of all PtAuBNps and their drug-loaded nanocomposites were characterised using UV-Vis spectroscopy, transmission electron microscopy (TEM), and nanoparticle tracking analysis (NTA). Drug encapsulation and drug loading studies were performed to determine the efficiency of PtAuBNps platforms. *In Vitro* studies were conducted to determine release profiles under simulated environments, cytotoxicity profiles through MTT and SRB studies and apoptosis induction using Duel EtBr/AO dyes. It is anticipated that utilizing novel chitosan capped PtAuBNps will reduce cytotoxic effects in normal HEK293 cell lines whilst inducing toxic effects on cancerous cell lines.

METHODS

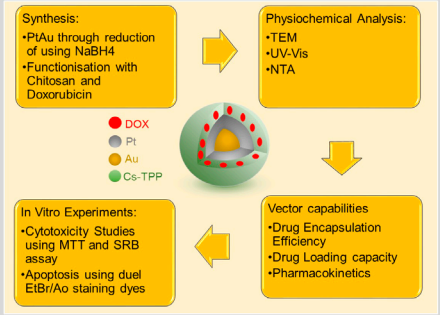

DISCUSSION

Ultrastructural analysis using TEM and NTA revealed all BNps and drug loaded Nanocomposites (Figure 1 A-D) to be spherical, homogenous and showing minimum aggregation. There was no noticeable change in the morphology of PtAuCs, however, crosslinking chitosan and subsequent addition of the drug demonstrated a size increase. Moreover, all functionalised BNps displayed high zeta potential (Table 1) indicating good Colloidal stability. Binding studies (Table 2) revealed high drug encapsulation efficiencies (~70%) and loading content capabilities. Drug release studies (Figure 3) revealed nanocomposites to display pH-triggered drug release, with faster release kinetics observed under acidic conditions. *In vitro* cytotoxicity profiles were determined using the MTT (Figure 4) and SRB assays (Figure 5), with up to 50% cell death recorded in the MCF-7 and HepG2 cell line. The nanocomposites exhibited high specificity towards cancerous cells and prevented harsh biological activity towards normal, HEK293 cell line. This finding was supported by Apoptosis studies (Figure 6), at their IC50 values drug encapsulated nanocarriers evoked cancer specific apoptosis induction in comparison to free Doxorubicin.

CONCLUSION

PtAuBNps were successfully synthesized and functionalised with DOX encapsulated chitosan. All BNps and drug loaded nanocomposites displayed favourable physico-chemical attributes with respect to small size, shape and colloidal stability. In addition, nanocomposites displayed pH triggered drug release that was shown to be cell specific through cytotoxicity and apoptosis induction studies. These positive attributes with further optimisations warrant future research.

REFERENCES

1. Zhang H, Toshima N. Synthesis of Au/Pt bimetallic nanoparticles with a Pt-rich shell and their high catalytic activities for aerobic glucose oxidation. *Journal of Colloid and Interface Science* 394 166-176 (2013).

ACKNOWLEDGEMENTS

1. Supervisor, Dr. M.Singh, Non-Viral Gene Delivery Laboratory, Discipline of Biochemistry and the University of KwaZulu Natal, Durban, South Africa

2. The National Research Foundation (NRF), Pretoria, South Africa.

RESULTS

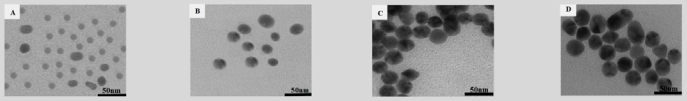

Figure 1. Transmission electron micrographs of (A) PtAuBNps, (B) PtAuCs, (C) CTD, (D) PACTD. Bar = 50 nm

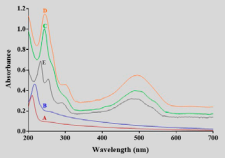

Figure 2. UV-Vis of (A) PtAuBNps, (B) PtAuCs, (C) CTD, (D) PACTD, (E) DOX

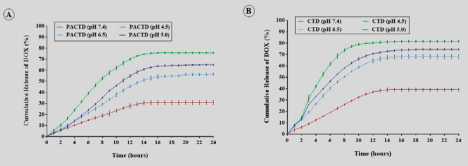

Figure 3. Drug Release Profile of **(A)** PACTD and **(B)** CTD under various neutral and acidic conditions

Table 1. Size Distribution and zeta potential of BNP and its Nano-conjugates. Data represented as mean ± SD

Sample	Particle Size (nm)	Zeta Potential (mV)
PtAuBNps	78.9 ± 8.5	-19.3 ± 0.9
PtAuCs	128.2 ± 3.7	58.5 ± 0.1
PACTD	131.1 ± 2.9	28.2 ± 1.5
CTD	147.8 ± 3.6	24.2 ± 3.1

Table 2. Drug loading efficiency(EE), theoretical drug content (TDC), actual drug content (ADC) and Drug loading content (LC) of nanocomposites.

Sample	TDC (µg)	EE (%)	ADC (µg)	LC (%)
CTD	116.00	71.85	83.34	14.62
PACTD	96.67	69.82	67.49	11.37

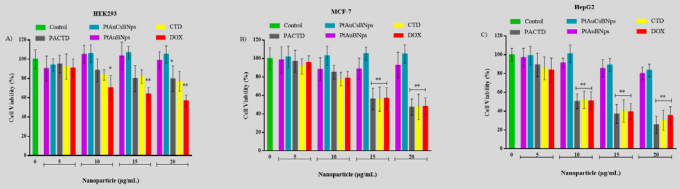

Figure 4: MTT cytotoxicity assay in cell lines: A) HEK293 , B) MCF-7 and C) HepG2. Each bar represents the mean ± SD (n=3), * p<0.05 and **p<0.01 were considered statistically significant as determined by the Dunnet test.

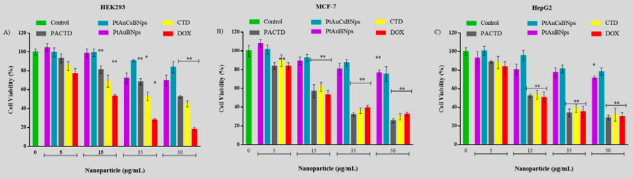

Figure 5: SRB cytotoxicity assay in cell lines: A) HEK293 , B) MCF-7 and C) HepG2. Each bar represents the mean ± SD (n=3), * p<0.05 and **p<0.01 were considered statistically significant as determined by the Dunnet test.

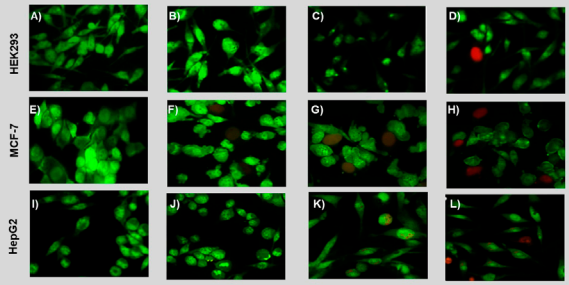

Figure 6: Apoptosis Induction assay in cell lines: **HEK293** , A) Control, B) PACTD, C) CTD, D) DOX ; **MFC-7**, E) Control, F) PACTD, G) CTD, H) DOX and **HepG2** I) Control, J) PACTD, K) CTD, H) DOX